ABSTRACT

CAPACITY, CODING, AND INTERFERENCE CANCELLATION IN MULTIUSER MULTICARRIER WIRELESS COMMUNICATIONS SYSTEMS

by
Christian Ibars Casas

Multicarrier modulation and multiuser systems have generated a great deal of research during the last decade. Orthogonal Frequency Division Multiplexing (OFDM) is a multicarrier modulation generated with the inverse Discrete Fourier Transform, which has been adopted for standards in wireless and wire-line communications. Multiuser wireless systems using multicarrier modulation suffer from the effects of dispersive fading channels, which create multi-access, inter-symbol, and inter-carrier interference (MAI, ISI, ICI). Nevertheless, channel dispersion also provides diversity, which can be exploited and has the potential to increase robustness against fading. Multiuser multicarrier systems can be implemented using Orthogonal Frequency Division Multiple Access (OFDMA), a flexible orthogonal multiplexing scheme that can implement time and frequency division multiplexing, and using multicarrier code division multiple access (MC-CDMA). Coding, interference cancellation, and resource sharing schemes to improve the performance of multiuser multicarrier systems on wireless channels were addressed in this dissertation.

Performance of multiple access schemes applied to a downlink multiuser wireless system was studied from an information theory perspective and from a more practical perspective. For time, frequency, and code division, implemented using OFDMA and MC-CDMA, the system outage capacity region was calculated for a correlated fading channel. It was found that receiver complexity determines which scheme offers larger capacity regions, and that OFDMA results in a better compromise between complexity and performance than MC-CDMA. From the more practical perspective of

bit error rate, the effects of channel coding and interleaving were investigated. Results in terms of coding bounds as well as simulation were obtained, showing that OFDMA-based orthogonal multiple access schemes are more sensitive to the effectiveness of the code to provide diversity than non-orthogonal, MC-CDMA-based schemes.

While cellular multiuser schemes suffer mainly from MAI, OFDM-based broadcasting systems suffer from ICI, in particular when operating as a single frequency network (SFN). It was found that for SFN the performance of a conventional OFDM receiver rapidly degrades when transmitters have frequency synchronization errors. Several methods based on linear and decision-feedback ICI cancellation were proposed and evaluated, showing improved robustness against ICI.

System function characterization of time-variant dispersive channels is important for understanding their effects on single carrier and multicarrier modulation. Using time-frequency duality it was shown that MC-CDMA and DS-CDMA are strictly dual on dispersive channels. This property was used to derive optimal matched filter structures, and to determine a criterion for the selection of spreading sequences for both DS and MC CDMA. The analysis of multiple antenna systems provided a unified framework for the study of DS-CDMA and MC-CDMA on time and frequency dispersive channels, which can also be used to compare their performance.

CAPACITY, CODING, AND INTERFERENCE CANCELLATION IN MULTIUSER MULTICARRIER WIRELESS COMMUNICATIONS SYSTEMS

by
Christian Ibars Casas

A Dissertation
Submitted to the Faculty of
New Jersey Institute of Technology
in Partial Fulfillment of the Requirements for the Degree of
Doctor of Philosophy in Electrical Engineering

Department of Electrical and Computer Engineering

August 2003

APPROVAL PAGE

CAPACITY, CODING, AND INTERFERENCE CANCELLATION IN MULTIUSER MULTICARRIER WIRELESS COMMUNICATIONS SYSTEMS

Christian Ibars Casas

Dr. Yeheskel Bar-Ness, Dissertation Advisor — Date
Distinguished Professor, Department of Electrical and Computer Engineering, NJIT

Dr. Alexander Haimovich, Committee Member — Date
Professor, Department of Electrical and Computer Engineering, NJIT

Dr. Hongya Ge, Committee Member — Date
Associate Professor, Department of Electrical and Computer Engineering, NJIT

Dr. Ali Abdi, Committee Member — Date
Assistant Professor, Department of Electrical and Computer Engineering, NJIT

Dr. Roy Yates, Committee Member — Date
Professor and Associate Director, WINLAB, Rutgers University

BIOGRAPHICAL SKETCH

Author: Christian Ibars Casas

Degree: Doctor of Philosophy

Date: August 2003

Undergraduate and Graduate Education:

- Doctor of Philosophy in Electrical Engineering,
  New Jersey Institute of Technology, 2003
- Master of Science in Electrical Engineering,
  Universitat Politècnica de Catalunya, Barcelona, Spain, 1999
- Master of Science in Electronics Engineering,
  Politecnico di Torino, Torino, Italy, 1999

Major: Electrical Engineering

Presentations and Publications:

C. Ibars and Y. Bar-Ness, "Inter-Carrier Interference Cancellation for OFDM Systems with Macrodiversity and Multiple Frequency Offsets," to appear in *Wireless Personal Communications, an international journal*, Kluwer Academic Publishers, 2003.

C. Ibars and Y. Bar-Ness, "Analysis of Time-Frequency Duality of MC and DS CDMA for Multi-Antenna Systems on Highly Time-Varying Wideband Channels," submitted, *IEEE Transactions on Wireless Communications*, August 2003.

C. Ibars and Y. Bar-Ness,"Outage capacities of a multi-carrier WLAN downlink under different resource sharing techniques," *Proc. IEEE International Symposium on Spread Spectrum Techniques and Applications (ISSSTA)*, vol. 1, pp. 144-149, Prague, Czech Republic, September 2002.

C. Ibars and Y. Bar-Ness, "OFDM detection in a macrodiversity system with multiple frequency offsets," *Proc. 3G Wireless*, San Francisco, CA, May 2002.

C. Ibars and Y. Bar-Ness, "The principle of time-frequency duality of DS and MC CDMA," *Proc. 36th. Annual Conference on Information Sciences and Systems (CISS)*, Princeton, New Jersey, March 2002.

C. Ibars and Y. Bar-Ness, "Rate-Adaptive Coded Multiuser OFDM for Downlink Wireless Systems," *Multi-Carrier Spread-Spectrum & Related Topics*, K. Fazel and S. Kaiser eds., pp. 199-207, Kluwer, 2002.

C. Ibars and Y. Bar-Ness, "Comparing the Performance of Coded Multiuser OFDM and Multi-Carrier CDMA," *Proc. of the 2001 IEEE Global Communications Conference (Globecom'01)*, vol. 2, pp. 881-885, San Antonio, TX, USA, November 2001.

Als meus pares (To my parents)

ACKNOWLEDGMENT

This work could not have been accomplished without the contribution of friendship, support and guidance of many people. First and foremost, I would like to express my sincere gratitude to my advisor, Dr. Yeheskel Bar-Ness for guiding me through the dissertation. He has taught me how to conduct strong research, and his encouragement and support during my studies have been invaluable. I would also like to express my appreciation to the distinguished members of the dissertation committee: Dr. Alexander Haimovich, Dr. Hongya Ge, Dr. Ali Abdi and Dr. Roy Yates. Their insightful comments have improved the quality of this dissertation.

Funding for my research was provided by the Ross Fellowship Memorial Fund. I am indebted to Dr. Ronald Kane and Dr. Sotirios Ziavras for ensuring the continuation of financial support.

Many thanks are due to Dr. John Cioffi, for his valuable discussions and advice, and for his logistic support during my stay at Stanford University, which I greatly enjoyed. I extend my gratitude to the members and visitors of his research group for providing a great research environment.

Everyone at the Center for Communications and Signal Processing Research deserves thanks for assistance during many stages of this work, and for generating a creative and enjoyable atmosphere to work in. Thanks to Mizhou Tan and Jianming Zhu for your help with my research. My colleagues Daniel Pérez Palomar and Albert Guillén Fàbregas also deserve special mention for their help in parts of this dissertation.

Finally, I sincerely thank Montse and my family for continued support and encouragement which have made possible this accomplishment and all of my friends at the CCSPR for making the past few years an exciting and enjoyable time.

TABLE OF CONTENTS

TABLE OF CONTENTS
(Continued)

Chapter Page

TABLE OF CONTENTS
(Continued)

TABLE OF CONTENTS
(Continued)

Chapter **Page**

LIST OF TABLES

LIST OF FIGURES

LIST OF FIGURES
(Continued)

Figure **Page**

LIST OF FIGURES
(Continued)

Figure **Page**

CHAPTER 1

INTRODUCTION

1.1 Multicarrier in Wireless

Multicarrier modulation is based on the principle of frequency division multiplexing (FDM), in which the frequency spectrum is subdivided in bands to allow multiple transmissions. Multicarrier modulation further subdivides a frequency band into several orthogonal sub-bands, which are used to transmit information in parallel. The first systems using multicarrier modulation were proposed four decades ago (e.g. the Kineplex system [1]) [2]. The main difficulty faced by these systems was that, in order to maintain the orthogonality of different sub-carriers and avoid interference, large guard bands had to be allowed, or otherwise very strict requirements on filter design were necessary. None of these solutions is satisfactory, since large guard bands result in low spectral efficiency and strict filter requirements in transceiver complexity. It was noted in [3, 4] that such impairments could be avoided by performing sub-carrier modulation digitally by means of the inverse discrete Fourier transform (IDFT), leading to what is known as orthogonal frequency division multiplexing (OFDM). In OFDM the sub-carrier spectra partially overlap, thereby reducing the required bandwidth while preserving orthogonality. Additionally, digital sub-carrier modulation by means of the fast Fourier transform (FFT) algorithm is nowadays possible using inexpensive signal processing integrated circuits.

Much of the popularity of wireless multicarrier systems lies in its robustness against wireless channel impairments, such as multipath propagation and frequency-selective signal fading. Longer symbol duration which results from a decreased data rate per sub-carrier reduces inter-symbol interference (ISI). ISI can be avoided using a cyclic prefix, thereby eliminating the need for complex equalization algorithms and

any resulting noise enhancement. On the other hand, OFDM suffers from some shortcomings. The peak to average power ratio (PAPR) of OFDM is notably higher than that of single-carrier modulations. A larger PAPR complicates the design of power amplifiers, requiring a wider linear characteristic. Analog to digital converters require a larger dynamic range as well. Additionally, OFDM is very sensitive to a frequency offset between transmitter and receiver, and to frequency-dispersive channels, which cause a loss of orthogonality among sub-carriers and result in inter-carrier interference (ICI).

Recently, OFDM has been introduced in many areas of wireless communications, such as terrestrial audio and video broadcasting (DAB, DVB-T) [5, 6], and wireless local area networks (WLAN), and was adopted in several standards (see Table 1.1 summarizing the physical layer characteristics). It is also a candidate for different proposals for 4th generation cellular communications systems. The DAB and DVB-T standards were introduced in Europe and subsequently adopted in many other countries. In the WLAN area, a very similar OFDM-based physical layer was adopted by IEEE 802.11a and ETSI Hiperlan for North America and Europe respectively [7,8].

Multiuser systems can be classified in two categories: broadcast systems, where a unique signal is sent and received by all users, and multiple access systems, in which different signals are sent and received by each user. Single frequency networks (SFNs), where all broadcast stations transmit the same signal at the same frequency, exploit an important advantage of MCM, and in particular of OFDM, for broadcast applications. SFNs rely on the immunity of OFDM to multipath, and result in increased received signal power and additional diversity. The classical approaches for multiple access (for the uplink) or multiplexing (for the downlink) are time, frequency, and code division multiple access (TDMA, FDMA, and CDMA respectively) or multiplexing (TDM, FDM, and CDM respectively). They can all be implemented on a

Table 1.1 Multicarrier Based Standards for Wireless Transmission

	DAB	DVB-T	IEEE 802.11a / Hiperlan
Established	ETSI, 1995	ETSI, 1997	IEEE, 1999/ ETSI, 2001
Number of sub-carriers	192-1536	1,705-6,817	52
Sub-carrier spacing	1 kHz - 8 kHz	1.16 kHz - 4.46 kHz	312.5 kHz
Modulation	QPSK	4 - 64-QAM	4 - 64-QAM
Frequency band	II, III, L	III, IV	unlicensed 5 GHz

multicarrier system. Orthogonal frequency division multiple access (OFDMA), also known as multiuser OFDM, is a general multiple access scheme that can implement TDMA/TDM and FDMA/FDM. CDMA/CDM can be implemented by multicarrier CDMA (MC-CDMA), also known as multicarrier spread spectrum (MC-SS). Other variants of a multicarrier CDMA implementation have been proposed in the literature, such as multicarrier DS-CDMA (MC-DS-CDMA) [9, 10], multitone CDMA (MT-CDMA) [11], and OFDM-CDMA [12]. These systems combine the use of CDMA and multicarrier in different ways. The reader may refer to [13] for an overview description of different multicarrier CDMA systems.

Multiple access systems can in turn be classified as uplink and downlink systems. Uplink and downlink have different constraints that must be accounted for by system designers. Their most fundamental difference is that the uplink is a multiple access channel (MAC) with several mobile users trying to access a single receiver, while the downlink corresponds, in information theory, to the broadcast channel (BC), with a single transmitter serving several mobile receivers. The capacity of MAC

and BC channels cannot generally be achieved by time division or frequency division multiplexing, but rather by code division multiplexing [14], which expanded interest on CDMA as a multiple access technique that could potentially achieve capacity for both uplink and downlink systems.

Lack of user synchronization poses a challenge for uplink multicarrier systems. MC-CDMA must rely on asynchronous multiuser detection and frequency offset correction, while OFDMA systems must ensure time and frequency synchronization by means of a feedback loop, which can be difficult and costly, unless ISI and ICI cancellation schemes are added to the receiver. On the other hand, the downlink involves only one transmitter wherein different users' signals can be transmitted synchronously in time and frequency. Finally, complexity constraints, which are placed on the mobile unit, are more stringent for the transmitter in the uplink system and for the receiver in the downlink system.

1.2 Dissertation Overview

In Chapter 2, OFDM, OFDMA, and MC-CDMA are described. In addition, the wireless channel is characterized by system functions, and multicarrier channel models are described. Basic results and definitions in the areas of information theory and coding for wireless channels are also provided.

Chapter 3 evaluates outage capacities of a multicarrier downlink system under different spectrum sharing techniques. The capacity regions and outage probabilities of TDM, FDM, and CDM, implemented with OFDMA and MC-CDMA, are given. It is shown that CDM has potentially a larger outage capacity region, which can however be smaller than TDM and FDM when suboptimal low-complexity detection methods are used.

Chapter 4 analyzes the performance of a multicarrier downlink system from the more practical point of view of bit and frame error rates. It is found that the use

of channel codes provides a greater performance improvement for OFDMA than for MC-CDMA. Useful performance bounds and approximations are provided and used to compare the two multiple access techniques.

Chapter 5 considers the effects of poor frequency synchronization between different OFDM transmitters in a SFN. Analysis of received signal to interference plus noise ratio (SINR) reveals high sensitivity of such systems to frequency offsets. Closed form expressions are provided for the SINR at the receiver side in the presence of multiple offsets. It is shown that linear and decision-feedback interference cancellation methods can be used to improve the SINR significantly, and therefore reduce the sensitivity to frequency offsets.

Chapter 6 establishes a unified framework for the analysis of multicarrier and direct sequence CDMA systems by determining a duality relationship among them, which is used to analyze the performance of CDMA systems in time-variant, frequency-selective fading channels. Optimal matched filter structures and design criteria for spreading sequences are also derived.

Finally, Chapter 7 summarizes the observations and contributions of this dissertation.

CHAPTER 2

MULTIUSER MULTICARRIER WIRELESS SYSTEMS

This chapter presents a brief introduction to multiuser multicarrier wireless systems. It is meant to define the multicarrier systems under study and to give the necessary background for their analysis. A clear definition for OFDMA and MC-CDMA is especially important to clarify the many different definitions and acronyms appearing in the literature [13]. In this dissertation, both OFDMA and MC-CDMA are assumed to be built upon an OFDM modem, which is well understood, commercially available, and very flexible for the implementation of multiuser systems. Other definitions of multicarrier CDMA are briefly mentioned and the reader is referred to the available literature.

The study of wireless systems requires an accurate characterization of the effects of the wireless channel, which is also provided in this chapter. Path loss, shadowing and multipath propagation are described. Furthermore, a statistical characterization of random fading based on the channel system functions is provided, and channel models for the simulation of multicarrier systems, as well as a block fading approximation used for its theoretical analysis, are described.

The concepts of ergodic and outage capacities, information-theoretic measures for time-varying channels, are also introduced. The main results on capacity of fading broadcast channels, used for the calculation of the capacity of multiuser multicarrier systems, are described. Furthermore, fundamental results on coding for fading channels are given, which lead to the definition of coding power gain and diversity gain, and to bounding techniques for the bit error rate (BER) of fading channels.

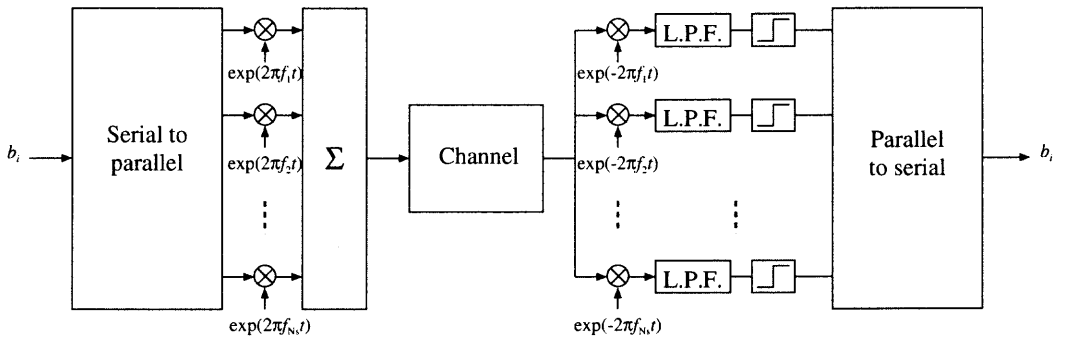

Figure 2.1 Multicarrier modem block diagram.

2.1 Multicarrier Modulation and OFDM

Multicarrier modulation uses several sub-carriers to transmit data. In orthogonal frequency division multiplexing sub-carriers are digitally modulated with the aid of the IDFT. Figure 2.1 shows the implementation of a multicarrier modem. A multi-carrier signal can be described as

$$x(t) = \Re\left\{\sum_{i=-\infty}^{\infty}\sum_{l=0}^{N_s-1} A_l b_{iN_s+l} \exp(j2\pi f_{c,l}t)p(t-iT)\right\}, \tag{2.1}$$

where A_l denotes the signal amplitude on sub-carrier l, b_{iN_s+l} denotes the symbol on the l^{th} sub-carrier for the i^{th} time interval, normalized to average unit power, $p(t)$ denotes a rectangular pulse shape, $p(t) = \Pi\left(\frac{t}{T}\right)$, N_s is the number of sub-carriers, T the multi-carrier symbol period, $j^2 = -1$, and $f_{c,l}$ denotes sub-carrier l frequency. Note that, since N_s sub-carriers are used to transmit in parallel, the symbol period on a sub-carrier is N_s times longer than the symbol period of the incoming data stream.

OFDM is a multicarrier modulation which performs sub-carrier modulation digitally. Blocks of N_s symbols are batch-processed by means of the IDFT to modulate the OFDM sub-carriers. The discrete output of the IDFT block resulting from an input of N_s symbols is known as OFDM block or OFDM symbol, and is denoted, for

$n = 0, 1, \cdots, N_s - 1$, by

$$x(n) = \frac{1}{\sqrt{N_s}} \sum_{l=0}^{N_s-1} A_l b_l \exp\left(j2\pi \frac{nl}{N_s}\right), \tag{2.2}$$

where variable n is used to describe discrete time domain and the IDFT is normalized by $1/\sqrt{N_s}$. The OFDM receiver processes incoming signals with the discrete Fourier transform (DFT), which digitally demodulates the multicarrier signal. IDFT and DFT can be efficiently implemented using the FFT algorithm. Without channel impairments, the IDFT/DFT pair ensure perfect signal reconstruction, which is easily seen by taking the DFT of $x(n)$ normalized by $\sqrt{N_s}$,

$$\begin{aligned} y(i) &= \frac{1}{N_s} \sum_{m=0}^{N_s-1} \sum_{l=0}^{N_s-1} A_l b_l \exp\left(j2\pi \frac{ml}{N_s}\right) \exp\left(-j2\pi \frac{im}{N_s}\right) \\ &= \frac{1}{N_s} \sum_{l=0}^{N_s-1} A_l b_l \sum_{m=0}^{N_s-1} \exp\left(j2\pi m \frac{l-i}{N_s}\right) = A_i b_i. \end{aligned} \tag{2.3}$$

In OFDM symbols are cyclically extended to avoid inter-symbol interference in non-ideal channels (those with non-zero delay spread) by means of a cyclic symbol prefix. An OFDM symbol with a cyclic prefix of N_{CP} samples is given by Equation (2.2) for $n = -N_{CP}, -N_{CP}+1, \cdots, N_s - 1$. As a result of the cyclic prefix, the spectral efficiency of OFDM is reduced by a factor of $\rho = \frac{N_s}{N_s+N_{CP}}$. The resulting complex baseband OFDM signal in continuous time domain is given by

$$x_{CP}(t) = \sum_{i=-\infty}^{\infty} \left(\sum_{l=0}^{N_s-1} A_l b_{iN_s+l} \exp\left(j2\pi \frac{l}{N_s} f_s t\right) \right) \omega(t - iT), \tag{2.4}$$

where $f_s = NT^{-1}$, with $N = N_s + N_{CP}$, is the channel symbol rate, which is the rate at which the digital to analog converter is fed, and $\omega(t)$ is a windowing function. Frequency separation between sub-carriers is given by $\Delta f = f_s/N_s$.

The windowing function is used to shape the power spectrum of OFDM signals in order to reduce the side lobe power. A raised cosine window is commonly used [15],

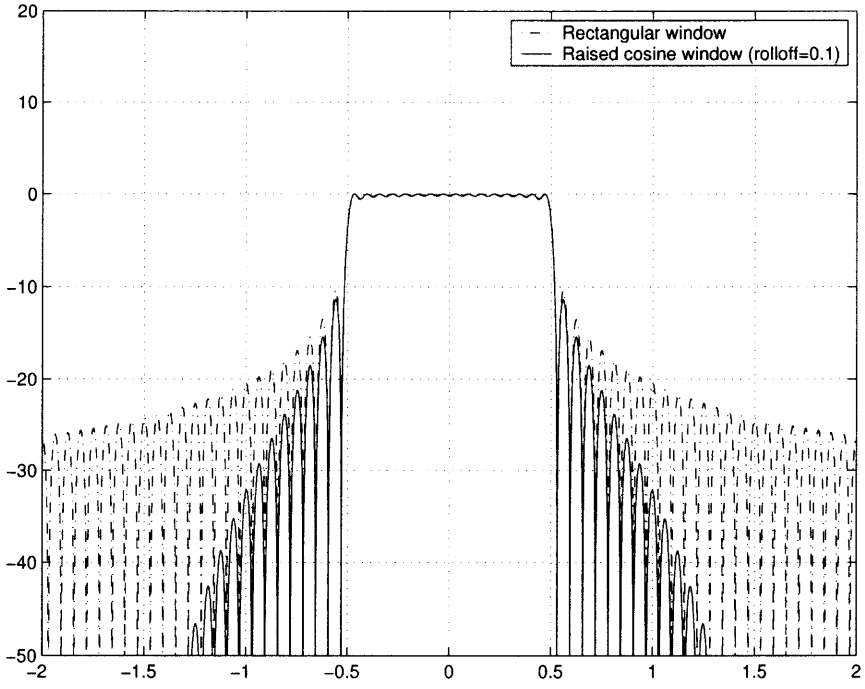

Figure 2.2 OFDM signal spectra without windowing and with a raised cosine window.

given by

$$\omega(t) = \begin{cases} 0.5 + 0.5\cos(\pi + t\pi/\beta T) & 0 \leq t \leq \beta T \\ 1 & \beta T \leq t \leq T \\ 0.5 + 0.5\cos((t-T)\pi/\beta T) & T \leq t \leq (1+\beta)T \end{cases}, \tag{2.5}$$

where β is the *roll-off factor*. Figure 2.2 shows the power spectrum of an OFDM signal before and after applying a raised cosine window with a roll-off factor of 0.1. The un-windowed signal uses a square pulse.

Assuming that there is no inter-block interference, it is useful to represent the OFDM signal in matrix notation. To do so the normalized IDFT matrix is defined as

$$\mathcal{F}^{-1} = \frac{1}{\sqrt{N_s}} \begin{bmatrix} 1 & 1 & 1 & \cdots & 1 \\ 1 & \exp\left(j2\pi\frac{1}{N_s}\right) & \exp\left(j2\pi\frac{2}{N_s}\right) & \cdots & \exp\left(j2\pi\frac{(N_s-1)}{N_s}\right) \\ 1 & \exp\left(j2\pi\frac{2}{N_s}\right) & \ddots & & \exp\left(j2\pi\frac{2(N_s-1)}{N_s}\right) \\ \vdots & \vdots & & \ddots & \vdots \\ 1 & \exp\left(j2\pi\frac{(N_s-1)}{N_s}\right) & \exp\left(j2\pi\frac{2(N_s-1)}{N_s}\right) & \cdots & \exp\left(j2\pi\frac{(N_s-1)^2}{N_s}\right) \end{bmatrix}$$

where a scaling factor of $1/\sqrt{N_s}$ has been applied to preserve average signal power. $\mathcal{F}^{-1}$ is unitary, therefore $\mathcal{F}^{-1} = \mathcal{F}^H$, where superscript ^{H} denotes Hermitian transpose, and $\mathcal{F}$ corresponds to the DFT transformation (scaled by a factor of $\sqrt{N_s}$) performed by the OFDM demodulator. Using matrix notation a transmitted OFDM symbol is given by

$$\mathbf{x} = \mathcal{F}^H \mathbf{A}\mathbf{b}, \tag{2.6}$$

where $\mathbf{A} = \text{diag}\{A_0, A_1, \cdots, A_{N_s-1}\}$ and $\mathbf{b} = [b_0, b_1, \cdots, b_{N_s-1}]$. As before, perfect reconstruction in an ideal channel is easily shown as

$$\mathbf{y} = \mathcal{F}\left(\mathcal{F}^H \mathbf{A}\mathbf{b}\right) = \mathbf{A}\mathbf{b}, \tag{2.7}$$

where the cyclic prefix was not included in the notation[1].

Transmission through a time-invariant channel with baseband impulse response $h(\tau)$ is considered next. The received continuous time, complex baseband OFDM signal is given by

$$y(t) = \int h(\tau) x_{CP}(t-\tau)\, d\tau + \eta(t), \tag{2.8}$$

[1]Throughout this dissertation cyclic prefix addition and removal is not considered in the notation unless it is relevant for the analysis. Additionally, the use of a cyclic prefix is implied whenever a cyclic convolution with the channel is assumed.

where $\eta(t)$ denotes additive white Gaussian noise (AWGN). The discrete-time baseband signal for $n = 1, 2, \cdots, N_s - 1$ is obtained by sampling $y(t)$ at rate f_s

$$y(n) = h(n) \circledast \frac{1}{\sqrt{N_s}} \sum_{l=0}^{N_s-1} A_l b_l \exp\left(j2\pi \frac{l}{N_s} n\right) + \eta(n).$$

In the expression, $\circledast$ denotes the circular convolution operator resulting from the use of a cyclic prefix [15], and $\eta(n)$ are discrete AWGN samples.

After performing the DFT on the received signal,

$$\begin{aligned} y(k) &= \frac{1}{\sqrt{N_s}} \sum_{n=0}^{N_s-1} y(n) \exp(-j2\pi nk/N_s) \\ &= H_k A_k b_k + \zeta_k \end{aligned} \tag{2.9}$$

is obtained, where H_k is a complex multiplicative coefficient, corresponding to the discrete baseband channel response at frequency $f = 2\pi k/N_s$. Furthermore, the term ζ_k represents AWGN at sub-carrier k and has variance σ_ζ^2 (the same in all sub-carriers). Using matrix notation it is obtained, for all sub-carriers,

$$\mathbf{y} = \mathbf{HAb} + \boldsymbol{\zeta}, \tag{2.10}$$

where $\mathbf{H} = \text{diag}\{H_0, H_1, \cdots, H_{N_s-1}\}$.

2.2 Multiuser Multicarrier Systems

2.2.1 OFDMA

In the previous section OFDM was described as a multicarrier modulation dedicated to a single user transmission. In a multiuser system with K users, K independent transmissions can be orthogonally multiplexed in a single OFDM signal. Such multiplexing can be easily understood in the case of a downlink system (Figure 2.3), since all data is multiplexed in a single transmitter. In an uplink system time and frequency synchronization must be very accurate in order to preserve sub-carrier orthogonality. Such system is referred to as OFDMA, or multiuser OFDM. The term OFDMA is

more appropriate for an uplink system, which is a multiple access system, whereas a downlink system is a multiplexing (rather than multiple access) system. Nevertheless, for the purpose of this dissertation the term OFDMA will be used indistinctively for uplink as well as downlink systems.

Every user in OFDMA is assigned one or more sub-carriers at any given time. Sub-carrier assignment may vary from one OFDM symbol to another in order to provide frequency diversity on a frequency-selective channel. This procedure, known as frequency interleaving or frequency hopping, is described in detail in later chapters. To provide a signal model for OFDMA define the sub-carrier set allocated to user k as $\mathcal{C}_k$, such that

$$\mathcal{C}_k \cap \mathcal{C}_j = \emptyset, \ k \neq j \tag{2.11}$$

$$\sum_{k=1}^{K} |\mathcal{C}_k| \leq N_s, \tag{2.12}$$

where $|\mathcal{X}|$ denotes the cardinality of set $\mathcal{X}$. Denote by $\mathcal{C}_k(l)$ the l^{th} element in $\mathcal{C}_k$. User k OFDMA signal can be expressed as

$$x_k(n) = \sum_{l=1}^{|\mathcal{C}_k|} A_l b_l \exp\left(j2\pi \frac{n\mathcal{C}_k(l)}{N_s}\right), \tag{2.13}$$

and the joint OFDMA signal for the synchronous case is given by

$$x(n) = \sum_{k=1}^{K} x_k(n). \tag{2.14}$$

In matrix notation,

$$\mathbf{x}_k = \mathcal{F}^H \mathbf{A} \mathbf{D}_k \mathbf{b}_k, \tag{2.15}$$

where $\mathbf{b}_k$ is a $|\mathcal{C}_k| \times 1$ vector containing $|\mathcal{C}_k|$ data symbols and $\mathbf{D}_k$ is a $N_s \times |\mathcal{C}_k|$ matrix mapping data symbols to positions specified by $\mathcal{C}_k$. $\mathbf{D}_k$ and $\mathcal{C}_k$ may be time-varying in order to implement frequency interleaving. Additionally, time division multiplexing

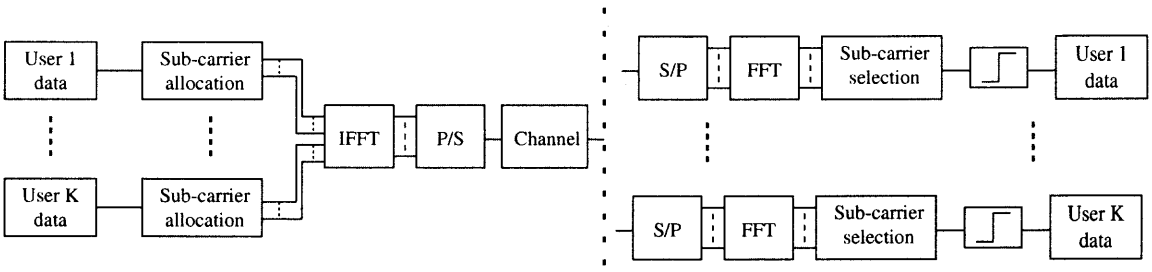

Figure 2.3 OFDMA transmitter for a downlink system.

can be implemented by setting $|\mathcal{C}_k| = N_s$ and $|\mathcal{C}_j| = 0, j \neq k$. The joint signal is given by

$$\mathbf{x} = \sum_{k=1}^{K} \mathcal{F}^H \mathbf{A}\mathbf{D}_k \mathbf{b}_k = \mathcal{F}^H \sum_{k=1}^{K} \mathbf{A}\mathbf{D}_k \mathbf{b}_k, \tag{2.16}$$

which may represent downlink or synchronous uplink.

2.2.2 Multicarrier CDMA

The term multicarrier CDMA (MC-CDMA) was used in [16] to identify an orthogonal multicarrier modulation in which data symbols are copied over all sub-carriers (operation known as spreading in the frequency domain), and encoded by different signature sequences in order to be distinguishable at the receiver. An MC-CDMA modem, shown in Figure 2.4, utilizes the signal structure of OFDM to obtain a set of N_s sub-carriers, where symbols are spread. Denote user k baseband, discrete time MC-CDMA signal by

$$x_{MC,k}(n) = \frac{1}{\sqrt{N_s}} \sum_{l=0}^{N_s-1} A_k b_k s_{k,l} \exp\left(j2\pi nl/N_s\right). \tag{2.17}$$

$\mathbf{s}_k = [s_{k,0}, s_{k,1}, \cdots, s_{k,N_s-1}]^T$ is the signature sequence of user k, also commonly referred to as spreading code, A_k the transmitted signal amplitude, and b_k a normalized data symbol. The *processing gain* or *spreading length* of this CDMA system is N_s. In

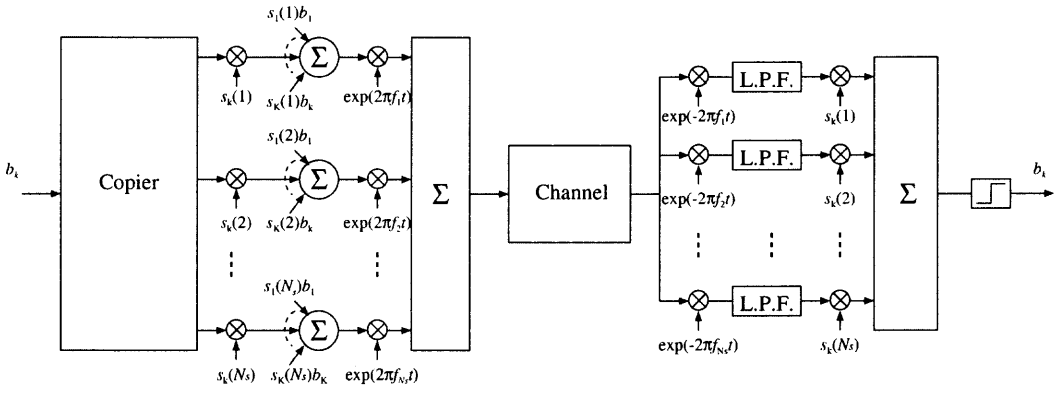

Figure 2.4 Multicarrier CDMA modem.

a system with K synchronous users, the transmitted signal is given by

$$x_{MC}(n) = \sum_{k=1}^{K} \frac{1}{\sqrt{N_s}} \sum_{l=0}^{N_s-1} A_k b_k s_{k,l} \exp\left(j2\pi nl/N_s\right). \tag{2.18}$$

From the signal model, notice the following differences between OFDMA and MC-CDMA:

- In MC-CDMA, all users use all sub-carriers simultaneously, while in OFDMA users are assigned disjoint sets of sub-carriers.
- In MC-CDMA, all users experience a bandwidth expansion of N_s for transmission of a data symbol, while in OFDMA there is no bandwidth expansion.

User j receiver detects the MC-CDMA signal by first performing an IDFT and then using a matched filter with its signature sequence $\mathbf{s}_j$. In an ideal channel,

$$\begin{aligned}
z_{MC,j} &= \frac{1}{\sqrt{N_s}} \sum_{m=0}^{N_s-1} s_{j,m}^* \sum_{n=0}^{N_S-1} x_{MC}(n) \exp\left(-j2\pi \frac{nm}{N_s}\right) \\
&= \frac{1}{N_s} \sum_{m=0}^{N_s-1} s_{j,m}^* \sum_{n=0}^{N_S-1} \sum_{k=1}^{K} \sum_{l=0}^{N_s-1} A_k b_k s_{k,l} \exp\left(j2\pi \frac{nl}{N_s}\right) \exp\left(-j2\pi \frac{nm}{N_s}\right) \\
&= \sum_{m=0}^{N_s-1} s_{j,m}^* \sum_{k=1}^{K} A_k b_k \frac{1}{N_s} \sum_{l=0}^{N_s-1} s_{k,l} \sum_{n=0}^{N_S-1} \exp\left(j2\pi \frac{n(l-m)}{N_s}\right) \\
&= \|\mathbf{s}_j\|^2 A_j b_j + \sum_{k \neq j} \langle \mathbf{s}_j, \mathbf{s}_k \rangle A_k b_k,
\end{aligned} \tag{2.19}$$

where superscript * denotes complex conjugate $\|\mathbf{s}_j\|^2 = \sum_{n=0}^{N_s-1} |s_{j,n}|^2$ is the squared norm of $\mathbf{s}_k$ and $\langle \mathbf{s}_j, \mathbf{s}_k \rangle = \sum_{n=0}^{N_s-1} s_{j,n}^* s_{k,n}$ is the inner product between $\mathbf{s}_j$ and $\mathbf{s}_k$. Besides the desired signal term, the second term in the right hand side of Equation (2.19) corresponds to multi-access interference (MAI). Note that, to achieve perfect reconstruction of the transmitted signal after the receiver matched filter, all signature sequences must be orthogonal. In matrix notation, with $\mathbf{S} = [\mathbf{s}_1\ \mathbf{s}_2\ \cdots\ \mathbf{s}_K]$, $\mathbf{b} = [b_1\ b_2\ \cdots\ b_K]^T$ and $\mathbf{A} = \text{diag}\{A_1, A_2, \cdots, A_K\}$, the transmitted signal of all users is given by

$$\mathbf{x}_{MC} = \mathcal{F}^H \mathbf{S}\mathbf{A}\mathbf{b}, \tag{2.20}$$

and the received, despread signal, after passing through an ideal channel by

$$z_{MC,j} = \mathbf{s}_j^H \mathcal{F}\mathcal{F}^H \mathbf{S}\mathbf{A}\mathbf{b}, \tag{2.21}$$

and for all users by

$$\mathbf{z}_{MC} = \mathbf{S}^H \mathcal{F}\mathcal{F}^H \mathbf{S}\mathbf{A}\mathbf{b}. \tag{2.22}$$

As it was described, MC-CDMA assigns a single code to every user and therefore it is limited to single rate applications. Research on MC-CDMA schemes supporting users with different transmission rates has resulted in two main approaches, namely fixed spreading length (FSL) and variable spreading length (VSL). On an FSL scheme, the same number of sub-carriers is used for all rates; hence the processing gain is equal. On a VSL scheme, transmissions having different rates are assigned different numbers of sub-carriers and the processing gain is different [17, 18]. Different solutions have been proposed to accommodate multiple rates in FSL schemes, among them coded FSL (CFSL) and multi-code FSL (MFSL) [18].

For MFSL, denote by M the total number of signature sequences. For every sequence, one information symbol can be transmitted on one MC-CDMA symbol,

which yields a symbol rate of $R_0 = (T)^{-1}$. Each user is allocated a set of sequences, $\mathcal{S}_k$, $|\mathcal{S}_k| \geq 1$, in order to meet its rate requirements. Its symbol rate is then given by $R_k = R_0|\mathcal{S}_k|$. A block diagram of MFSL MC-CDMA is shown in Figure 2.5. Sequence allocation is such that

$$\mathcal{S}_k \cap \mathcal{S}_j = \emptyset, \ k \neq j \tag{2.23}$$

$$\sum_{k=1}^{K} |\mathcal{S}_k| = M. \tag{2.24}$$

A transmitted MFSL MC-CDMA symbol for user k is represented as

$$\mathbf{x}_{MC,k} = \mathcal{F}^H \mathbf{S}_k \mathbf{A}_k \mathbf{b}_k, \tag{2.25}$$

where $\mathbf{S}_k$ is a matrix whose columns are the sequences in $\mathcal{S}_k$, and $\mathbf{A}_k$ is a $|\mathcal{S}_k| \times |\mathcal{S}_k|$ diagonal matrix with the amplitudes of symbols in vector $\mathbf{b}_k$, which contains $|\mathcal{S}_k|$ user k symbols. For K users,

$$\mathbf{x}_{MC} = \sum_{k=1}^{K} \mathcal{F}^H \mathbf{S}_k \mathbf{A}_k \mathbf{b}_k, \tag{2.26}$$

which, defining $\mathbf{S} = [\mathbf{S}_1, \mathbf{S}_2, \cdots, \mathbf{S}_K]$, $\mathbf{A} = \text{diag}\{\mathbf{A}_1, \mathbf{A}_2, \cdots, \mathbf{A}_K\}$, and $\mathbf{b} = [\mathbf{b}_1^T, \mathbf{b}_2^T, \cdots, \mathbf{b}_K^T]^T$, becomes

$$\mathbf{x}_{MC} = \mathcal{F}^H \mathbf{S} \mathbf{A} \mathbf{b}. \tag{2.27}$$

The more general MFSL notation, which can also be used for single code MC-CDMA ($|\mathcal{S}_k| = 1$ for every k), is used throughout this dissertation to represent MC-CDMA.

2.2.3 Multiuser Detection for MC-CDMA

In Section 2.2.2 a receiver structure which simply despreads transmitted symbols was described, and it was shown that it achieves perfect reconstruction of the transmitted signal when orthogonal codes are used over an ideal channel. But the wireless

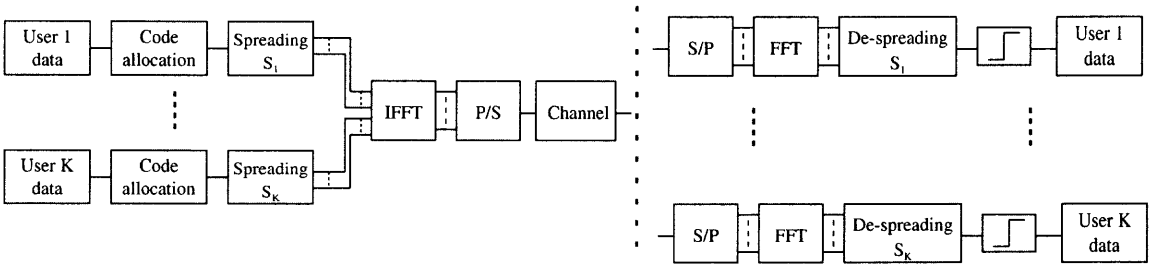

Figure 2.5 Multi-code MC-CDMA modem block diagram.

channel, described in detail in Section 2.3, is frequency-selective, therefore attenuation of a multicarrier signal varies for different sub-carriers. This effect raises two issues for an MC-CDMA receiver: first, an optimal combining strategy must be found that maximizes received signal power over background noise. Secondly, the channel distorts spreading sequences and despreading cannot achieve perfect reconstruction. Therefore, the desired signal suffers interference from other users' signals, or MAI.

Modified MC-CDMA receivers, known as multiuser detectors (MUDs) have been proposed to address these issues [13,19]. In general MUDs outperform the aforementioned detector at the expense of increased complexity. Some MUDs require joint detection of all users' signals, adding complexity to the downlink receiver, where only detection of the desired user's signal is necessary. On the other hand, linear multiuser detectors, which perform a linear transformation on the received symbols, do not need to detect all users' signals. There are two main approaches to linear multiuser detection: to completely eliminate MAI or to maximize the desired user's SNR. The former is known as *decorrelating detector*, or *decorrelator*, and the latter as *minimum mean square error (MMSE) detector.*

Denote the signal at the receiver, corresponding to all users, for the uplink, and after the DFT, by

$$\mathbf{y}_{MC}^{u} = \sum_{k=1}^{K} \mathbf{H}_k \mathbf{S}_k \mathbf{A}_k \mathbf{b}_k + \boldsymbol{\zeta}, \tag{2.28}$$

where $\mathbf{H}_k$ is the frequency domain channel from transmitter k to the receiver, and $\boldsymbol{\zeta}$ denotes AWGN. Note that for multiuser detection it is necessary to consider all users' signals. The notation represents multi-code MC-CDMA. For the downlink, the signal corresponding to all users at receiver j is

$$\begin{aligned} \mathbf{y}^d_{MC,j} &= \mathbf{H}_j \sum_{k=1}^{K} \mathbf{S}_k \mathbf{A}_k \mathbf{b}_k + \boldsymbol{\zeta}_j \\ &= \mathbf{H}_j \mathbf{S} \mathbf{A} \mathbf{b} + \boldsymbol{\zeta}_j, \end{aligned} \tag{2.29}$$

where $\mathbf{H}_j$ is the channel from the transmitter to receiver j, and vector $\mathbf{y}_{MC,j}$ contains all users' signals. The block diagram of a linear MUD is shown in Figure 2.6. The first step in the detection process is to despread all users' signals using a matched filter bank, which performs the operations of maximal ratio combining and despreading, yielding

$$\mathbf{z}^u_{MC} = (\sum_{k=1}^{K} \mathbf{H}_k \mathbf{S}_k)^H ((\sum_{k=1}^{K} \mathbf{H}_k \mathbf{S}_k) \mathbf{A} \mathbf{b} + \boldsymbol{\zeta}) \tag{2.30}$$

$$\mathbf{z}^d_{MC,j} = (\mathbf{H}_j \mathbf{S})^H (\mathbf{H}_j \mathbf{S} \mathbf{A} \mathbf{b} + \boldsymbol{\zeta}_j), \tag{2.31}$$

for uplink and downlink respectively. Defining $\mathbf{R}^u = (\sum_{k=1}^{K} \mathbf{H}_k \mathbf{S}_k)^H (\sum_{k=1}^{K} \mathbf{H}_k \mathbf{S}_k)$ and $\mathbf{R}^d_j = (\mathbf{H}_j \mathbf{S})^H \mathbf{H}_j \mathbf{S}$ as the uplink and downlink *channel-modified code cross-correlation matrices*, Equations (2.30) and (2.31) become

$$\mathbf{z}^u_{MC} = \mathbf{R}^u \mathbf{A} \mathbf{b} + \boldsymbol{\xi}^u \tag{2.32}$$

$$\mathbf{z}^d_{MC,j} = \mathbf{R}^d_j \mathbf{A} \mathbf{b} + \boldsymbol{\xi}^d_j. \tag{2.33}$$

The signal after the matched filter is processed by $\mathbf{T}$, which is intended to increase the SINR of the received signal:

$$\mathbf{z}^{T,u}_{MC} = \mathbf{T} \mathbf{z}^u_{MC} \tag{2.34}$$

$$\mathbf{z}^{T,d}_{MC,j} = \mathbf{T} \mathbf{z}^d_{MC,j}. \tag{2.35}$$

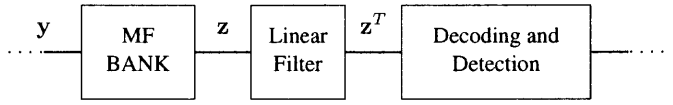

Figure 2.6 Block diagram of a linear multiuser detector.

For the uplink, all users can be detected from $\mathbf{z}_{MC}^{T,u}$, while for the downlink the desired user can be extracted from $\mathbf{z}_{MC,j}^{T,d}$. For the decorrelator MUD,

$$\mathbf{T} = \mathbf{R}^{-1}, \tag{2.36}$$

while for the MMSE detector

$$\mathbf{T} = (\mathbf{R} + \sigma_\zeta^2 \mathbf{A}^{-2})^{-1}, \tag{2.37}$$

where $\mathbf{R}$ denotes uplink or downlink cross-correlation matrices $\mathbf{R}^u$ and $\mathbf{R}^d$. The derivation of Equations (2.36) and (2.37) can be found in Appendix A, as well as the SINR of $\mathbf{z}_{MC}^T$.

2.2.4 Macrodiversity and Single Frequency Networks

Single frequency networks (SFNs) are a different type of multiuser systems based on OFDM modulation, used in broadcasting. SFNs have an extensive coverage area, reached by sending an identical signal from multiple transmit stations. The use of several geographically separated transmitters defines a class of transmitter diversity known as *macrodiversity*. A SFN with uniformly placed transmitters is shown in Figure 2.7. Note that coverage areas overlap, therefore each transmit station signal is received in adjacent coverage areas in addition to its own. The main difference between SFNs and multiuser systems described in the previous section is that in a SFN the same signal is transmitted to all receivers, hence there is no need for multiple access or multiplexing.

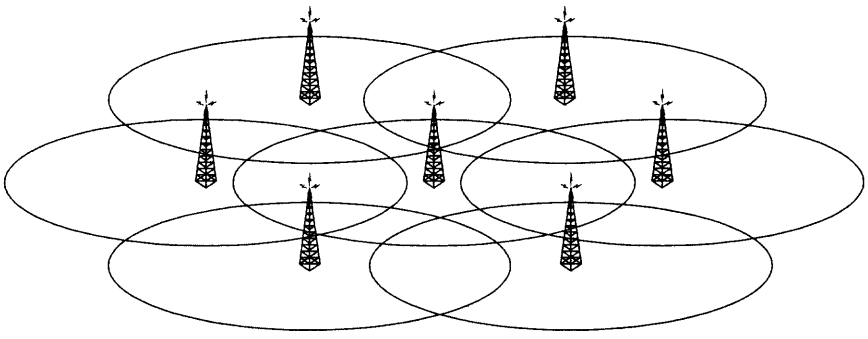

Figure 2.7 Macrodiversity in a single frequency network.

Macrodiversity improves system performance by making several signal replicas, undergoing independent channels, available to the receiver[2]. This effect, known as *artificial multipath*, provides diversity while increasing the received signal power[3]. It was shown in [20] that coverage and signal quality of SFN broadcast systems is superior compared to systems using frequency reuse due to transmit macrodiversity. On the other hand, artificial multipath may result in very large delay spread. While this complicates equalization in single carrier modulation systems, it does not in OFDM systems, since ISI can be eliminated by simply increasing the symbol length (increasing the number of sub-carriers) and the length of the cyclic prefix.

As mentioned earlier, several transmit stations contribute to the signal received by users, which can be represented (in baseband) by

$$y(t) = \sum_{i=1}^{N_T} \left(\int h^i(\tau) x^i(t-\tau)\, d\tau \right) + \eta(t), \tag{2.38}$$

where $h^i(\tau)$ denotes the complex baseband channel response from station i to the receiver (the relative delay of signals from different transmitters is incorporated in

[2]In [20] it is pointed out that channels from different stations in a SFN may be correlated. Nevertheless, macrodiversity improves the performance even with correlated channels.
[3]Macrodiversity provides diversity against shadowing. Using space-time coding at the transmitters macrodiversity can also provide diversity against frequency-selective fading.

$h^i(\tau)$). After the DFT, and in matrix notation,

$$\mathbf{y} = \sum_{i=1}^{N_T} \mathbf{H}^i \mathbf{A}^i \mathbf{b} + \boldsymbol{\zeta} \tag{2.39}$$

is obtained, where $\mathbf{H}^i$ and $\mathbf{A}^i$ represent the channel coefficients in the frequency domain and the signal amplitude respectively, for transmitter i.

2.3 Dispersive Radio Channels

The transmission channel for radio communications is characterized in this section. The wireless channel is a very challenging environment, and must be described accurately in order to design transmission schemes which provide reliable communication. A channel description that fits the needs of this dissertation, including a multicarrier frequency domain channel model, is provided. More complete treatment of this subject can be found in [21, 22].

The effects of radio channels are usually classified into three main categories:

- *Propagation path loss*, which describes the signal attenuation from transmitter to receiver. Antenna gains and cable losses are usually incorporated into the path loss factor.
- *Shadowing*, which describes a statistical variation in path loss.
- *Multipath propagation*, which describes the effects of signals arriving at the receiver from multiple paths, with different delays and amplitudes, and from different directions.

The following sections describe these effects in detail.

2.3.1 Path Loss and Shadowing

A number of path loss models have been derived from empirical measurements, [23, 24]. These models take into consideration the effects of distance, antenna heights,

frequency, and type of terrain (rural, urban, or hilly). The simplest path loss model consists of a distance-dependent factor,

$$\mathcal{L} = d^{-\alpha}. \tag{2.40}$$

α is the path loss exponent, and it typically ranges from 2 to 4 [22], being smaller when there is line of sight (LOS) between transmitter and receiver.

Path loss models fail to describe large signal strength variations on two locations at a same distance from the transmitter. These fluctuations may be the result of additional attenuation due to the presence of large objects, such as a large building. This phenomenon is known as shadowing and its characterization is usually done statistically, using a log-normal distribution. Additional attenuation due to shadowing is given by

$$\mathcal{L}_{Sh} = 10^{\sigma_{sh}\xi}, \tag{2.41}$$

where σ_{sh} is the log-normal standard deviation and ξ is a Gaussian random variable with zero mean and unit variance, $\xi \sim \mathcal{N}(0,1)$. Typical values for log-normal standard deviation are 6 to 8 dB. Shadowing and path loss attenuation are usually constant over the frequency band of a band-pass signal, such as the signals studied in this dissertation. For a moving receiver, shadowing and path loss will result in time variation of the channel, as the environment around the receiver varies and so does the distance to the transmitter. However, such time variation is very slow compared to fast signal strength fluctuations caused by multipath propagation.

2.3.2 Multipath Propagation

Multiple reflections of the transmitted signal on mountains, buildings, and vehicles produce different propagation paths to the receiver. As a result, a number of signal replicas arrive with different amplitude, phase, and delay, creating a fluctuation of

the signal strength. Such phenomenon is known as *multipath fading*, and the signal strength may have a dependence on frequency within the band of a pass-band signal, while rapidly changing in space and time. Multipath propagation is usually characterized statistically, and different models exist depending on the signal bandwidth and type of transmission (indoor or outdoor, and type of outdoor environment). A mathematical description of multipath propagation is provided in this chapter in terms of the low-pass equivalent channel response, which describes the channel response to the low-pass complex envelope of a band-pass signal. The relationship between a pass-band signal $s(t)$ and its complex low-pass equivalent $x(t)$ is given by

$$s(t) = \Re\left\{x(t)\exp(j2\pi f_c t\right\}. \tag{2.42}$$

A narrowband channel model can be characterized by a time-varying complex coefficient $A\exp(j\theta(t))$. It was shown by Clarke [25] that the contribution of many signal replicas with different amplitude and phase can be characterized by a channel response with uniformly distributed phase, $\theta \sim I[0, 2\pi)$, and Rayleigh distributed amplitude, with probability density function (pdf)

$$f_{Ra}(r) = \begin{cases} \frac{r}{\sigma^2}\exp\frac{-r^2}{2\sigma^2}, & 0 \leq r \leq \infty \\ 0, & r < 0 \end{cases}. \tag{2.43}$$

Such distribution is the phase and envelope representation of a complex Gaussian random variable, where real and imaginary components have a Gaussian pdf with zero mean and equal variance. Where a line of sight path exists, the received signal can be characterized as the sum of a deterministic component and a random, Rayleigh-distributed component. The resulting random variable has a Rice distribution, with pdf

$$f_{Ri}(r) = \begin{cases} \frac{r}{\sigma^2}\exp\left(-\frac{r^2+v^2}{2\sigma^2}\right) I_0\left(\frac{rv}{\sigma^2}\right), & 0 \leq r \leq \infty \\ 0, & r < 0 \end{cases}, \tag{2.44}$$

where $I_0(\cdot)$ is the zero-order modified Bessel function of the first kind.

2.3.3 Time-Frequency Duality and System Functions Representation of Dispersive Channels

Time-frequency analysis is a very useful tool in electrical engineering, since transforming between time and frequency domains simplifies the analysis of many systems. The principle of time-frequency duality was formalized by P. Bello in [26], and is similar to voltage-current duality in electric circuits. Based on the equivalence of a time or frequency representation, it goes on to define time-frequency dual systems, which can be represented by the same mathematical operators in time and frequency domains respectively. The main application of time-frequency duality was the characterization in [27–29] of time and frequency dispersive (TDFD) channels by their system functions, which are the channel responses to impulses and sinusoids. More recently these results were extended to consider the spatial domain in [30,31]. In [30] wide-sense stationary (WSS) channels in time, frequency and space are characterized, and in [31] a set of system functions is defined for them. Such characterization is very relevant when one considers the effect that spatial correlation of the channel has on system performance [32–34].

A direct result of time-frequency duality is that a signal processing device can be equivalently described in terms of dual input and output variables (e.g. t and f) by the corresponding dual operators. Additionally, two signal processing devices are dual when their dual operators have the same mathematical form. As an example, consider a device described by

$$Y(f) = f\left(x(t)\right). \tag{2.45}$$

The dual operator of $f(x(t))$ determines the time domain output from the frequency domain input,

$$y(t) = g\left(X(f)\right). \tag{2.46}$$

Furthermore, the dual device is described by

$$Y(f) = g\left(x(t)\right). \tag{2.47}$$

Finally, more complex signal processing systems can also be described as dual if they satisfy the duality condition (their dual operators having the same mathematical form) when regarded as multi-input, multi-output devices.

In Section 2.3.2 it was mentioned that multipath propagation leads to delay spread, which is also known as time dispersion, since, if an impulse function is transmitted, the channel disperses its energy over time. In a mobile environment, different paths arriving to the receiver from different directions (and possibly reflected from moving objects) suffer different Doppler frequency shifts, leading to Doppler spread, or frequency dispersion. Hence, in general, mobile radio channels are dispersive in time and frequency, or doubly dispersive, and must be characterized by time-varying functions. A complete description of such channels appears in [27], in the dual domains of time t and Doppler frequency ν, and of frequency f and delay τ, which are related by

$$\tau \overset{\mathcal{F}_\tau}{\longleftrightarrow} f \tag{2.48}$$

$$t \overset{\mathcal{F}_t}{\longleftrightarrow} \nu, \tag{2.49}$$

where $\mathcal{F}$ denotes a Fourier transform (and inverse) relationship.

Characterizing the channel in any two of the four domains results in four of the Bello system functions in [27]:

1. The *Input delay-spread function* is the time-variant impulse response of the channel, denoted by $g(t, \tau)$. The received signal can be described as

$$y(t) = \int x(t - \tau) g(t, \tau) \, d\tau, \tag{2.50}$$

where τ is the *delay* variable, representing path delay, and t is the *time* variable, representing time variation induced by receiver/transmitter mobility, or a changing environment.

2. The *time-variant transfer function*, $T(f, t)$, represents the time-varying channel response to a tone at frequency $f_c + f$ and time t. It is related to the input delay-spread function by

$$T(f, t) = \mathcal{F}_\tau \{g(t, \tau)\} = \int g(t, \tau) \exp(-j2\pi f \tau) \, d\tau. \tag{2.51}$$

The output signal in terms of $T(f, t)$ is given by

$$y(t) = \int X(f) T(f, t) \exp(j2\pi f t) \, df. \tag{2.52}$$

3. The *Output Doppler-spread function*, $G(f, \nu)$, describes the channel in terms of frequency and Doppler frequency. It satisfies

$$G(f, \nu) = \mathcal{F}_t \{T(f, t)\} = \int T(f, t) \exp(-j2\pi \nu t) \, dt, \tag{2.53}$$

and the output signal is given by

$$Y(f) = \int X(f - \nu) G(f - \nu, \nu) \, d\nu. \tag{2.54}$$

4. The *Delay-Doppler-spread function*, $U(\tau, \nu)$, satisfies

$$U(\tau, \nu) = \mathcal{F}_t \{g(t, \tau)\} = \int g(t, \tau) \exp(-j2\pi \nu t) \, dt, \tag{2.55}$$

and the output signal is given by

$$y(t) = \int\int x(t-\tau)\exp(j2\pi\nu t)U(\tau,\nu)\ d\nu d\tau. \tag{2.56}$$

From the equivalence of the channel representation with any of the system functions presented it is concluded that time and Doppler frequency are dual domains, and delay and frequency are also dual domains. Furthermore, four additional system functions can be obtained as the dual operators of the ones described. These are summarized in Table 2.1, and the expressions for the output signal are given in Table 2.2. Finally, the description of the channel is completed by Table 2.3, which summarizes the relationship of the different system functions in terms of time/delay and frequency/Doppler frequency Fourier transforms.

Table 2.1 Duality Correspondence of Channel System Functions

	Function			Dual function	
t,τ	*Input delay-spread f.*	$g(t,\tau)$	f,ν	*Input Doppler-spread f.*	$H(f,\nu)$
f,t	*Time-variant transfer f.*	$T(f,t)$	t,f	*Frequency-dependent modulation f.*	$M(t,f)$
τ,ν	*Delay-Doppler-spread f.*	$U(\tau,\nu)$	ν,τ	*Doppler-delay-spread f.*	$V(\nu,\tau)$
f,ν	*Output Doppler-spread f.*	$G(f,\nu)$	t,τ	*Output delay-spread f.*	$h(t,\tau)$

2.3.4 Statistical Characterization of Dispersive Channels

In Section 2.3.2 it was noted that the channel response to a narrowband signal at frequency $f_c + f$ and time t, given by $T(f,t)$, could be characterized as complex Gaussian. Since the other functions are linear transformations of $T(f,t)$, and therefore also complex Gaussian, all can be fully characterized by their autocorrelation functions,

Table 2.2 Input-Output Relationship of Dual Channel Functions

Function	Output
Input Doppler-spread f. $H(f,\nu)$	$Y(f) = \int X(f-\nu)H(f,\nu)\ d\nu$
Frequency-dependent modulation f. $M(t,f)$	$Y(f) = \int x(t)M(t,f)\exp(-j2\pi ft)\ dt$
Doppler-delay-spread f. $V(\nu,\tau)$	$Y(f) = \int\int X(f-\nu)\exp(-j2\pi\tau f)V(\nu,\tau)\ d\tau d\nu$
Output delay-spread f. $h(t,\tau)$	$y(t) = \int x(t-\tau)h(t-\tau,\tau)\ d\tau$

defined by

$$R_g(t_1,t_2;\tau_1,\tau_2), \text{for } g(t,\tau),$$

$$R_T(f_1,f_2;t_1,t_2), \text{for } T(f,t),$$

$$R_G(f_1,f_2;\nu_1,\nu_2), \text{for } G(f,\nu),$$

$$R_U(\tau_1,\tau_2;\nu_1,\nu_2), \text{for } U(\tau,\nu).$$

The autocorrelation functions for the dual channel functions can be defined similarly. A channel is said to be *wide sense stationary* (WSS) if the correlation functions depend only on the time difference $\Delta t = t_2 - t_1$. It can be shown that for WSS channels, fading on signals arriving with different Doppler shifts is uncorrelated. Additionally, a channel is defined as *uncorrelated scattering* (US) if the correlation functions depend only on $\Delta f = \nu_2 - \nu_1$. For such channel fading on signals arriving with different delays is uncorrelated. A channel is said to be *wide sense stationary, uncorrelated*

Table 2.3 Fourier Transform Correspondence of Channel System Functions

Function	time/Doppler freq. FT	delay/freq. FT	double time/Doppler freq. FT and freq./delay FT
$g(t,\tau)$	$U(\tau,\nu)$	$T(f,t)$	$G(f,\nu)$
$H(f,\nu)$	$V(\nu,\tau)$	$M(t,f)$	$h(t,\tau)$
$T(f,t)$	$G(f,\nu)$	$g(t,\tau)$	$U(\tau,\nu)$
$M(t,f)$	$h(t,\tau)$	$H(f,\nu)$	$V(\nu,\tau)$
$U(\tau,\nu)$	$g(t,\tau)$	$G(f,\nu)$	$T(f,t)$
$V(\nu,\tau)$	$H(f,\nu)$	$h(t,\tau)$	$M(t,f)$
$G(f,\nu)$	$T(f,t)$	$U(\tau,\nu)$	$g(t,\tau)$
$h(t,\tau)$	$M(t,f)$	$V(\nu,\tau)$	$H(f,\nu)$

scattering (WSSUS) if it is both WSS and US [27]. Therefore, for a WSSUS channel,

$$R_g(t_1,t_2;\tau_1,\tau_2) = P_g(\Delta t,\tau)\delta(\tau-\eta), \tag{2.57}$$

$$R_T(f_1,f_2;t_1,t_2) = R_T(\Delta f,\Delta t), \tag{2.58}$$

$$R_G(f_1,f_2;\nu_1,\nu_2) = P_G(\Delta f,\nu)\delta(\nu-\mu), \tag{2.59}$$

$$R_U(\tau_1,\tau_2;\nu_1,\nu_2) = P_U(\tau,\nu)\delta(\tau-\eta)\delta(\nu-\mu), \tag{2.60}$$

where $P(x)$ denotes the power spectrum, and similar results were obtained for the dual channel functions. All channels considered in this dissertation can be characterized as WSSUS channels. Furthermore, Equations (2.57)-(2.60) are related by double Fourier transforms in the corresponding domains [27].

Time and frequency dispersion of a WSSUS channel can be characterized by its *power delay profile* and by its *Doppler spectrum*, respectively. The former is defined

as

$$s_d(\tau) = \int P_U(\tau, \nu)\ d\nu, \tag{2.61}$$

which determines the signal power received with delay τ. Two additional parameters related to time dispersion are the *mean delay*

$$\bar{\tau} = \frac{\int \tau s_d(\tau)\ d\tau}{\int s_d(\tau)\ d\tau}, \tag{2.62}$$

and the *r.m.s delay spread*

$$\tau_{rms} = \sqrt{\frac{\int (\tau - \bar{\tau})^2 s_d(\tau)\ d\tau}{\int s_d(\tau)\ d\tau}}. \tag{2.63}$$

The Doppler spectrum is defined as

$$s_D(\nu) = \int P_U(\tau, \nu)\ d\tau, \tag{2.64}$$

which determines the signal power receiver with a frequency shift of ν. *Mean Doppler shift* and *r.m.s. Doppler spread* can be defined similarly to mean delay and r.m.s. delay spread.

An alternative characterization of time and frequency dispersion is by the correlation function, $R_T(\Delta f, \Delta t)$, which determines the similarity of the channel response at frequencies separated Δf and instants separated Δt. Variation of the channel in frequency is known as *frequency selectivity*, while variation of the channel in time is known as *time selectivity*, or *time variance*. The frequency selectivity of a channel can be characterized by $R_T(\Delta f, 0)$, and is therefore determined by the power delay profile, as can be seen by noting that

$$\begin{aligned} R_T(\Delta f, 0) &= \int \int P_U(\tau, \nu) \exp(-j2\pi\Delta f\tau)\ d\tau d\nu \\ &= \int s_d(\tau) \exp(-j2\pi\Delta f\tau)\ d\tau, \end{aligned} \tag{2.65}$$

where the double integral is a double Fourier transform. For a channel with an exponential power delay profile the frequency correlation function of the channel is given by [35]

$$R_T(\Delta f, 0) = \frac{1 - j2\pi\tau_d\Delta f}{1 + (2\pi\tau_d\Delta f)^2}. \tag{2.66}$$

The *coherence bandwidth*, B_c, is a measure of frequency selectivity and is defined as the smallest frequency separation for which the correlation function falls below a prescribed level (usually 0.9 or 0.5). Since $R_T(\Delta f, 0)$ and $s_d(\tau)$ are related by a Fourier transform, it follows that $B_c \propto \tau_{rms}^{-1}$.

Time selectivity of the channel is given by

$$\begin{aligned} R_T(0, \Delta t) &= \int\int P_U(\tau, \nu) \exp(-j2\pi\Delta t\nu)\ d\nu d\tau \\ &= \int s_D(\nu) \exp(-j2\pi\Delta t\nu)\ d\nu, \end{aligned} \tag{2.67}$$

therefore it is determined by the Doppler spectrum. Clarke and Gans [25,36] developed a model for the Doppler spectrum, given by

$$s_D(f) = \frac{1.5}{\pi f_m \sqrt{1 - \left(\frac{f - f_c}{f_m}\right)}}, \tag{2.68}$$

where f_m is the maximum Doppler shift and f_c is the carrier frequency. f_m is related to the mobile speed and carrier frequency by

$$f_m = \frac{v}{\lambda}, \tag{2.69}$$

where $\lambda = c/f_c$ is the corresponding wavelength. The time correlation function of the channel can be readily obtained with Equation (2.67), and is given by

$$R_T(0, \Delta t) = J_0(2\pi f_d \Delta t), \tag{2.70}$$

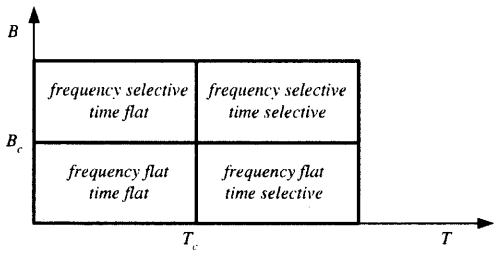

Figure 2.8 Channel classification according to coherence time and bandwidth.

where $J_0(x)$ is the zero order Bessel function of the first kind. The *coherence time*, T_c, is a measure of time selectivity and, similar to the coherence bandwidth, is defined as the smallest time interval for which the correlation function falls below a certain level. Since $R_T(\Delta f, 0)$ and $s_D(\nu)$ are Fourier transform pairs, T_c is inversely proportional to the r.m.s. Doppler spread.

Depending to the relationship between signal bandwidth B and B_c, and symbol period T and T_c, the channel is classified as [37]:

- *Frequency flat, time flat* when $T \ll T_c$ and $B \ll B_c$.
- *Frequency selective, time flat* when $T \ll T_c$ and $B > B_c$.
- *Frequency flat, time selective* when $T > T_c$ and $B \ll B_c$.
- *Frequency selective, time selective* when $T > T_c$ and $B > B_c$.

Figure 2.8 illustrates this channel classification.

2.3.5 Multicarrier Channel Models

For the study of multicarrier systems it is useful to represent the channel in both time and frequency domains. In the time domain, the input delay-spread function $g(t, \tau)$ can be modeled as a tapped delay line (Figure 2.9), denoted by

$$g(t, \tau) = \sum_{l=0}^{L} a_l(t)\delta(t - \tau_l(t)), \tag{2.71}$$

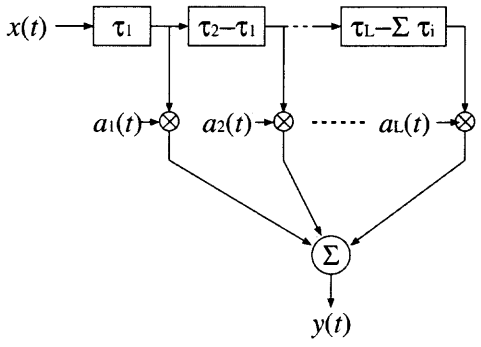

Figure 2.9 Tapped delay line model of the channel impulse response.

where L is the number of paths, $a_l(t)$ a complex coefficient representing each path's amplitude and phase, and $\tau_l(t)$ represents path delay. It is assumed that $\tau_l(t) < \tau_m(t)$ if $l < m$. Each tap represents a cluster of paths and is assigned a representative delay. Amplitude gain and phase of each path are characterized statistically; amplitude according to a Rayleigh distribution, and phase according to a uniform distribution in $[0, 2\pi)$. The received signal is given by

$$y(t) = \int x(t-\tau)g(t,\tau)\, d\tau. \tag{2.72}$$

The maximum path delay τ_L must not exceed the duration of the cyclic prefix of OFDM, and the OFDM symbol length must satisfy $T \gg \tau_L$. On the other hand, in order to ensure sub-carrier orthogonality and avoid ICI, the channel response must be fairly constant over the time interval and therefore the latter must satisfy $T \ll T_c$.

In the frequency domain, the channel can be modeled as a vector of coefficients $\mathbf{h}(t) = [h_0(t), h_1(t), \cdots, h_{N_s-1}(t)]$, representing the channel transfer function $T(f,t)$, obtained as $h_i(t) = T(f_i, t)$, where f_i is the sub-carrier frequency, and where time dependence is eliminated for time-invariant channels[4].

A block approximation of the transfer function model was also used to simplify theoretical analysis of coded multicarrier systems. Such model is termed *multicarrier*

[4]An alternative notation used for the channel is $\mathbf{H} = \text{diag}\{H_0, H_1, \cdots, H_{N_s-1}\}$, where H_i=h_i.

block fading channel (MCBFC), and it was used in [38]. The MCBFC is similar to the block fading channel (BFC) model widely used in single-carrier systems (see, e.g. [39,40]). In this model channel coefficients are divided in blocks B_j^i of time length L_t symbols and frequency width L_f sub-carriers, as in Figure 2.10. Block size L_t and L_f depend on the channel coherence time and coherence bandwidth respectively. Fading coefficients satisfy:

- $h_i(n_1) = h_j(n_2)$ if they are in the same block.
- $h_i(n_1)$ and $h_j(n_2)$ are independent otherwise.

The number of blocks along the frequency axis, F, is limited by the coherence bandwidth B_c and the signal bandwidth B to $F = \lceil \frac{B}{B_c} \rceil$, where $\lceil x \rceil$ denotes the smallest integer larger than x. The number of blocks along the time axis, denoted by T, may be limited by delay constraints or transmission packet length. Otherwise, T is considered infinitely large.

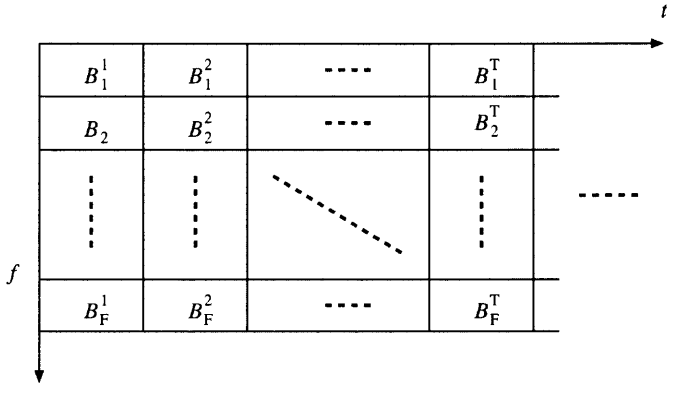

Figure 2.10 Multicarrier block fading channel.

2.4 Ergodic and Outage Capacities

An information-theoretic model of a multiuser multicarrier system is needed to evaluate the capacity of the downlink in Chapter 3, which involves a single transmitter and

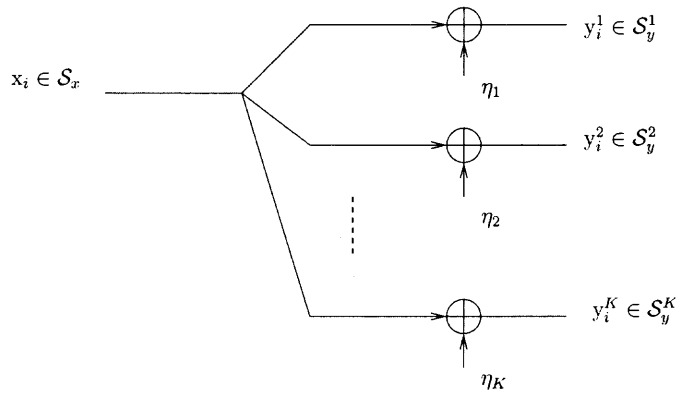

Figure 2.11 Gaussian broadcast channel.

several receivers. Such scenario corresponds to the BC in information theory, provided that the system is isolated from other downlink transmissions. If this condition is not satisfied, the more general model of the interference channel, which involves several transmitters and receivers, applies. The capacity region of broadcast channels has only been solved in some particular cases, such as the degraded broadcast channel [41] and, more recently, the fading channel [42, 43].

The capacity of the Gaussian BC, derived in [44,45], is the starting point for an information-theoretic model of a multicarrier downlink. Consider the discrete-time communication system in Figure 2.11. A codeword x_i from an input codebook $\mathcal{S}_x$ is transmitted to K receivers over K AWGN channels. $\eta_1, \eta_2, \cdots, \eta_K$ are Gaussian noise samples with variances $\sigma_1^2, \sigma_2^2, \cdots, \sigma_K^2$ respectively. Each receiver decodes a codeword $y_1, y_2, \cdots, y_K$ from alphabets $\mathcal{S}_y^1, \mathcal{S}_y^2, \cdots, \mathcal{S}_y^K$. The capacity region for this channel is defined as the mutual information for the pairs $\{X, Y^1\}, \{X, Y^2\}, \cdots, \{X, Y^K\}$, maximized over input alphabet X. Assuming that $\sigma_1^2 < \sigma_2^2 < \cdots < \sigma_K^2$, the capacity region for such channel, in bits per symbol constellation dimension per channel use, is defined by

$$\begin{aligned} C_k(\mathbf{p}) &= \frac{1}{2}\log_2\left(1 + \frac{p_k}{\sigma_k^2 + \sum_{j:\sigma_k^2<\sigma_j^2} p_j}\right) \text{(bits/dim)} \\ k &= 1, 2, \cdots, K, \end{aligned} \tag{2.73}$$

where p_k is power assigned to convey information to receiver k. Equation (2.73) is an extension of the result in [14] to K users.

To extend the Gaussian BC results to fading channels it is assumed that the channel remains constant during the transmission of an entire codeword. Under this condition the channel can be represented by a set of coefficients $\mathbf{h} = [h_1, h_2, \cdots, h_K]$ representing amplitude gains or, alternatively, by scaling the noise variances to $\bar{\sigma}_1^2, \bar{\sigma}_2^2, \cdots, \bar{\sigma}_K^2$, where $\bar{\sigma}_i^2 = \sigma_i^2/|h_i|^2$. The latter representation was used in [42,43] to derive the capacity of a fading BC. From it, it follows that capacity conditioned on the joint channel state $\mathbf{h}$, or instantaneous channel capacity, is given by

$$\begin{aligned} C_k(\mathbf{p},\mathbf{h}) &= \frac{1}{2}\log_2\left(1+\frac{p_k}{\bar{\sigma}_k^2+\sum_{j:\bar{\sigma}_k^2<\bar{\sigma}_j^2} p_j}\right) \\ &= \frac{1}{2}\log_2\left(1+\frac{p_k|h_k|^2}{\sigma_k^2+\sum_{j:\frac{\sigma_k^2}{|h_k|^2}<\frac{\sigma_j^2}{|h_j|^2}} p_j|h_k|^2}\right) \text{ (bits/dim)} \\ k &= 1, 2, \cdots, K. \end{aligned} \tag{2.74}$$

Although it is not explicit in the notation, $\mathbf{p}$ may depend on the channel state $\mathbf{h}$. If the channel vector $\mathbf{h}$ varies randomly, as in fading channels, so does its instantaneous capacity. This leads to the concepts of ergodic, delay-limited, and outage capacities, defined as follows [46]:

Ergodic capacity is the average of the instantaneous capacity taken over the channel vector,

$$C_{E,k} := E_{\mathbf{h}}[C_k(\mathbf{p},\mathbf{h})]. \tag{2.75}$$

Delay-limited capacity is the maximum rate achievable with finite delay.

Outage capacity is defined as the rate C_o for which the probability that the instantaneous capacity is smaller than C_o is equal to the *outage probability*, denoted

by constant p_o. Therefore,

$$p_o = Pr(C_k(\mathbf{p}, \mathbf{h}) < C_o), \tag{2.76}$$

and

$$Pr(C_k(\mathbf{p}, \mathbf{h}) < C_o) = p_o. \tag{2.77}$$

Note that delay-limited capacity can be seen as outage capacity with zero outage probability.

Two types of power constraints are meaningful for wireless systems, namely, long term and short term. A long term power constraint limits the average of available power to a fixed value,

$$E_{\mathbf{h}}\left[\sum_{k=1}^{K} p_k(\mathbf{h})\right] \leq \bar{P}. \tag{2.78}$$

This in fact does not limit peak power, but rather average energy consumption per time unit, thus it is useful for battery-operated devices. A short term power constraint limits the power available on a given channel state,

$$\sum_{k=1}^{K} p_k(\mathbf{h}) \leq \bar{P}, \tag{2.79}$$

or the average on a limited number of states,

$$\frac{1}{L}\sum_{l=1}^{L}\sum_{k=1}^{K} p_k(\mathbf{h}_l) \leq \bar{P}. \tag{2.80}$$

Such constraint, which limits peak and average power, is important for systems operating on peak power restrictions, such as cellular systems or systems using an unlicensed frequency band[5].

The results in Equations (2.73) and (2.74) were extended to consider several parallel broadcast channels in [47] and [48]. For M parallel Gaussian BC, where each

[5]A more general power constraint can be derived as a mixture of the ones described.

can be described by the model in fig 2.11, denote the noise powers for channel m by $\sigma^2_{m,1}, \sigma^2_{m,2}, \cdots, \sigma^2_{m,K}$. Also, define a power allocation matrix $\mathbf{P} = \{P_{m,k}\}$, where $\{P_{m,k}\}$ denotes power allocated to user k on channel m . The channel capacity region is defined by

$$\begin{aligned} C_k(\mathbf{P}) &= \sum_{m=1}^{M} \frac{1}{2} \log_2 \left(1 + \frac{P_{m,k}}{\sigma^2_{m,k} + \sum_{j:\sigma^2_{m,k}<\sigma^2_{m,j}} P_{m,j}} \right) (bits/dim) \\ k &= 1, 2, \cdots, K. \end{aligned} \tag{2.81}$$

Additionally, denote the channel state by vectors $\mathbf{h}_1, \mathbf{h}_2, \cdots, \mathbf{h}_K$, where $\mathbf{h}_k = [h_1, h_2, \cdots, h_M]^T$, for users $1, 2, \cdots, K$ respectively. The instantaneous capacity for parallel fading BC, conditioned on the channel state, is obtained following the same approach used to obtain Equation (2.74), and is given by

$$C_k(\mathbf{P}, \mathbf{h}) = \sum_{i=1}^{M} \frac{1}{2} \log_2 \left(1 + \frac{P_{i,k}|h_{i,k}|^2}{\sigma^2_k + \sum_{j:|h_{i,k}|<|h_{i,j}|} P_{i,j}|h_{i,j}|^2} \right), \tag{2.82}$$

2.5 Coding on Multicarrier Wireless Systems

It has been noted that outage probability, although not a lower bound on BER, is a good indicator of such performance for coded systems on fading channels with limited diversity [40]. Nevertheless, actual BER of systems using channel coding must be determined through analysis of such code, which is considered in Chapter 4. In fading channels, coding not only provides power gain by increasing the code free distance, but also diversity gain. For the purposes of code analysis, define the received signal as

$$y(i) = H(i)Ax(i) + \xi(i), \tag{2.83}$$

where i is the symbol index, $H(i)$ denotes the channel coefficients for each i after signal reception, A is the signal amplitude, $x(i)$ denotes normalized coded symbols, and $\xi(i)$ denotes noise and interference. The interpretation of these variables is different for OFDMA and for MC-CDMA:

- For OFDMA $H(i)$ are complex Gaussian variables, and $\xi(i)$ is AWGN with power $\sigma^2 = N_0/2$. Correlation between different $H(i)$ depends not only on time and frequency correlation of the channel, but also on whether time and frequency interleaving are used. On a channel with time and frequency dispersion both kinds of interleaving should be used to maximize diversity. If the interleaving depth is unlimited one can assume that each consecutive coefficient $H(i)$ is independent, which leads to the *independent fading channel* model. If interleaving is limited by delay constraints, an approach that minimizes correlation among consecutive $H(i)$ is performing periodic interleaving, that is, transmitting consecutive symbols apart in time or frequency by at least the coherence time or bandwidth, respectively. With such approach, for a time interleaving depth of T times the coherence time and for a bandwidth of F times the coherence bandwidth up to FT consecutive $H(i)$ are independent. Furthermore, if channel coefficients of symbols adjacent in time or frequency are highly correlated the multicarrier block fading channel approximation described in Section 2.3 may be used.

- For MC-CDMA, $H(i)$ are channel coefficients after despreading and multiuser detection, while $\xi(i)$ is colored Gaussian noise and interference. Correlation among successive channel coefficients and among noise samples depends on the type of detection scheme used. Unlike in OFDMA, frequency interleaving is not helpful since symbols already occupy the entire multiuser signal bandwidth. On the other hand, time interleaving can be implemented in a similar way as in OFDMA.

The Euclidean distance between two codewords $\mathbf{w}_i$ and $\mathbf{w}_j$ is obtained, conditioned on the channel coefficients, from Equation (2.83),

$$\begin{aligned} d_E^2(i,j|\mathbf{H}) &= ||\mathbf{w}_i - \mathbf{w}_j||^2 \\ &= A^2 \sum_{l=1}^{L_c} |H(l)\left(x_i(l) - x_j(l)\right)|^2 \\ &= E_s R_c \sum_{l \in \mathcal{K}} |(x_i(l) - x_j(l))H(l)|^2, \end{aligned} \tag{2.84}$$

where $A^2 = E_s R_c$, and L_c is the codeword length. The second expression is obtained by adding only the terms where the two codeword symbols differ. Such set of symbols is denoted by $\mathcal{K}$, and its cardinality $|\mathcal{K}|$ is given by the Hamming distance between $\mathbf{w}_i$ and $\mathbf{w}_j$, $d_H(i,j)$. In addition, R_c is the code rate, E_s is the symbol energy, and $x_i(l)$ and $x_j(l)$ are normalized symbols in codewords i, j.

The pairwise error probability (PEP) is defined as the probability to mistakenly detect codeword $\mathbf{w}_j$ when $\mathbf{w}_i$ was sent. For the maximum likelihood decoder, and conditioned on the channel states, it is given by

$$Pr(\mathbf{w}_i \rightarrow \mathbf{w}_j|\mathbf{H}) = Q\left(\sqrt{\frac{d_E^2(i,j|\mathbf{H})}{2N_0}}\right), \tag{2.85}$$

where $\mathbf{H}$ is a vector containing the elements $\{H(j), j \in \mathcal{K}\}$. The average PEP is found taking the expectation on the channel coefficients,

$$Pr(\mathbf{w}_i \rightarrow \mathbf{w}_j) = E_{\mathbf{H}}\left[Pr(\mathbf{w}_i \rightarrow \mathbf{w}_j|\mathbf{H})\right]. \tag{2.86}$$

2.5.1 Power Gain and Diversity Gain

In general, Equation (2.86) is difficult to solve analytically. Nevertheless, for some simplified cases it is possible to obtain upper bounds on the PEP which provide insight on how to design codes for fading channels, and lead to the definitions of power gain and diversity gain. Independent Rayleigh fading channel and MCBFC are considered.

Independent fading channel: The Euclidean distance can be expressed as

$$d_E^2(i,j|\mathbf{H}) = E_s R_c X. \tag{2.87}$$

where $X = \sum_{l\in\mathcal{K}} |(x_i(l) - x_j(l))H(l)|^2$ is a random variable with moment generating function [49]

$$\Phi_X(s) = \prod_{l\in\mathcal{K}} \frac{1}{1 - s|x_i(l) - x_j(l)|^2}. \tag{2.88}$$

Using this result and the Chernoff bound on $Q(x)$,

$$Q(x) \leq \frac{1}{2} e^{-\frac{x^2}{2}}, \tag{2.89}$$

it is possible to upper-bound the average PEP in Equation (2.86) as

$$\begin{aligned} P(\mathbf{w}_i \to \mathbf{w}_j) &= E_{\mathbf{H}}\left[Q\left(\sqrt{\frac{d_E^2(i,j|\mathbf{H})}{2N_0}}\right)\right] \\ &\leq \frac{1}{2} E_{\mathbf{H}}\left[e^{-\frac{d_E^2(i,j|\mathbf{H})}{4N_0}}\right] \\ &= \frac{1}{2}\Phi_X(s)_{|s=-\frac{E_s R_c}{4N_0}} \\ &= \frac{1}{2}\prod_{l\in\mathcal{K}} \frac{1}{1 + \frac{E_s R_c}{4N_0}|x_i(l) - x_j(l)|^2} \\ &\approx \frac{1}{2}\frac{1}{\left(\frac{E_s R_c}{4N_0}\Gamma\right)^{d_H(i,j)}}, \end{aligned} \tag{2.90}$$

where Γ is defined as

$$\Gamma = \left(\prod_{l\in\mathcal{K}} |x_i(l) - x_j(l)|^2\right)^{1/d_H(i,j)}. \tag{2.91}$$

If binary symbols are used in each dimension (e.g. 2-psk, or 4-psk), X is a chi-square distribution with $n_d d_H(i,j)$ degrees of freedom, with n_d being the number of dimensions of each symbol. In such case, the moment generating function of X is given by

$$\Phi_X^b(s) = \left(\frac{1}{1 - 4s}\right)^{d_H(i,j)}, \tag{2.92}$$

and the PEP can be bounded as

$$\begin{aligned} P(\mathbf{w}_i \to \mathbf{w}_j) &= \frac{1}{2}\Phi_X(s)_{|s=-\frac{E_s R_c}{4N_0}} \\ &= \frac{1}{2}\left(\frac{1}{1+\frac{E_s R_c}{N_0}}\right)^{d_H(i,j)} \\ &\approx \frac{1}{2}\left(\frac{E_s R_c}{N_0}\right)^{-d_H(i,j)}. \end{aligned} \tag{2.93}$$

MCBFC: a similar expression for the PEP can be obtained by grouping symbols $x_i(l), x_j(l)$, $l \in \mathcal{K}$ that are transmitted in the same block. Doing so, the Euclidean distance is given by

$$\begin{aligned} d_E^2(i,j|\mathbf{H}) &= A^2 \sum_{l=1}^{L_c} |H(l)\left(x_i(l) - x_j(l)\right)|^2 \\ &= E_s R_c \sum_{b\in\mathcal{B}} \left(\sum_{l\in\mathcal{K}_b} |x_i(l) - x_j(l)|^2\right) |H_b|^2, \end{aligned} \tag{2.94}$$

where $\mathcal{B}$ denotes the set of channel blocks in which a non-empty set $\mathcal{K}_b$ of symbols from $\mathbf{w}_i$ and $\mathbf{w}_j$ differ, and H_b are the channel coefficients for those blocks. As in Equation (2.87), define the Euclidean distance as

$$d_E^2(i,j|\mathbf{H}) = E_s R_c X_b, \tag{2.95}$$

where $X_b = \sum_{b\in\mathcal{B}} \left(\sum_{l\in\mathcal{K}_b} |x_i(l) - x_j(l)|^2\right) |H_b|^2$ is a random variable with moment generating function

$$\Phi_X(s) = \prod_{b\in\mathcal{B}} \frac{1}{1 - s\sum_{l\in\mathcal{K}_b} |x_i(l) - x_j(l)|^2}. \tag{2.96}$$

Following the development for independent fading channels, it is easy to obtain an upper bound for the PEP,

$$\begin{aligned} P(\mathbf{w}_i \to \mathbf{w}_j) &= E_{\mathbf{H}}\left[Q\left(\sqrt{\frac{d_E^2(i,j|\mathbf{H})}{2N_0}}\right)\right] \\ &\leq \frac{1}{2}E_{\mathbf{H}}\left[e^{-\frac{d_E^2(i,j|\mathbf{H})}{4N_0}}\right] \\ &= \frac{1}{2}\Phi_X(s)_{|s=-\frac{E_sR_c}{4N_0}} \\ &= \frac{1}{2}\prod_{l\in\mathcal{K}}\frac{1}{1+\frac{E_sR_c}{4N_0}|x_i(l)-x_j(l)|^2} \\ &\approx \frac{1}{2}\frac{1}{\left(\frac{E_sR_c}{4N_0}\Gamma\right)^{\mathcal{B}}}, \end{aligned} \tag{2.97}$$

where Γ is re-defined as

$$\Gamma = \left(\prod_{b\in\mathcal{B}}\left(\sum_{l\in\mathcal{K}_b}|x_i(l)-x_j(l)|^2\right)\right)^{1/|\mathcal{B}|}. \tag{2.98}$$

Comparing Equation (2.97) to the uncoded symbol error rate expression leads to the concept of code power gain and diversity gain. For a Gaussian channel, where $H(i)=1$, define power gain as the increase in the minimum Euclidean distance with respect to uncoded modulation,

$$\Psi = \frac{\min d_E^2(i,j)}{\min(x_i - x_j)}, \tag{2.99}$$

where the minimum is taken over the entire codebook in the numerator and over all the constellation symbols in the denominator. For binary modulation,

$$\Psi = \frac{\min d_E^2(i,j)}{2E_s} = \frac{d_{free}2E_sR_c}{2E_s} = d_{free}R_c, \tag{2.100}$$

where d_{free} denotes the code minimum free distance. Notice that the code power gain depends solely on the Euclidean code distance spectrum.

To define the code diversity gain, consider a channel with Rayleigh fading and diversity (thus with $FT > 1$, and $|\mathcal{B}| > 1$ in general). The code diversity gain is

defined in analogy to systems with diversity (time, frequency or antenna), where the error rate is proportional to $(E_b/N_0)^{-L}$, with L representing the diversity order. Therefore, the code diversity gain is defined by the pair of codewords yielding the largest exponent in Equation (2.97), given by

$$\Upsilon = \min_{i,j} |\mathcal{B}|. \tag{2.101}$$

For independent fading, $\Upsilon = d_{free}$, since Hamming distance determines diversity. The definition of diversity gain as the slope of the BER curve can be used to extend this concept to channels with correlated fading (without using the MCBFC approximation), or channels with other fading distributions, where the diversity gain depends on the following:

- Code Hamming distance spectrum.
- Received SNR distribution.
- Correlation between channel coefficients H_i.
- Channel diversity, determined by the number of resolvable paths.
- Interleaving depth.

2.5.2 Bit Error Rate Bounds

The Euclidean distance and PEP, given by Equations (2.84) and (2.85) respectively, can be used to derive the *nearest neighbor* lower bound on the BER, given, for BPSK or QPSK modulation, by

$$P_e > \min_{j \neq i} E_{\mathbf{H}} \left[P(\mathbf{w}_i \rightarrow \mathbf{w}_j | \mathbf{H}) \right]. \tag{2.102}$$

The union bound, found by adding the PEP for all possible codewords, has been used as an upper bound for the BER; for a geometrically uniform code[6] it is given by

$$P_e < E_{\mathbf{H}}\left[\sum_{j\neq 0}\omega_j P(\mathbf{w}_0 \rightarrow \mathbf{w}_j|\mathbf{H})\right], \tag{2.103}$$

where $\mathbf{w}_0$ is the all-zeros codeword, and ω_j is the error event weight. Adding for all possible codewords is usually impractical, but due to the equal likelihood of all errors at the same Hamming distance the calculation can be simplified for channels with no diversity and for independent Rayleigh channels. Denote the code distance spectrum by the 3-tuple $(B_{\omega,d}, \omega, d)$, where $B_{\omega,d}$ denotes the multiplicity (number) of error events with error weight ω at Hamming distance d. The union bound simplifies to

$$P_e < E_{\mathbf{H}}\left[\sum_{d=d_{free}}^{\infty}\sum_{\omega=1}^{\infty}\omega B_{\omega,d} P_d(\mathbf{w}_i \rightarrow \mathbf{w}_j|\mathbf{H})\right], \tag{2.104}$$

where $P_d(\mathbf{w}_i \rightarrow \mathbf{w}_j|\mathbf{H})$ is the probability of deciding for a codeword at distance d. Finally, since normally error events of smaller distances dominate the error probability, the union bound can be truncated at a certain distance above the code free distance, $d_T > d_{free}$,

$$P_e < E_{\mathbf{H}}\left[\sum_{d=d_{free}}^{d_T}\sum_{\omega=1}^{\infty}\omega B_{\omega,d} P_d(\mathbf{w}_i \rightarrow \mathbf{w}_j|\mathbf{H})\right]. \tag{2.105}$$

BER bounds for OFDMA and MC-CDMA on MCBFC are obtained in Chapter 4.

2.6 Chapter Summary

In this introductory chapter orthogonal frequency division multiplexing was described, and basic models for multiuser multicarrier systems under study in this dissertation were established. A comprehensive description of the wireless channel was given,

[6]All codes of interest in this dissertation are geometrically uniform, meaning that the distance spectrum from any codeword is identical.

emphasizing its modeling for multicarrier systems. Finally, channel capacity and coding results for fading channels, of relevance for this dissertation, were reviewed.

CHAPTER 3

OUTAGE CAPACITIES OF A MULTICARRIER DOWNLINK SYSTEM

Different alternatives for multiuser communications using multicarrier modulation, namely OFDMA and MC-CDMA, were presented in the previous chapter. The objective of this chapter is to evaluate their capacity and performance, taking into consideration system complexity, for the downlink. From an information theory perspective, the downlink fits the model of a broadcast channel, where a single transmitter sends information to multiple receivers. By including OFDM modulation and detection strategy in the analysis, the results in this chapter are on system capacity, which is always limited by the capacity of the channel.

Existing results on ergodic and outage capacities for fading BC by Li and Goldsmith in [42, 43] do not address multicarrier implementations for the classic approaches of TDM, FDM, and CDM. Results on system capacity are important in the design of medium access control algorithms, for the evolution of standards using OFDM (such as IEEE 802.11a [7], and ETSI Hiperlan [8]), and also for the design of future systems using OFDM.

The paradigm of low-mobility data users is addressed by considering outage capacity, rather than ergodic capacity. Results on outage capacity are significant for systems in which transmission takes place on a single channel state. The next section addresses the channel model for such system, based on an idealized OFDM system (without channel estimation or synchronization errors at the receiver). In addition, throughout the chapter lack of channel state information at the transmitter (CSIT) is assumed, in agreement with the current standards implementations mentioned earlier.

The definitions of ergodic, delay-limited, and outage capacity can be extended to this scenario noting that power allocation does not assume knowledge of the channel.

3.1 Information-theoretic Considerations of Multicarrier Broadcast Channels

To model a multicarrier system note that:

- Multicarrier systems of interest operate in frequency-selective fading channels; nevertheless, fading in each sub-carrier is flat.
- Under the assumptions of perfect time and frequency synchronization, different sub-carriers are orthogonal. Therefore, symbols or codewords sent over these sub-carriers do not interfere with each other, and can be seen as if being sent through parallel channels.

Such interpretation of multicarrier requires the use of the frequency-domain, transfer function channel model, described in Section 2.3.5. For user k it is represented by vector $\mathbf{h}_k = [h_{1,k}, h_{2,k}, \cdots, h_{N_s,k}]$, where $h_{i,k}$ is a complex Gaussian random variable denoting the channel coefficient of sub-carrier i,. Clearly, sub-carrier channels are correlated as determined by the channel delay spread, with the correlation coefficient approximated by Equation (2.66). In addition, AWGN power is assumed to be equal on all receivers. A block diagram of the OFDM downlink with the parallel channel interpretation is shown in Figure 3.1.

It was already mentioned that time, frequency, and code division multiplexing or multiple access can be implemented using OFDM. TDM and FDM are orthogonal resource allocation techniques, where a single user is transmitting at a given time or frequency. As such, they can be implemented using OFDMA: in TDM all sub-carriers are assigned to each user for a fraction of time, whereas in FDM a fixed number of

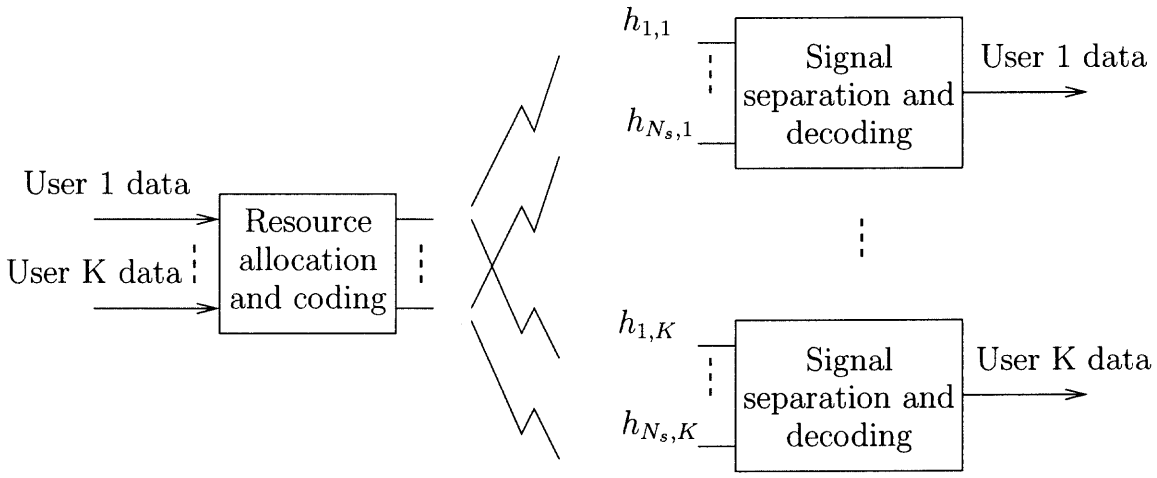

Figure 3.1 Multicarrier WLAN downlink system model.

sub-carriers is allocated to each user all the time[1]. In TDM the channel is shared by allocating different OFDM symbols to different users, while in FDM a portion of each OFDM symbol is given to each user, which limits the number of FDM users to N_s. Furthermore, OFDMA is flexible enough to implement hybrid TDM-FDM systems, depending on the choice of the mapping matrices $\mathbf{D}_k$, described in section 2.2.

Code division can be implemented using spread spectrum MC-CDMA, described in Section 2.2.2, by allocating different spreading codes to different users. The distinctive feature of MC-CDMA is that the entire band of the OFDM signal is assigned to all users all the time, which are then separated by multiuser detection, taking advantage of their spreading codes. The capacity of CDM with MC-CDMA is therefore dependent on the receiver, as shown in Section 3.2.4. In MC-CDMA the number of users is limited to the number of codes used. Furthermore, different transmission rates are possible using multi-code MC-CDMA.

Finding the outage capacity regions implies finding the best power allocation for a given TDM, FDM, or CDM scheme. To that end a power allocation matrix

[1]Note that this is not FDM in its strict sense because the sub-carrier spectra overlap. Nevertheless, OFDM preserves the orthogonality property of frequency division.

$\mathbf{P} = [\mathbf{p}_1, \mathbf{p}_2, \cdots, \mathbf{p}_K]$ is defined, where $\mathbf{p_k} = [P_{1,k}, P_{2,k}, \cdots, P_{N_s,k}]^T$ contain the power allocated to user k for each sub-carrier. This definition is general enough to consider TDM, FDM, and CDM: for TDM, all but one $\mathbf{p}_k$ are all-zero vectors at any given time; for FDM, $\mathbf{p}_k$ are orthogonal for different k, that is, the inner product $\langle \mathbf{p}_i, \mathbf{p}_j \rangle = 0, j \neq i$; for CDM there are no such restrictions on $\mathbf{P}$. A short term average power constraint for the power allocation matrix is defined with $\sum_{i=1}^{N_s} \sum_{k=1}^{K} P_{i,k} \leq \overline{P}$, which has the advantage of limiting transmit power peaks, which might cause interference and possibly exceed the maximum transmit power allowed to operate in an unlicensed band such as the 5GHz band. Furthermore, it is shown that a short term power constraint is not more restrictive than a long-term average power constraint when considering the no-CSIT case.

3.2 Outage Capacities Without CSIT

The parallel channel interpretation of the transmitted OFDM signal is instrumental in deriving the outage capacity regions. The instantaneous channel capacity of a wireless channel is dependent on channel fading, and thus varies randomly. An outage is declared when the data rate exceeds instantaneous capacity, with the outage capacity for a given outage probability p_0 defined in Equation (2.77). Multiuser outage capacity regions under different spectrum sharing techniques are derived in the following sections by maximizing multiuser mutual information over all possible power allocations satisfying a short term average power constraint.

3.2.1 Time Division Multiplexing

In time division multiplexing all sub-carriers are assigned to a single user at a given time. Define a time allocation vector $\boldsymbol{\tau} = [\tau_1, \tau_2, \cdots, \tau_K]$, such that $\sum_{k=1}^{K} \tau_k = 1$, where τ_k represents the fraction of time when user k is transmitting. The maximum instantaneous mutual information between the transmitted signal and the signal

received by user k is given by

$$C_k^{TDM}(\mathbf{h}_k, \mathbf{P}^{TDM}) = \tau_k \sum_{i=1}^{N_s} \frac{1}{2} \log_2 \left(1 + \frac{P_{i,k}^{TDM} |h_{i,k}|^2}{\sigma_k^2} \right) (b/dim), \tag{3.1}$$

where σ_k^2 is user k receiver Gaussian noise variance, and capacity, expressed in bits per channel use per symbol dimension, is achieved using Gaussian signaling [14]. Additionally, the power allocation matrix for TDM during period τ_k when user k is transmitting satisfies $\mathbf{P}^{TDM} = [\mathbf{0}, \cdots, \mathbf{p}_k^{TDM}, \cdots, \mathbf{0}]$.

The outage probability for user k and a rate R_k using TDM is defined as

$$Pr_{o,k}^{TDM}(R_k, \mathbf{P}^{TDM}) = Pr(C_k^{TDM}(\mathbf{h}_k, \mathbf{P}^{TDM}) < R_k). \tag{3.2}$$

In Equations (3.1) and (3.2) the dependence of instantaneous capacity and outage probability on the power allocation matrix $\mathbf{P}^{TDM}$ is indicated. Denote by $p_{C_k^{TDM}}(x)$ the pdf of C_k^{TDM}. Then, the outage probability is given by

$$Pr_{o,k}^{TDM}(R_k, \mathbf{P}^{TDM}) = \int_0^{R_k} p_{C_k^{TDM}}(x)\, dx. \tag{3.3}$$

The outage capacity for user k with outage probability p_o is the rate $R_{po,k}^{TDM}$ satisfying

$$Pr_{o,k}^{TDM}(R_{po,k}^{TDM}, \mathbf{P}^{TDM}) = Pr(C_k^{TDM}(\mathbf{h}_k, \mathbf{P}^{TDM}) < R_{po,k}^{TDM}) = p_o. \tag{3.4}$$

and can be solved numerically using Equation (3.3). In order to find the capacity region, define a rate reward vector $\boldsymbol{\mu} = [\mu_1, \mu_2, \cdots, \mu_K]^T$ such that $\sum_{i=1}^K \mu_i = 1$, and an outage capacity vector $\mathbf{R}_{p_o}^{TDM} = [R_{po,1}^{TDM}, R_{po,2}^{TDM}, \cdots, R_{po,K}^{TDM}]^T$, and then maximize

$$\boldsymbol{\mu}^T \mathbf{R}_{po}^{TDM}, \tag{3.5}$$

subject to

$$\sum_{k=1}^{K}\sum_{i=1}^{N_s} P_{i,k}^{TDM} \leq \overline{P} \tag{3.6}$$

$$\sum_{k=1}^{K} \tau_k = 1. \tag{3.7}$$

Clearly, maximizing $\boldsymbol{\mu}^T \mathbf{R}_{p_o}^{TDM}$ is tantamount to minimizing $\boldsymbol{\mu}^T \mathbf{Pr}_o^{TDM}$, where $\mathbf{Pr}_o^{TDM} = [Pr_{o,1}^{TDM}, Pr_{o,2}^{TDM}, \cdots, Pr_{o,K}^{TDM}]^T$ is the outage probability vector [43]. Under a short term power constraint, the maximization of the mutual information for one channel state is independent of other channel states, since the same power $\overline{P}$ is applied for all states. Therefore, maximization of the instantaneous mutual information $\mathbf{C}^{TDM}(\mathbf{h}_{1-K}) = [C_1^{TDM}(\mathbf{h}_1), C_2^{TDM}(\mathbf{h}_2), \cdots, C_K^{TDM}(\mathbf{h}_K)]^T$ for every channel state ensures that the outage probability $\boldsymbol{\mu}^T \mathbf{Pr}_o^{TDM}$ is minimized.

To derive the optimal power allocation, a random power allocation strategy is first assumed. Since the transmitter has no information about the channel, then channel state and power allocation policy are statistically independent, and the instantaneous mutual information for any channel state is

$$\mathbf{C}^{TDM}(\mathbf{h}_{1-K}) = E_{\mathbf{P}^{TDM}}\left[\mathbf{C}^{TDM}(\mathbf{h}_{1-K}, \mathbf{P}^{TDM})\right], \tag{3.8}$$

and

$$\boldsymbol{\mu}^T \mathbf{C}^{TDM}(\mathbf{h}_{1-K}) = E_{\mathbf{P}^{TDM}}\left[\boldsymbol{\mu}^T \mathbf{C}^{TDM}(\mathbf{h}_{1-K}, \mathbf{P}^{TDM})\right]. \tag{3.9}$$

Given the convexity of the *log* function, by Jensen's inequality ([14], p.25) it is obtained that

$$E_{\mathbf{P}^{TDM}}\left[\boldsymbol{\mu}^T \mathbf{C}^{TDM}(\mathbf{h}_{1-K}, \mathbf{P}^{TDM})\right] \leq \boldsymbol{\mu}^T \mathbf{C}^{TDM}(\mathbf{h}_{1-K}, E_{\mathbf{P}^{TDM}}[\mathbf{P}^{TDM}]), \tag{3.10}$$

and therefore a fixed power allocation policy (independent from the channel state) for each user, in time and frequency (along sub-carriers), maximizes the outage capacity

region. As a result, the region boundary can be reached varying the time allocation vector.

3.2.2 Frequency Division Multiplexing

In frequency division disjoint sets of sub-carriers are allocated to different users so that each sub-carrier is allocated to only one user for the entire frame. Define K disjoint sub-carrier sets $\mathcal{C}_1, \mathcal{C}_2, \cdots, \mathcal{C}_K$ such that $\bigcup_{k=1}^{K} \mathcal{C}_k$ contains all N_s sub-carriers. The maximum instantaneous mutual information for user k is, for FDM,

$$C_k^{FDM}(\mathbf{h}_k) = \sum_{i \in \mathcal{C}_k} \frac{1}{2} \log_2 \left(1 + \frac{P_{i,k}^{FDM} |h_{i,k}|^2}{\sigma_k^2} \right) (b/dim), \tag{3.11}$$

where the power allocation matrix columns satisfy $\langle \mathbf{p}_i, \mathbf{p}_j \rangle = 0, j \neq i$, and capacity is also achieved with Gaussian signaling. Outage probability and outage capacity are defined from Equation (3.11) as in Equations (3.2) and (3.4). To determine the outage capacity, a rate reward vector $\boldsymbol{\mu}$ is defined as in the TDM case and the maximization problem becomes

$$\boldsymbol{\mu}^T \mathbf{R}_{po}^{FDM}, \tag{3.12}$$

subject to

$$\sum_{i=1}^{N_s} \sum_{k=1}^{K} P_{i,k}^{FDM} \leq \overline{P}. \tag{3.13}$$

One can see that, without CSIT, a fixed power allocation maximizes capacity following the same arguments as in the TDM case; therefore all points in the region boundary can be obtained by varying sub-carrier allocation.

3.2.3 Code Division Multiplexing

In CDM, signals to all active users are transmitted simultaneously using all sub-carriers and separated at the receiver by successive decoding. The maximum instan-

taneous mutual information for user k is given by

$$C_k^{CDM}(\mathbf{h}_{1-K}) = \sum_{i=1}^{Ns} \frac{1}{2} \log_2 \left(1 + \frac{P_{i,k}|h_{i,k}|^2}{\sigma_k^2 + \sum_{j:|h_{i,k}|<|h_{i,j}|} P_{i,j}|h_{i,j}|^2} \right), \tag{3.14}$$

which is the instantaneous mutual information for a set of parallel BC, achieved with Gaussian signaling [48]. The channel capacity is obtained defining outage probability and outage capacity (as in Equations (3.2) and (3.4)) from Equation (3.14), and can be achieved by successive decoding [42]. Although its optimality is not shown, a uniform power allocation policy is considered when calculating the capacity region to compare it with TDM and FDM.

3.2.4 CDM with MC-CDMA Spread Spectrum

Code division can be implemented using multicarrier spread spectrum as described in Section 2.2.2. With successive decoding different users' signals are detected in a certain order and then subtracted from the remaining signal; it was mentioned that successive decoding achieves capacity in fading BC, but such performance comes at the expense of considerable receiver complexity, and a practical implementation requires the use of powerful coding that reduces performance degradation caused by decoding errors [50]. Therefore, it is of interest to investigate what is the performance of MC-CDMA for different simplified detectors which do not require successive decoding. In this section outage capacities of MC-CDMA using decorrelating and MMSE MUDs with a set of orthogonal spreading codes are derived. In the following the notation represents multi-code MC-CDMA with a total of M signature sequences, used to achieve different rates.

Denote user k received MC-CDMA signal, after transmission through the channel, the matched filter bank, and despreading, by (cf Equation (2.33))

$$\begin{aligned} \mathbf{z}_k &= (\mathbf{H}_k\mathbf{S})^H(\mathbf{H}_k\mathbf{S}\mathbf{A}\mathbf{b} + \boldsymbol{\zeta}_k) \\ &= \mathbf{R}_k\mathbf{A}\mathbf{b} + \boldsymbol{\xi}_k, \end{aligned} \tag{3.15}$$

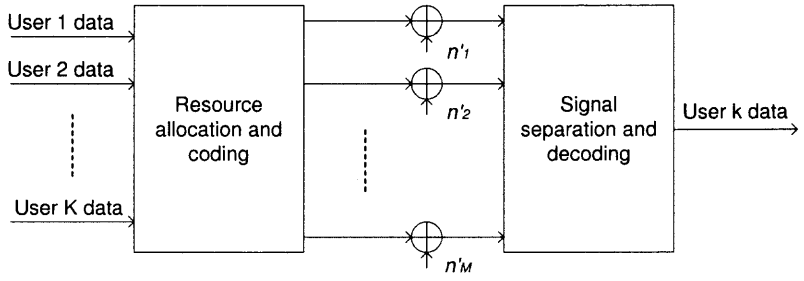

Figure 3.2 Equivalent MC-CDMA parallel channel set transceiver.

where $\mathbf{z} = [z_1, z_2, \cdots, z_M]^T$ is the received signal vector for receiver k, $\mathbf{H}_k = \text{diag}\{\mathbf{h}_k\}$ is a diagonal matrix whose diagonal elements are the channel coefficients, $\boldsymbol{\zeta}_k$ is a $M \times 1$ vector of AWGN with covariance matrix $\sigma_k^2 \mathbf{I}_M$, and $\boldsymbol{\xi}_k$ has covariance matrix $\sigma_k^2 \mathbf{R}_k$. The output of the decorrelating MUD is

$$\mathbf{z}_k^D = \mathbf{b} + \boldsymbol{\xi}_k^D,$$

where $\boldsymbol{\xi}_k^D$ has variance $\sigma_k^2 \mathbf{R}_k^{-1}$ (see Appendix A). By viewing spreading, despreading, and decorrelating matrices as part of the channel, the system can be modeled as M parallel channels, consisting of the signals that are spread using the M different signature sequences, as shown in Figure 3.2, with noise $\boldsymbol{\xi}_k^D$.

The M parallel channel model can be used to derive the instantaneous capacity of MC-CDMA. To that end, define a power allocation matrix $\mathbf{P}_{MC} = [\mathbf{p}_1, \mathbf{p}_2 \cdots, \mathbf{p}_K]$, where $\mathbf{p}_k$ are $M \times 1$ column vectors containing power allocated to each signature sequence for user k, subject to a short-term average power constraint $\sum_{i=1}^{M} \sum_{k=1}^{K} P_{i,k} \leq \overline{P}$. Since each user is allocated disjoint sets of codes, the columns of $\mathbf{P}_{MC}$ are orthogonal, and $\langle \mathbf{p}_i, \mathbf{p}_j \rangle = 0, j \neq i$[2]. For the decorrelating detector, the maximum

[2]For MC-CDMA, the orthogonality on $\mathbf{p}_k$ means that only one user allocates non-zero power to any given code, e.g. if a code belongs to $\mathcal{S}_k$, then only user k allocates power to that code.

instantaneous mutual information for user k is

$$\begin{aligned} C_k^D(\mathbf{H}_k) &= \sum_{i \in \mathcal{S}_k} \frac{1}{2} \log_2 \left(1 + \frac{P_{i,k}}{E[|\xi_{i,k}^D|]^2} \right) \\ &= \sum_{i \in \mathcal{S}_k} \frac{1}{2} \log_2 \left(1 + \frac{P_{i,k} \rho_{i,k}^{-1}}{\sigma_k^2} \right) (b/dim), \end{aligned} \tag{3.16}$$

where the summation is over the set of codes assigned to user k, given by $\mathcal{S}_k$. Additionally, $\rho_{k,i} = E[|\xi_{k,i}^D|]^2/\sigma_k^2$ is the *noise enhancement factor*, which depends on the channel state $\mathbf{H}_k$, and capacity is also achieved using Gaussian signaling.

The MMSE detector uses the transformation minimizing the mean square error on the received signal vector, and is given by $\mathbf{M}_k = (\mathbf{R}_k + \sigma_k^2 \mathbf{A}^{-2})^{-1}$, where $\mathbf{A}^2$ is a diagonal matrix with diagonal elements $[\mathbf{A}^2]_{i,i} = \sum_{k=1}^K P_{i,k}$. The MMSE output is

$$\mathbf{z}_k^M = \mathbf{M}_k \mathbf{R}_k \mathbf{A} \mathbf{b} + \boldsymbol{\xi}_k^M, \tag{3.17}$$

where $\boldsymbol{\xi}_k^M$ is Gaussian noise with variance $\sigma_k^2 [\mathbf{M}_k \mathbf{R}_k \mathbf{M}_k^H]_{k,k}$ (see Appendix A). Unlike the decorrelating detector, the MMSE detector does not result in an orthogonal set of sub-channels. The signal corresponding to spreading code j can be expressed as

$$[\mathbf{z}_k^M]_j = [\mathbf{M}_k \mathbf{R}_k]_{j,j} [\mathbf{A}\mathbf{b}]_j + \sum_{l \neq j} [\mathbf{M}_k \mathbf{R}_k]_{j,l} [\mathbf{A}\mathbf{b}]_l + [\boldsymbol{\xi}_k^M]_j. \tag{3.18}$$

Residual MAI, represented by the second term in Equation (3.18), is treated as noise by this detector. Assuming MAI to be Gaussian-distributed (in [19] it is verified that this approximation results in a small error) it is possible to combine noise and MAI terms in Equation (3.18), resulting in

$$[\mathbf{z}_k^M]_j = [\mathbf{M}_k \mathbf{R}_k]_{j,j} [\mathbf{A}\mathbf{b}]_j + I_j, \tag{3.19}$$

where noise plus interference term has variance $E[|I_j|^2] = [\mathbf{M}_k \mathbf{R}_k \mathbf{M}_k^H]_{j,j} \sigma_k^2 + \sum_{l \neq j} |[\mathbf{M}_k \mathbf{R}_k \mathbf{A}]_{j,l}|^2$. The parallel channel interpretation can now be used and the

maximum instantaneous mutual information for user k is similar to Equation (3.16):

$$C_k^M(\mathbf{H}_{1-K}) = \sum_{i \in \mathcal{S}_k} \frac{1}{2} \log_2 \left(1 + \frac{P_{i,k}}{E[|I_k|^2]}\right), \tag{3.20}$$

where I_k depends on the channel state $\mathbf{H}$. Note that Equations (3.16), (3.20), and (3.11) are mathematically equivalent, therefore the analysis of CDM with MC-CDMA can be carried out, with the equivalent channel model in figure 3.2, as the analysis of FDM, with spreading codes rather than sub-carriers being parallel channels. Therefore, defining outage probability and outage capacity from Equations (3.16) or (3.20) as in Equations (3.2) and (3.4), the outage capacity region can be found defining a rate reward vector $\boldsymbol{\mu}$ and maximizing

$$\boldsymbol{\mu}^T \mathbf{R}_{po}^{MC}, \tag{3.21}$$

subject to

$$\sum_{i=1}^{M} \sum_{k=1}^{K} P_{i,k}^{MC} \leq \overline{P}. \tag{3.22}$$

Uniform power allocation maximizes capacity (as in TDM and FDM); therefore points in the boundary of the capacity region can be achieved by varying spreading code allocation.

3.3 Numerical Results

Outage capacity regions were calculated numerically following the procedure described in previous sections. Table 3.1 summarizes the system parameters assumed for numerical analysis, which correspond to the IEEE802.11a standard. Out of 52 sub-carriers, 4 are used as pilot signals for channel estimation at the receiver side. It is assumed that the cyclic prefix completely eliminates inter-symbol interference and thus the system is interference-free in the TDM and FDM cases. r.m.s delay spread is set to 25 ns, a typical value for indoor environments, and the channel is Rayleigh

fading. For FDM, sub-carriers allocated to each user were interleaved in order to minimize fading correlation. For MC-CDMA, it is assumed that 48 orthogonal spreading sequences are distributed among active users.

Table 3.1 Simulation Parameters

Sub-carriers (N_s)	Data sub-carriers	Freq. spacing	Symbol rate
52	48	312.5 kHz	250 kbaud
Channel type	Delay spread	Outage prob.	Sequences (MC-CDMA)
Indoor propagation	25 ns	0.1, 0.01	Walsh-Hadamard, M=48

Figures 3.3 and 3.4 show the capacity region for TDM, FDM, and MC-CDMA as well as the channel capacity using CDM for a two active users having average SNR difference of 25 dB (SNR=30 dB for user 1 and SNR=5 dB for user 2). The capacity region for CDM was obtained assuming a fixed decoding order (the user with better average SNR is decoded first). Outage probabilities of 0.1 and 0.01 were considered for Figure 3.3 and Figure 3.4 respectively. It can be seen that channel capacity using CDM is significantly larger than the capacity of TDM and FDM. However, when CDM is implemented using MC-CDMA and a low-complexity receiver, capacity decreases to a point where TDM and FDM are preferable. A slight advantage of TDM over FDM can be noticed, and is due to the fact that in TDM each user employs all sub-carriers and therefore exploits the channel frequency diversity better than in FDM. Outage capacity regions for the same system when the user SNR difference is 5 dB (SNR=15 dB for user 1 and SNR=10 dB for user 2) are shown for outage probability 0.1 in Figure 3.5 and 0.01 in Figure 3.6. Notice that the theoretical advantage of CDM has greatly diminished and the capacity region is only slightly greater than that of TDM.

Figure 3.7 shows user 1 (solid lines) and user 2 (dashed lines) capacity for different power levels with outage probability 0.1 and a 20 dB difference in average

SNR between users (worse user SNR in parenthesis in plots). In these simulations resources (power, and time, bandwidth or number of codes) have been allocated in equal parts to both users, except for the CDM case where such allocation results in very poor performance for the user having lower SNR. Thus, more power has been allocated to the weak user in the CDM case. One can see that the capacities of MC-CDMA with decorrelating and MMSE detectors become close for increasing SNR. This fact should be expected since the MMSE transformation approaches the decorrelating transformation for large SNR values. Finally, Figure 3.8 shows user 1 (solid lines) and user 2 (dashed lines) outage probabilities for different power levels wherein the transmission rates are 50 Mbps for user 1 and 20 Mbps for user 2 (SNR in parenthesis). It is interesting to see that the slope of the curves corresponding to MC-CDMA is lower than the rest. Given the direct relationship between the slope of the outage probability curve and diversity, it is concluded that MC-CDMA with multi-code does not make good use of channel frequency diversity.

3.4 Chapter Summary

In this chapter the performance, in terms of outage capacity, of a multicarrier downlink system was evaluated. Different multiplexing techniques, namely time division, frequency division, and code division, were studied. For code division, a multicarrier CDMA implementation with orthogonal codes and suboptimal (linear) detection was also considered. Results showed the outage capacity regions for such system, as well as achievable rates and outage probabilities for different SNR. From the results it is concluded that, although code division exhibits theoretically the largest capacity region, a suboptimal implementation with multi-code MC-CDMA with decorrelating or MMSE MUDs has inferior performance than time or frequency division.

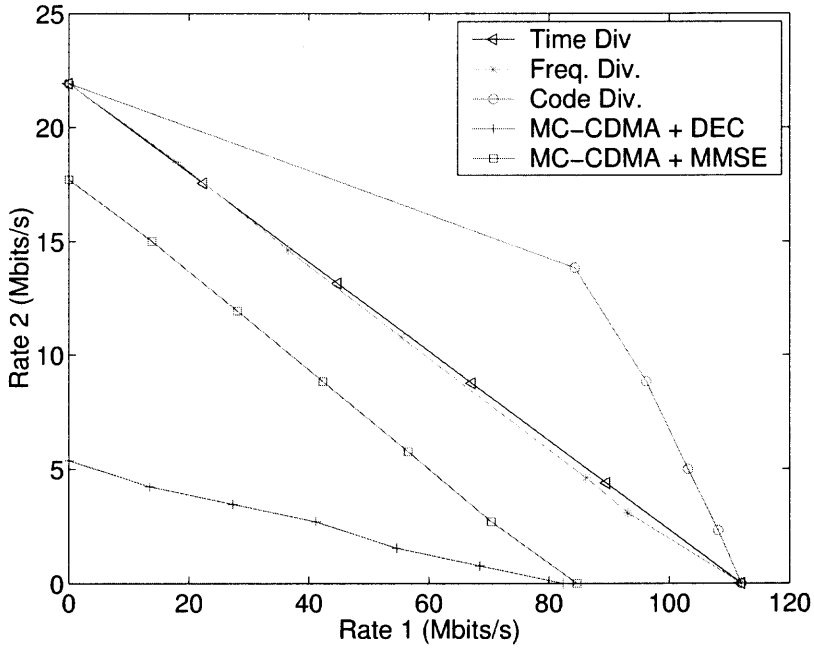

Figure 3.3 Capacity regions for different spectrum sharing techniques for SNR difference of 25 dB and outage probability 0.1.

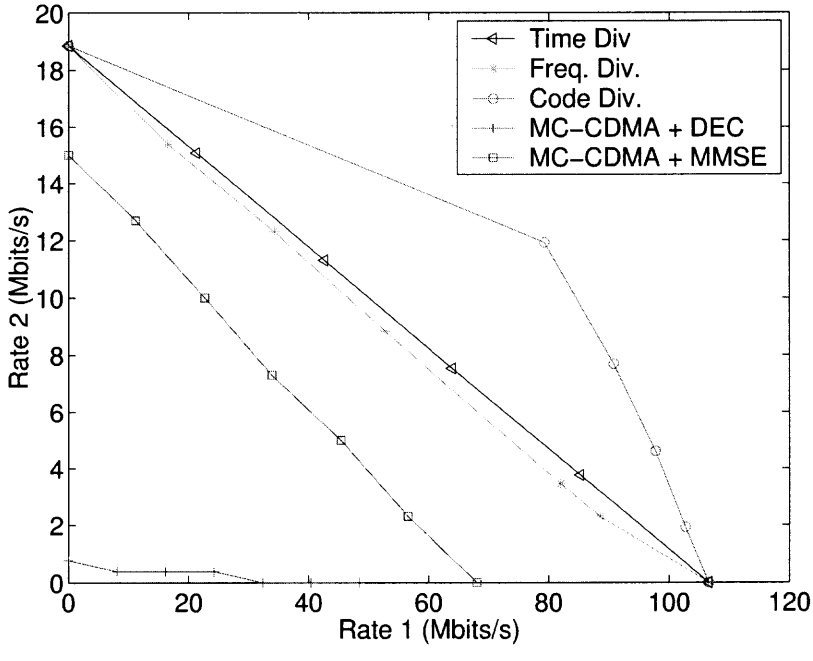

Figure 3.4 Capacity regions for different spectrum sharing techniques for SNR difference of 25 dB and outage probability 0.01.

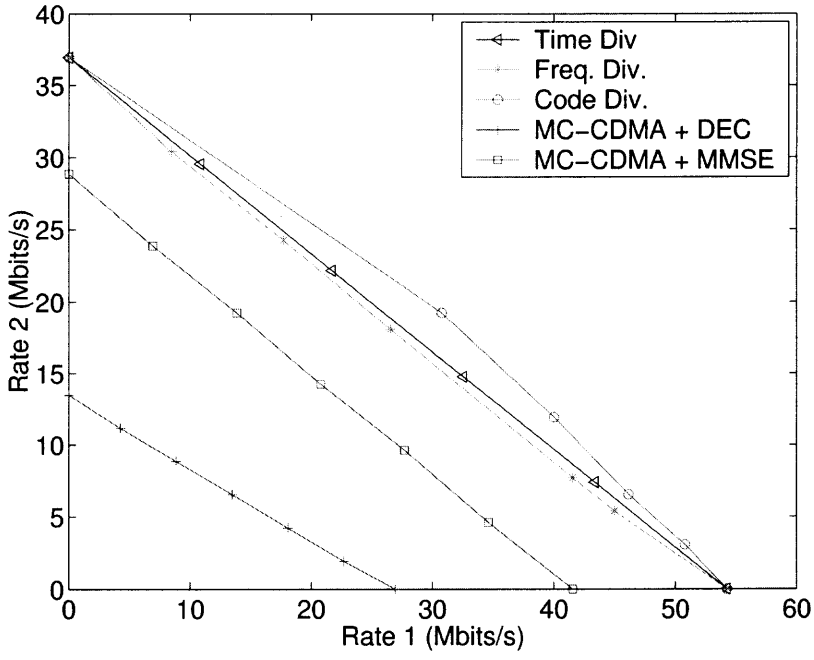

Figure 3.5 Capacity regions for different spectrum sharing techniques for SNR difference of 5 dB and outage probability 0.1.

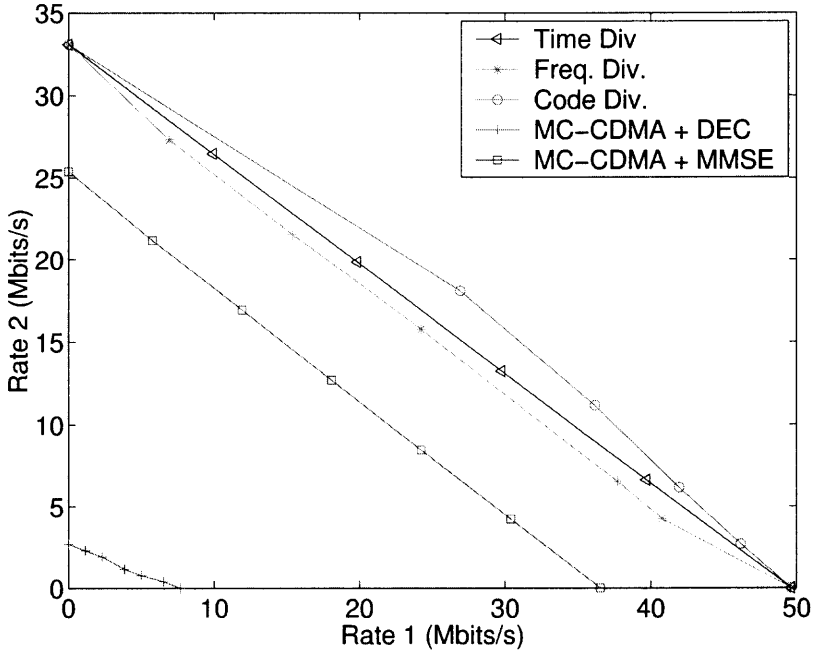

Figure 3.6 Capacity regions for different spectrum sharing techniques for SNR difference of 5 dB and outage probability 0.01.

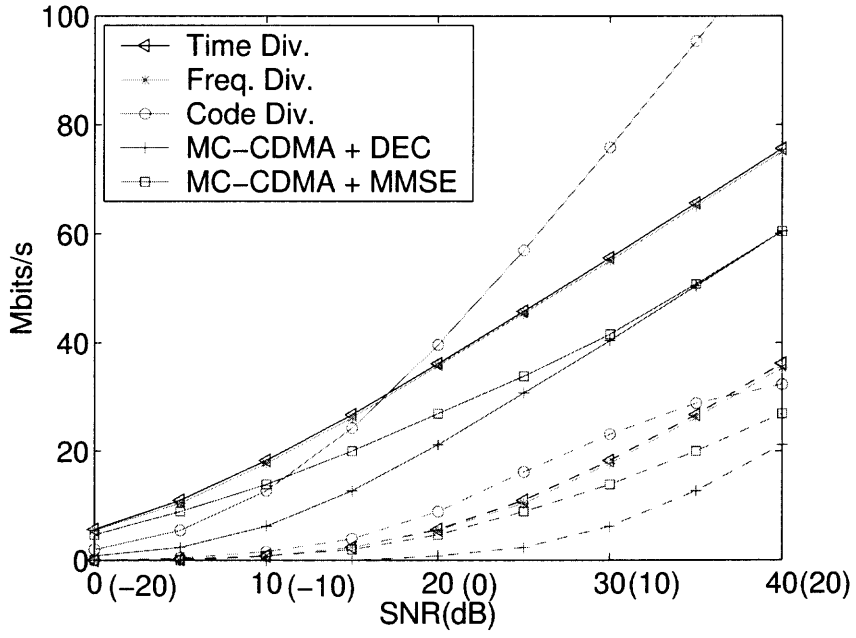

Figure 3.7 Rates for user 1 (solid lines) and user 2 (dashed lines) for different transmit power levels for SNR difference of 20 dB and outage probability 0.1

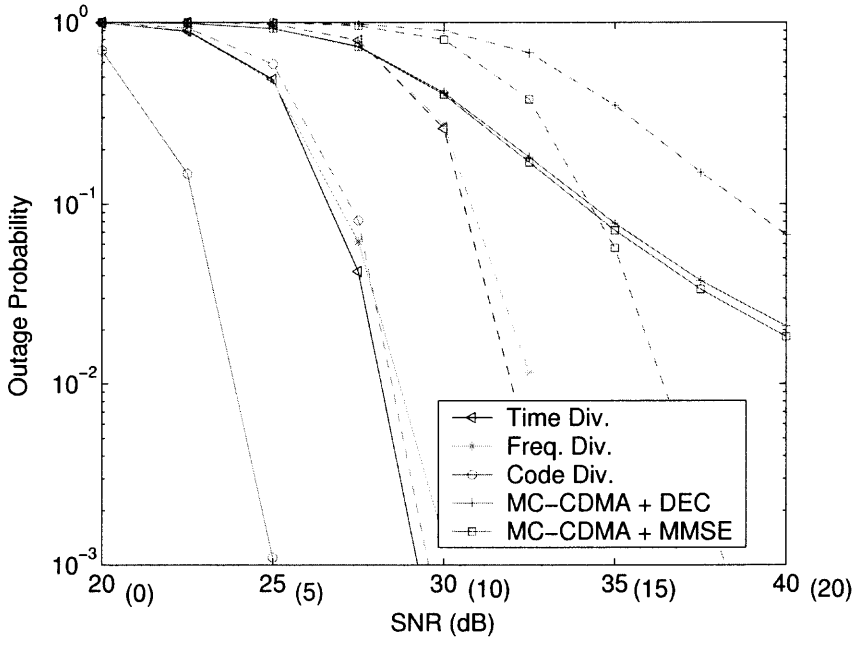

Figure 3.8 Outage probabilities for SNR difference of 20 dB for user 1 (solid lines) with rate 50 Mb/s and user 2 (dashed lines) with rate 20 Mb/s.

CHAPTER 4

CODED PERFORMANCE OF MC-CDMA AND OFDMA

The performance of MC-CDMA and OFDMA in terms of outage capacities analyzed in the previous chapter provides information on the maximum achievable capacity of a system given an outage probability. Since outage capacity only provides an upper bound on the performance of a real system, for practical purposes it is useful to evaluate systems in terms of their BER, which depends on the type of code, modulation, and multiple access technique being used.

BER performance of OFDMA and MC-CDMA without channel encoding is well known (see [51] for the latter). MC-CDMA exploits channel frequency diversity by transmitting each user's symbols over all sub-carriers, while OFDMA cannot do so because each symbol is transmitted over a single sub-carrier, and thus it performs poorly on frequency-selective channels. On the other hand, it was shown in Chapter 3 that OFDMA (used for time or frequency division multiplexing) can outperform MC-CDMA in terms of outage capacity. If outage capacity results are interpreted as an indication to the performance of coded systems [40], this result suggests that OFDMA can have a larger coding gain than MC-CDMA; hence the need to evaluate the performance of coded systems.

In this chapter, the coding gain-complexity trade-off of OFDMA and MC-CDMA is described qualitatively as a starting point to analyze the performance of coded systems through the analysis of equivalent multi-frequency codes [52] as well as simulation. Furthermore, it is shown that rate-adaptive encoding greatly improves the performance of OFDMA.

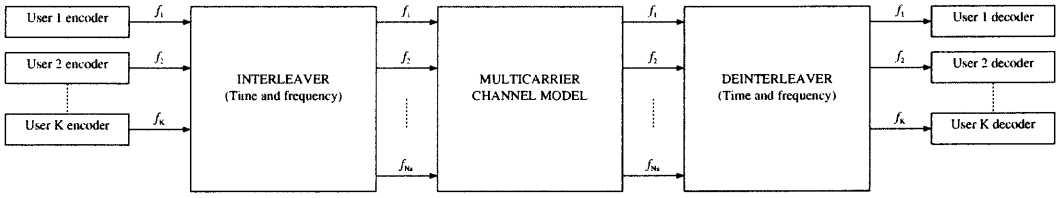

Figure 4.1 OFDMA block diagram.

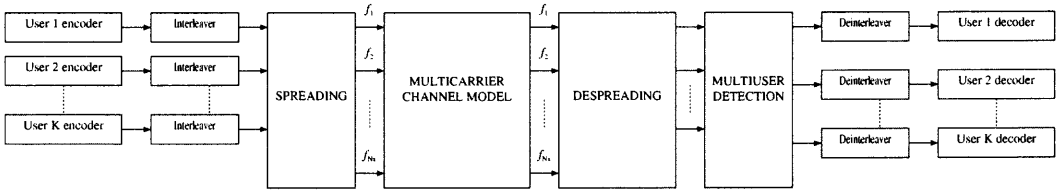

Figure 4.2 MC-CDMA block diagram.

4.1 Coding Gain-Complexity Trade-off for OFDMA and MC-CDMA

In this chapter, refer to the block diagrams in Figures 4.1 and 4.2 for coded OFDMA and MC-CDMA respectively. The channel is represented in the frequency domain. Interleaving is on time and frequency for OFDMA and on time only for MC-CDMA[1].

In Section 2.5 the coding gain was divided into power gain and diversity gain. It was argued that the power gain depends solely on the code distance spectrum, while diversity gain depends on other factors, such as SNR distribution and channel diversity. Using the multicarrier block fading channel approximation of Section 2.3 it was possible to distinguish between channel time and frequency diversity, which OFDMA and MC-CDMA exploit as follows:

- Assuming that the coherence time is larger than the symbol period and smaller than the interleaving depth, channel coding and interleaving provide code diversity for both OFDMA and MC-CDMA.

[1]Frequency interleaving for OFDMA is also known as orthogonal frequency hopping.

- Assuming that the coherence bandwidth is larger than the sub-carrier bandwidth and smaller than the multiuser signal bandwidth (OFDM signal bandwidth), MC-CDMA inherently exploits frequency diversity through frequency spreading, while channel coding and frequency interleaving provides code diversity for OFDMA.

Therefore, it is expected that the code diversity gain be larger for OFDMA than for MC-CDMA, since part of the diversity gain in MC-CDMA is inherent in spreading.

It was also shown in Section 2.5 that code diversity depends on the code minimum Hamming distance, which increases with code complexity. Therefore a trade-off exists between code diversity gain and complexity. Since uncoded OFDMA has no diversity, it is expected that increasing the code complexity results in more remarkable gains for OFDMA than for MC-CDMA. Two extreme cases of uncoded BER and outage probabilities (interpreted as an approximation to the BER with the best possible code) are shown for OFDMA and MC-CDMA (using only one code per user) in Figures 4.3 and 4.4 respectively, obtained with the parameters in table 4.1. Notice from Figure 4.3 that the BER is similar or higher for OFDMA than for MC-CDMA when the system is at full load (32 users for 32 sub-carriers). In addition, the BER does not improve for OFDMA at half load (only 16 users active for 32 sub-carriers), while there is considerable improvement for MC-CDMA at half load. On the other hand, Figure 4.4 shows that outage probability at full load is lower for OFDMA with frequency interleaving than for MC-CDMA. Results for half load for OFDMA were obtained using all available bandwidth (e.g. all sub-carriers were assigned to the active users, resulting in two sub-carriers per user). Figure 4.4 shows this improvement, as well as the improvement obtained with frequency interleaving.

Table 4.1 Comparison Parameters

Sub-carriers	Users	Spreading seqs.	Spectral efficiency
32	16,32	32 Walsh-Hadamard	1 bit/sym/dim
Modulation	Channel model	r.m.s delay spread	sub-carrier spacing
QPSK	Exponential delay spread	25 ns	312.5 kHz

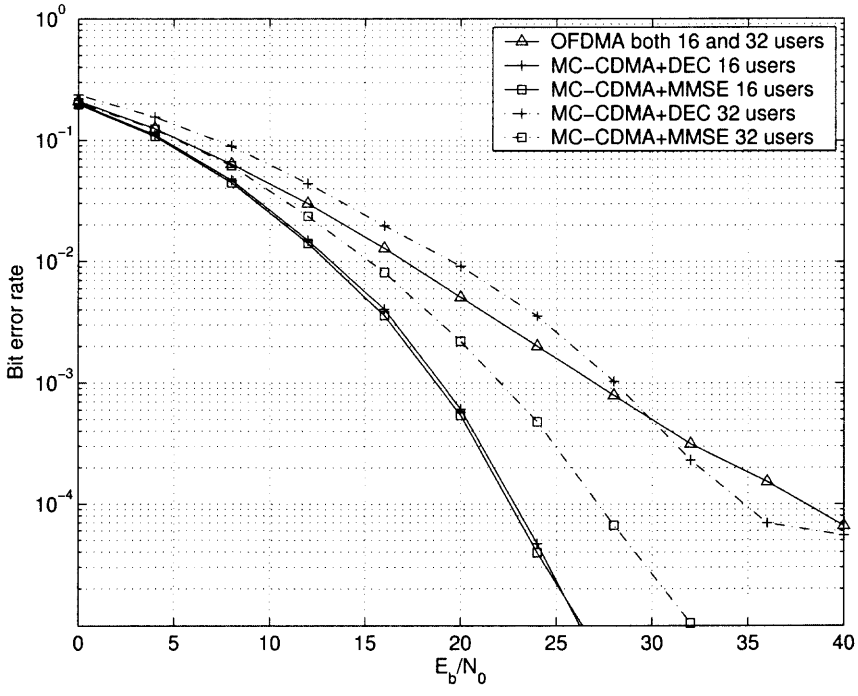

Figure 4.3 Bit error rate for uncoded OFDMA and MC-CDMA.

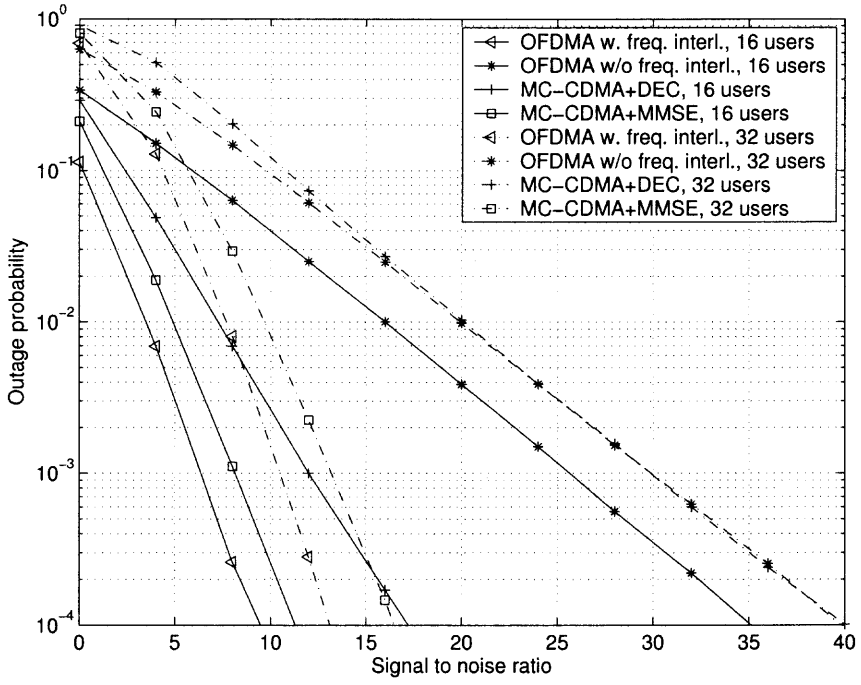

Figure 4.4 Outage probabilities for OFDMA and MC-CDMA.

4.2 Bit Error Rate of Coded OFDMA

For the purpose of coded performance analysis, denote the demultiplexed symbols for user k by

$$y_k(i) = H_k(i)Ax_k(i) + \xi_k(i), \tag{4.1}$$

where $H_k(i)$ represents the channel coefficient at the time and frequency of transmission of $x_k(i)$, which depends on the interleaving pattern, i is the symbol index, and $\xi_k(i)$ is white Gaussian noise with variance $N_0/2$. The MCBFC channel model is used to simplify the analysis and calculation of the nearest neighbor bound and the transfer function bound, described in Section 2.5. In addition, for simplicity the analysis focuses on binary codes using BPSK modulation.

Periodic interleaving reduces correlation among consecutive symbols in a MCBFC by transmitting them on different channel blocks. As a result, for a channel with FT blocks, FT consecutive channel coefficients are independent, although chan-

$x(1) \quad \cdots$ $x(FT+1)$ $\vdots$	$x(F+1) \quad \cdots$ $x(F(T+1)+1)$ $\vdots$	$\cdots$ $\vdots$	$x(F(T-1)+1) \cdots$ $x(F(2T-1)+1)$ $\vdots$
$x(2) \quad \cdots$ $x(FT+2)$ $\vdots$	$x(F+2) \quad \cdots$ $x(F(T+1)+2)$ $\vdots$	$\cdots$ $\vdots$	$x(F(T-1)+2) \cdots$ $x(F(2T-1)+2)$ $\vdots$
$\vdots$	$\vdots$	$\ddots$	$\vdots$
$x(F) \quad \cdots$ $x(F(T+1))$ $\vdots$	$x(2F) \quad \cdots$ $x(F(T+2))$ $\vdots$	$\cdots$ $\vdots$	$x(FT) \quad \cdots$ $x(2FT)$ $\vdots$

Figure 4.5 Arrangement of transmitted symbols in OFDM with periodic interleaving.

nel coefficients exactly FT symbols apart are fully correlated (for BPSK, this means that data transmitted FT bits apart undergo the same channel). An example of periodic interleaving is shown in Figure 4.5. The arrangement of symbols represents transmission with OFDM. Each row represents a sub-carrier, and consecutive symbols are placed in different blocks in time and frequency. After the number of blocks FT has been reached, next symbol is placed in the first block. This procedure is repeated until all blocks are filled. This hints that not only the error weight but also the position of the erroneous bits shall be taken into account when calculating the pairwise error probability. The analysis can be done in the same way as the analysis of coded performance over block fading channels [40, 53] noting that the number of blocks is FT.

The nearest neighbor lower bound for the BER in Equation (2.102) can be easily calculated by simple inspection of the positions of symbol errors. Figure 4.6 shows this procedure applied to the minimum distance error event of a convolutional code with generator polynomials (7,5), for channels with diversity $FT = 2$ and $FT = 4$ (branches are labeled with the pairs of transmitted bits). $\alpha, \beta, \gamma, \delta$ represent the channel coefficients for different blocks. The expressions for minimum Euclidean

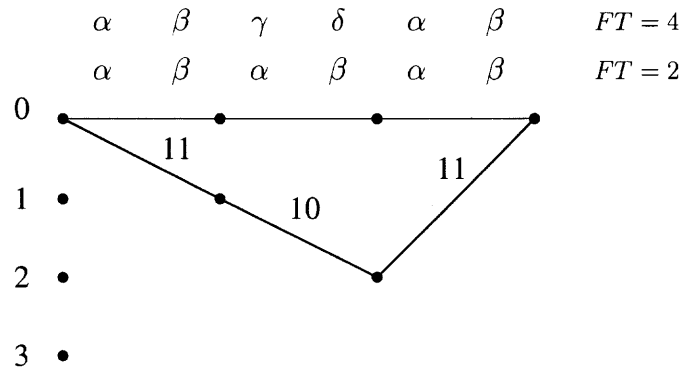

Figure 4.6 Minimum distance error event for a code with generators (7,5) on a MCBFC with $FT = 2$ and $FT = 4$.

distance are given by

$$d^2_{E,min} = 4E_sR_c(3\alpha^2 + 2\beta^2), \tag{4.2}$$

$$d^2_{E,min} = 4E_sR_c(2\alpha^2 + 2\beta^2 + \gamma^2), \tag{4.3}$$

respectively. Note from Equation (4.3) that the code diversity is 2 for $FT = 2$ and 3 for $FT = 4$. In this example, the expressions for the nearest neighbor lower bound on BER are

$$P_e > E_{\alpha,\beta}\left[Q\left(\sqrt{\frac{2E_sR_c(3\alpha^2 + 2\beta^2)}{N_0}}\right)\right] \tag{4.4}$$

$$P_e > E_{\alpha,\beta,\gamma}\left[Q\left(\sqrt{\frac{2E_sR_c(2\alpha^2 + 2\beta^2 + \gamma^2)}{N_0}}\right)\right]. \tag{4.5}$$

Lower bounds for other codes and other values of FT can be obtained following the analysis of their trellis in a similar way as depicted in Figure 4.6.

Calculation of an upper bound can be done according to Equation (2.103). Equations (2.104)-(2.105) are not valid for MCBFC, due to fading correlation. Furthermore, calculating the PEP for all codewords in the codebook as in Equation (2.103) is impractical. A useful approach to calculate the union bound consists in constructing the code transfer function distinguishing between errors on each channel

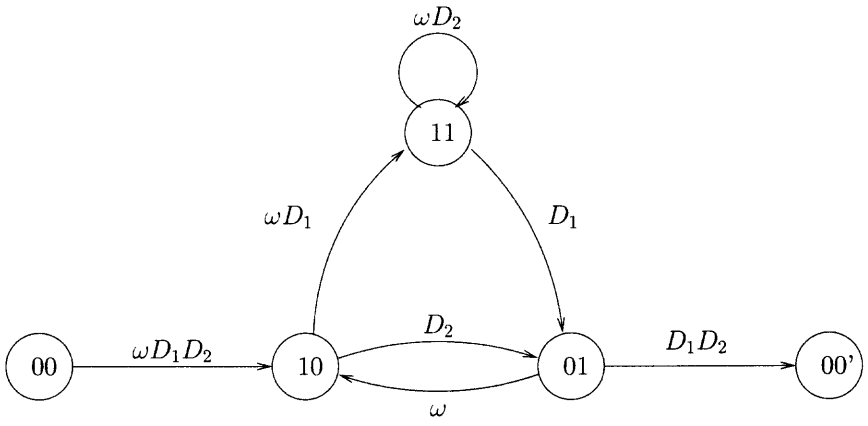

Figure 4.7 State diagram for the code with generators (7,5) and diversity 2.

state. This approach was used in [52] for the analysis of multi-frequency trellis codes and also in [53, 54]. The corresponding transfer function is easily constructed from the properly labeled code split-state diagram, which in turn is obtained from the code trellis [52]. Figures 4.7 and 4.8 show the diagrams for the rate 1/2 code with generators (7,5) for $FT = 2$ and $FT = 4$, respectively. $D_1, D_2, \cdots, D_4$ represent the error weight of each state transition, while ω represents the information error weight (number of erroneous uncoded bits). The diagram for FT=4 was obtained considering an equivalent code in which four output symbols were stacked together. The corresponding trellis diagram is shown in Figure 4.9. The transfer function for the diagram in Figure 4.7 is

$$T(D_1, D_2, \omega) = \frac{D_1^2 D_2^3 \omega + D_1^4 D_2^2 \omega^2 - D_1^2 D_2^4 \omega^2}{1 - 2D_2\omega - D_1^2\omega^2 + D_2^2\omega^2}, \tag{4.6}$$

where the same procedure used to obtain the un-modified transfer function (the one obtained setting $D_1 = D_2 = D$) in ([37], p.791) was used. The function corresponding to state diagram in figure 4.8 can also be found in closed form.

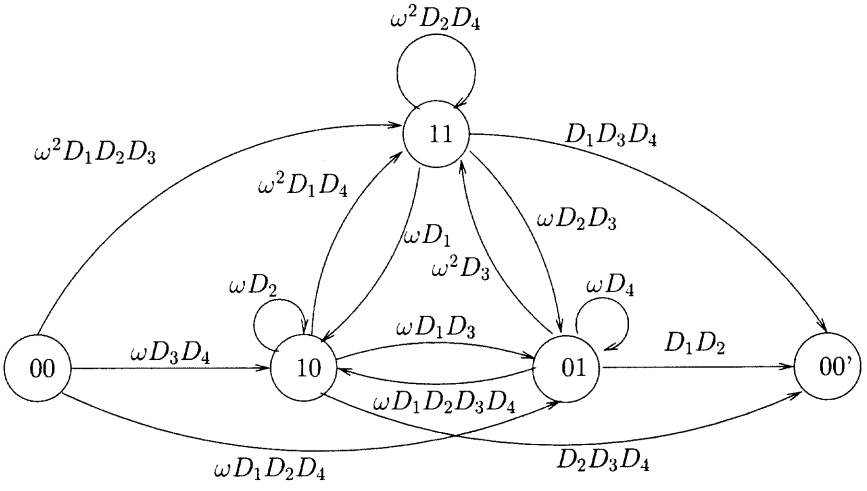

Figure 4.8 State diagram for the code with generators (7,5) and diversity 4.

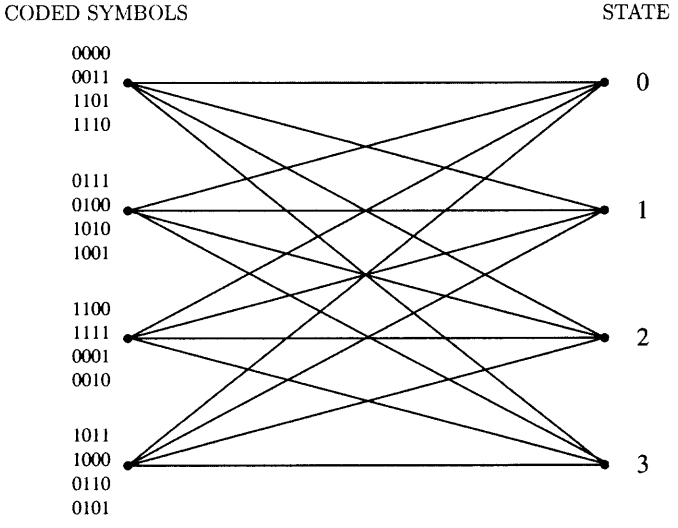

Figure 4.9 Trellis diagram for a 4-frequency code with generators (7,5).

The transfer function can be used to find the transfer function bound ([37], p. 569), which for a channel with FT blocks is given by

$$P_e < E_{\mathbf{H}}\left[\frac{\partial}{\partial\omega}T(D_1, D_2, \cdots, D_{FT}, \omega)_{|\omega=1, D_i=exp(-(E_s/N_0)R_c|H(i)|^2)}\right]. \quad (4.7)$$

To calculate the union bound, consider the series expansion of $T(D_1, D_2, \cdots, D_{FT}, \omega)$, and the n-tuple $(B_{\mathbf{d},\omega}, d_1, d_2, \cdots, d_{FT}, \omega)$, where $B_{\mathbf{d},\omega}$ denotes the multiplicity of error events with weight ω at Hamming distances $\mathbf{d} = [d_1, d_2, \cdots, d_{FT}]$ on the respective channel blocks. The bound is found adding over all $\mathbf{d}$[2],

$$P_e \leq E_{\mathbf{H}}\left[\sum_{d_1=d_{free,1}}^{\infty}, \sum_{d_2=d_{free,2}}^{\infty}, \cdots, \sum_{d_{FT}=d_{free,FT}}^{\infty}\sum_{\omega=1}^{\infty}\omega B_{\mathbf{d},\omega}P_{\mathbf{d}}(\mathbf{w}_0 \to \mathbf{w}_j|\mathbf{H})\right], \quad (4.8)$$

where $d_{free,1}, d_{free,2}, \cdots, d_{free,FT}$, are the code free distances for the respective blocks[3], and $P_{\mathbf{d}}(\mathbf{w}_0 \to \mathbf{w}_j|\mathbf{H})$ is the PEP of a codeword at distance $\mathbf{d}$. The union bound can be truncated by limiting the summations to $\mathbf{d}_T = [d_1^T, d_2^T, \cdots, d_{FT}^T]$.

Even though they are easy to calculate, Equations (4.7) and (4.8) lead to loose upper bounds due to errors with larger Hamming distances which may have low diversity and relatively high probability. Additionally, the overlap of the integration regions that make the PEP produces a poor approximation to the actual BER. A modified union bound was presented in [53] to mitigate this effect. It relies on limiting the error probability, obtained by adding all PEP, to 0.5 or 1 (depending on whether bit or frame error rate is sought), replacing Equations (4.7) and (4.8) by

$$P_e < E_{\mathbf{H}}\left[\min\left(0.5, \left[\frac{\partial}{\partial\omega}T(D_1, D_2, \cdots, D_{FT}, \omega)_{|\omega=1, D_i=exp(-(E_b/N_0)R_c|H(i)|^2)}\right]\right)\right] \quad (4.9)$$

[2]Note that for MCBFC codeword distances on all channel states must be distinguished, hence the use of distance vector $\mathbf{d}$ instead of a scalar as in Equation (2.104).

[3]These need not necessarily add to d_{free}, since the minimum free distances of different blocks may correspond to different codewords, however, $d_{free} \geq d_{free,1} + d_{free,2} + \cdots + d_{free,FT}$

and

$$P_e \leq E_{\mathbf{H}}\left[\min\left(0.5, \left[\sum_{d_1=d_{free,1}}^{\infty}, \sum_{d_2=d_{free,2}}^{\infty}, \cdots, \sum_{d_{FT}=d_{free,FT}}^{\infty}\sum_{\omega=1}^{\infty}\omega B_{\mathbf{d},\omega}P_{\mathbf{d}}(\mathbf{w}_0 \rightarrow \mathbf{w}_j|\mathbf{H})\right]\right)\right] \tag{4.10}$$

respectively. Although numerical calculation of this bound may be more complex, it is much tighter for fading channels with low diversity than the union bound.

4.3 Practical Code Design for OFDMA

4.3.1 Diversity Bounds

In an independent fading channel the minimum squared Euclidean distance is given by Equation (2.87). In the case of correlated fading, using the block fading channel described in Section 2.3, the squared Euclidean distance is given by Equation (2.94). Due to fading correlation, the Hamming distance no longer determines code diversity, as it can be seen from Equation (2.98); nevertheless, it provides an upper bound. Other upper bounds on code diversity are the number of channel blocks FT, and the Singleton bound [40, 55], given by

$$\delta_{\min} \leq 1 + \left\lfloor FT\left(1 - \frac{R_c}{\log_2|S|}\right)\right\rfloor, \tag{4.11}$$

where FT is the total number of blocks and S is the constellation size (per dimension). Values for Equation (4.11) are shown in Table 4.2 for binary symbols. High-rate codes have smaller δ_{min} than low-rate codes, and therefore the latter have in general a higher diversity gain, from which a significant performance improvement is expected.

4.3.2 Rate-adaptive Codes

A multiuser system usually has a variable load, and is customarily designed to operate at partial capacity in order to be able to deal with peaks of load demand. A non-

Table 4.2 Maximum Diversity Achievable for FT=8

Code rate	0.75	0.5	0.25	0.125
Maximum $\delta_{\min}$	3	5	7	8

adaptive FDM/TDM scheme allocates a portion of bandwidth/time to an active user regardless of the total number of users in the system. As a consequence, a significant portion of the bandwidth is unused most of the time. Alternatively, this bandwidth may be utilized by an adaptive coding scheme which uses different code rates depending on the number of active users, thereby increasing coding gain.

Punctured codes can be used to implement adaptive encoding without compromising receiver complexity, since a single hardware implementation can decode all rates. In rate-compatible punctured convolutional (RCPC) codes, introduced in [56], the non-punctured bits of higher-rate codes are not punctured in lower-rate codes either. Given a base code, a set of puncturing patterns can be chosen to accommodate different code rates. With a decoding period p and a base code with rate $1/n$, the following rates can be achieved:

$$R_c = \frac{p}{np}, \frac{p}{np-1}, \frac{p}{np-2}, \cdots, \frac{p}{p+1}. \tag{4.12}$$

When very few users are active, nested codes, also variable rate codes, are appropriate for very low rates. Nested codes are obtained from a base code with rate $1/n$ using additional generator polynomials. In this fashion it is possible to obtain codes of rate $\{1/(n+1), 1/(n+2), \cdots, 1/(n+m)\}$ for an arbitrary m . Table 4.3 summarizes the minimum rates of a set of RCPC and nested codes for a 32-user system employed in the simulations.

Due to finite rate resolution of the codes chosen, there is a rate loss from the minimum rate possible given the bandwidth and number of users. It can be seen in

table 4.3 that the rate loss is minimal for the example considered. Furthermore, finer rate resolution can be achieved by increasing the puncturing period of RCPC codes.

Table 4.3 RCPC Codes and Nested Codes with Puncturing Period $p = 8$ and Base Code Rate 1/4

Users	Minimum rate / Bits per dimension	RCPC code rate	Punctured bits	Nested code rate	Rate loss
32	0.5	0.5	16	-	0
28	0.437	0.444	14	-	0.007
24	0.375	0.381	11	-	0.006
20	0.312	0.32	7	-	0.007
16	0.25	0.25	0	-	0
12	0.187	-	-	0.2	0.012
8	0.125	-	-	0.125	0
4	0.062	-	-	0.062	0

4.4 Bit Error Rate of Coded MC-CDMA

The equivalent MC-CDMA parallel channel set transceiver introduced in Chapter 3 is used to define a simplified expression for the received signal, analogous to Equation (4.1). According to the model, denote the received signal for user k by

$$y_k(i) = H'_k(i)Ax_k(i) + \xi'_k(i), \tag{4.13}$$

where the equivalent channel coefficients $H'_k(i)$, as well as the covariance of noise samples $\xi'_k(i)$, depend on the channel matrix, the spreading code matrix, and the MUD. In addition to the equivalent channel model, interleaving must also be considered. Clearly, frequency interleaving is not possible since symbols are already transmitted over all sub-carriers. On the other hand, periodic time interleaving is, hence

coding can provide time diversity in the MCBFC in addition to inherent frequency diversity achieved by spreading. It follows that the maximum achievable diversity gain over the uncoded system is given by the number of time blocks, T.

4.4.1 BER with Decorrelating Detector

For the decorrelating detector, the received signal is simplified to

$$y_k(i) = Ax_k(i) + \xi_k^D(i), \tag{4.14}$$

where $\xi_k^D(i)$ has covariance $\rho_k^D(i)\sigma_\zeta^2 = \rho_k^D(i)N_0/2$, with the noise enhancement factor $\rho_k^D(i)$ defined in Appendix A. The dependence of the noise enhancement factor on the channel state where symbol i is transmitted is expressed by index i. Using the equivalent MC-CDMA channel model, the nearest neighbor lower bound is calculated similarly to OFDMA. The analysis is carried out depending on the degree of time diversity.

No time diversity: the Euclidean distance is given by

$$d_E^2(i,j) = E_s R_c \sum_{l\in\mathcal{K}} |x_i(l) - x_j(l)|^2, \tag{4.15}$$

which is independent from the channel state, and the PEP (also for no time diversity) is given by

$$P(\mathbf{w}_i \to \mathbf{w}_j|\mathbf{H}) = Q\left(\sqrt{\frac{d_E^2(i,j)}{2\rho_k^D N_0}}\right), \tag{4.16}$$

which depends on the channel state through ρ_k^D (the dependence on symbol index i was eliminated since all symbols are transmitted on the same channel state in this case). The BER can thus be lower-bounded by

$$P_e > \min_{j\neq i} E_{\mathbf{H}}\left[Q\left(\sqrt{\frac{d_E^2(i,j)}{2\rho_k^D N_0}}\right)\right]. \tag{4.17}$$

For the rate 1/2 code with generators (7,5) and BPSK modulation considered for OFDMA, and assuming $F = 2$,

$$P_e > E_{\alpha,\beta}\left[Q\left(\sqrt{\frac{2E_sR_c5}{\rho_k^D N_0}}\right)\right] \tag{4.18}$$

since $d_{free} = 5$. This lower bound can be calculated numerically. The BER can be upper-bounded using the same technique used for OFDMA but considering time diversity only, and noise enhancement rather than the channel coefficients. For no time diversity there is only one state to consider, and using the fact that $D_1 = D_2 = D$ the transfer function in Equation (4.6) simplifies to

$$T(D,\omega) = \frac{D^5\omega}{1 - 2D\omega}, \tag{4.19}$$

Also, the modified transfer function bound and union bound, obtained by limiting the error probability to 0.5, are found similarly to Equations (4.9) and (4.10).

With time diversity: with time interleaving, the noise enhancement factor $\rho_k^D(i)$ of consecutive symbols is independent (albeit equal for symbols located T symbols apart). In such case it is also necessary to take into account the position of symbol errors in an identical manner as in OFDMA. For the example code, and for $T = 2$, the BER is lower-bounded by

$$P_e > E_{\alpha,\beta}\left[Q\left(\sqrt{\frac{2E_sR_c}{N_0}\left(\frac{3}{\rho_k^D(\alpha)} + \frac{2}{\rho_k^D(\beta)}\right)}\right)\right], \tag{4.20}$$

where $\rho_{k,}^D(\alpha)$ and $\rho_{k,}^D(\beta)$ are the noise enhancement factors produced by each of the channels (denoted by α and β). The upper bound is found as in OFDMA. For example, for $T = 2$, the code transfer function is given by Equation (4.6), and, the modified transfer function bound and union bound are obtained similarly to Equations (4.9) and (4.10) considering only the channel time blocks T.

4.4.2 BER with MMSE Detector

Denote the received signal by

$$y_k(i) = Ax_k(i) + e_k(i), \tag{4.21}$$

where $e_k(i)$ is the minimum mean square error, with covariance given by

$$E[|e_k(i)|^2] = \sigma^2[\mathbf{M}(i)]_{k,k} \tag{4.22}$$

as shown in Appendix A. The error $e_k(i)$ depends on channel, spreading codes, number of active users, and SNR. Using Equation (4.21), the Euclidean distance is given by

$$d_E^2(i,j) = E_s R_c \sum_{l \in \mathcal{K}} |x_i(l) - x_j(l)|^2. \tag{4.23}$$

As with the decorrelating detector, the analysis depends on the degree of time diversity.

No time diversity: using BPSK, the Euclidean distance can be expressed as

$$d_E^2(i,j) = 4E_s R_c d_H(i,j), \tag{4.24}$$

where $d_H(i,j)$ was defined in chapter 2 as the Hamming distance between codewords $\mathbf{w}_i$ and $\mathbf{w}_j$. The PEP is given by (see Appendix A)

$$P(\mathbf{w}_i \to \mathbf{w}_j|\mathbf{H}) = Q\left(\sqrt{d_H(i,j)\left(\frac{E_s R_c}{E[|e_k|^2]} - 1\right)}\right), \tag{4.25}$$

where the dependence of e_k on i was eliminated since all symbols are transmitted in the same channel state, resulting in the same e_k. The bit error probability can thus be lower-bounded by

$$P_e > \min_{j \neq i} E_{\mathbf{H}}\left[Q\left(\sqrt{d_H(i,j)\left(\frac{E_s R_c}{E[|e_k|^2]} - 1\right)}\right)\right] \tag{4.26}$$

For the rate 1/2 code with generators (7,5) (considered for OFDMA), $d_{free} = 5$, and

$$P_e > E_{\mathbf{H}} \left[Q \left(\sqrt{5 \left(\frac{E_s R_c}{E[|e_k|^2]} - 1 \right)} \right) \right], \tag{4.27}$$

which can be calculated by the Monte-Carlo integration method. Similarly as in the decorrelator case, the BER can be upper-bounded using the same technique used with the decorrelating detector, but considering the error $e_k(i)$ rather than noise enhancement. For no time diversity the transfer function is also given by Equation (4.19).

With time diversity: making the same assumptions regarding interleaving as in the previous section, the MMSE $e_k(i)$ of consecutive symbols is independent for T symbols (and fully correlated for data transmitted T symbols apart). The symbol error position must be taken into account as well, with the BER lower bound being calculated in similarly to the decorrelating detector. For the example code, and for $T = 2$, the BER is lower-bounded by

$$P_e > E_{\alpha,\beta} \left[Q \left(\sqrt{3 \left(\frac{E_s R_c}{E[|e_k(\alpha)|^2]} - 1 \right) + 2 \left(\frac{E_s R_c}{E[|e_k(\beta)|^2]} - 1 \right)} \right) \right], \tag{4.28}$$

where $E[|e_k(\alpha)|^2]$ and $E[|e_k(\beta)|^2]$ are the MMSE produced by each of the channels. The upper bound is found as with the decorrelating detector (therefore, for $T = 2$, the code transfer function is given by Equation (4.6), and, the modified transfer function bound and union bound are obtained similarly to Equations (4.9) and (4.10), also considering only the channel time blocks T.

4.5 Performance Comparison of Coded OFDMA and Coded MC-CDMA

4.5.1 Bit Error Rate Bounds

The methodology for bounding the BER of OFDMA and MC-CDMA was used to examine and compare the performance of a single cell downlink system. Modulation,

Table 4.4 Comparison Parameters

Sub-carriers	Users	Spreading seqs.	Modulation
32	16,24,32	32 Walsh-Hadamard	BPSK
Code Generators	Freq. div. F	Time div. T	Frame Size
(7,5)	1,2,4	1	100 symbols

coding and multiple access parameters used are listed in Table 4.4. Figure 4.10 shows simulated performance and calculated bounds of an OFDMA system with code rate 1/2 without diversity and with diversity 2, showing the benefit of code diversity on BER.

Figures 4.11, and 4.12 show the results for MC-CDMA with the decorrelating detector operating at 50% load and 100% load for different diversity orders. Note that, at 50% load, an increase in channel diversity resulted in significant performance improvements attributable to the inherent frequency diversity of MC-CDMA. On the other hand, at 100% load, an increase in channel diversity left the performance of the decorrelating detector almost unchanged, showing a poor diversity capability of this scheme. Figures 4.13, and 4.14 depict the same results for MC-CDMA with the MMSE detector. In this case channel diversity resulted in improved performance at both 50% and 100% load, although the improvement is more remarkable at half load.

In order to compare the performance of OFDMA and MC-CDMA, Figures 4.15 and 4.16 show simulated BER and performance bounds for MC-CDMA operating at 50% and 100% respectively, and for OFDMA. Notice that the performance of OFDMA was similar to MC-CDMA at 50% load and superior at 100% load.

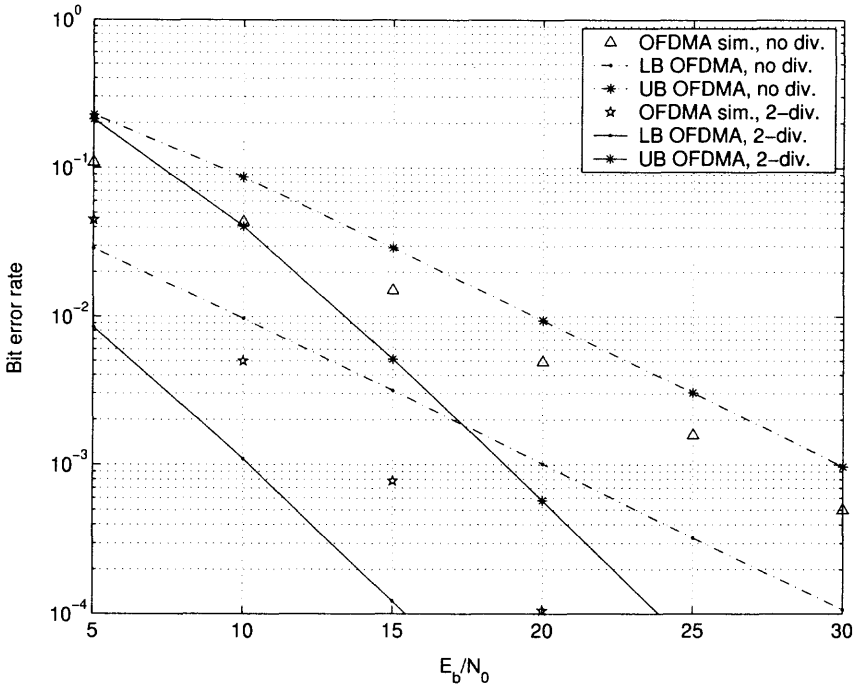

Figure 4.10 Upper bound, lower bound, and simulation of coded OFDMA with rate 1/2 (7,5) code, without diversity and with diversity 2.

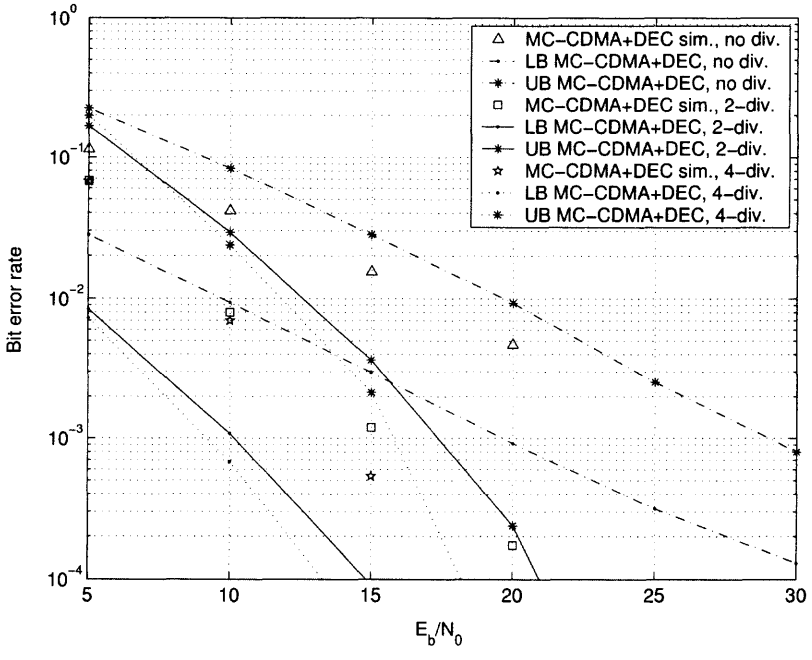

Figure 4.11 Upper bound, lower bound, and simulation of coded MC-CDMA+DEC with rate 1/2 (7,5) code, 50% load with different diversity orders.

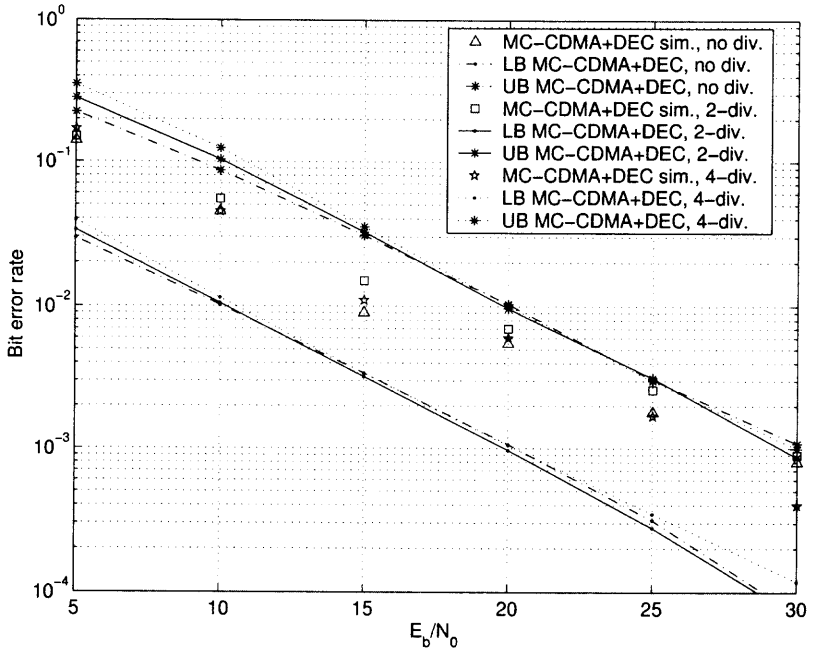

Figure 4.12 Upper bound, lower bound, and simulation of coded MC-CDMA+DEC with rate 1/2 (7,5) code, 100% load. with different diversity orders.

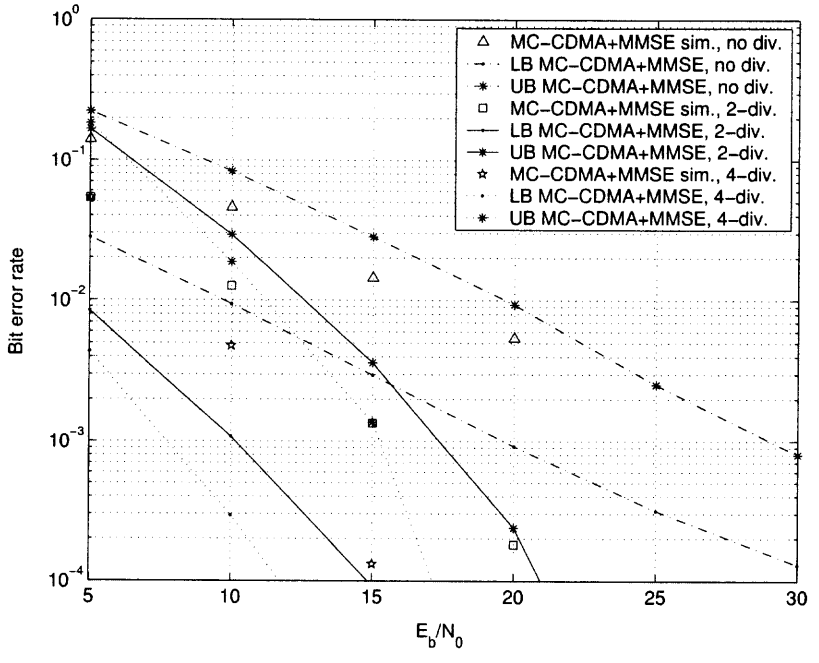

Figure 4.13 Upper bound, lower bound, and simulation of coded MC-CDMA+MMSE with rate 1/2 (7,5) code, 50% load with different diversity orders.

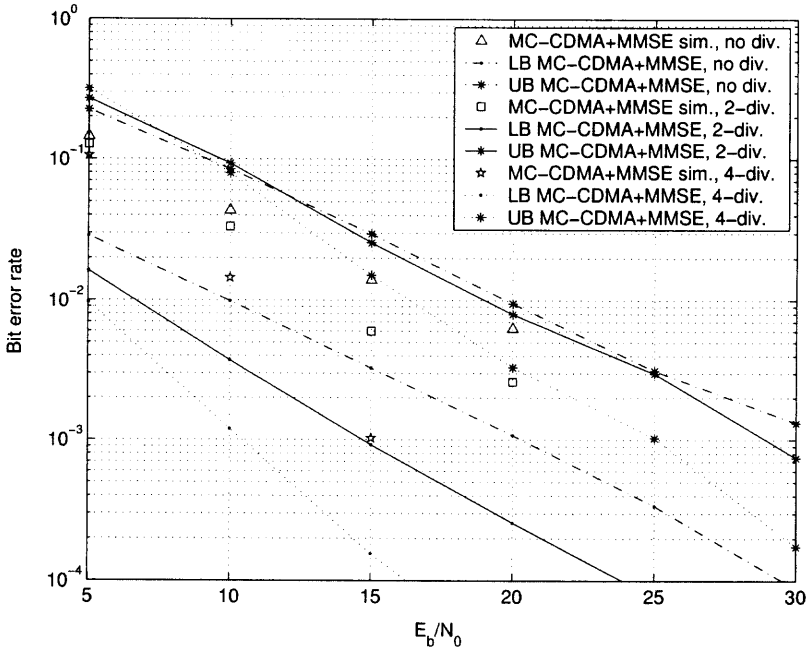

Figure 4.14 Upper bound, lower bound, and simulation of coded MC-CDMA+MMSE with rate 1/2 (7,5) code, 100% load with different diversity orders.

4.5.2 Bit Error Rate Simulation

While results in the previous section were restricted to a 4-state code with generators (7,5) to simplify the analysis, in this section more powerful codes are evaluated through simulation using the parameters in Table 4.5. The BER of OFDMA using rate-adaptive codes, with the code rate being chosen according to system load, is shown in Figure 4.17 for RCPC codes with a 64-state base code of rate 1/4 and generators (133,117,123,127) , using optimal puncturing patterns from [57] for puncturing period 8. The additional generators for nested codes are (135,173,145,137,155, 157,175) [57]. Figures 4.18 and 4.19 compare the performance of OFDMA with fixed rate and with rate-adaptive codes and of MC-CDMA with decorrelator and MMSE detectors and a rate 1/2 code with generators (171,133). In figure 4.18 the BER at $E_b/N_0 = 8dB$ is shown for different rates, demonstrating a substantial improvement of the performance of OFDMA at low load using rate adaptation, which makes OFDMA superior to MC-CDMA for any system load. Figure 4.19 shows the E_b/N_0 required

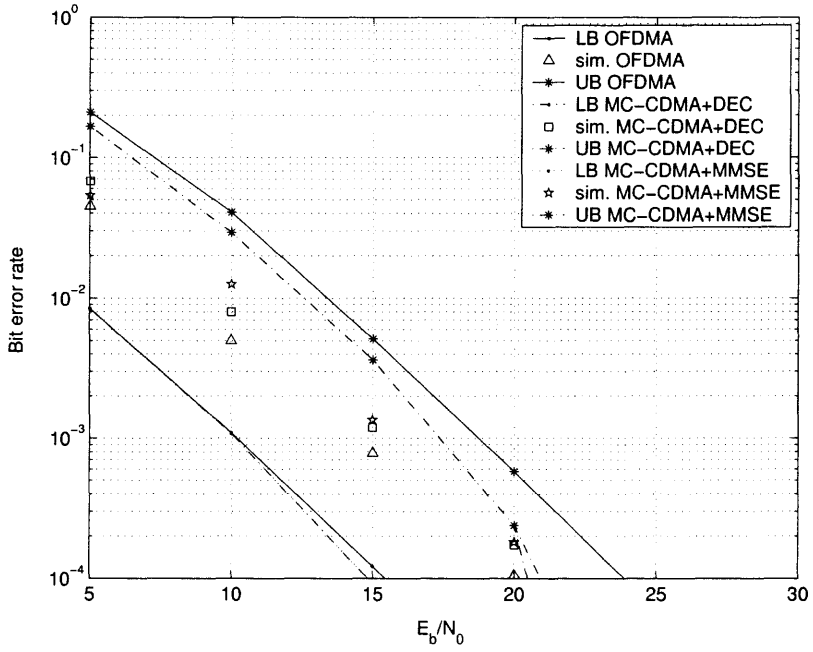

Figure 4.15 Comparison of OFDMA and MC-CDMA at 50% load.

for a BER of 10^{-3}, and a similar conclusion can be reached.

Table 4.5 Comparison Simulation Parameters

Sub-carriers	Users	Spreading seqs.	Modulation
32	16,24,32	32 Walsh-Hadamard	BPSK
Code Rate	Freq. div. F	Time div. T	Frame Size
OFDMA: see Table 4.3	8	1	100 symbols
MC-CDMA: 1/2			

4.6 Summary and Conclusions

In this chapter the tools to calculate bounds to the bit error rate of OFDMA and MC-CDMA were provided. It was also shown that the performance of OFDMA can

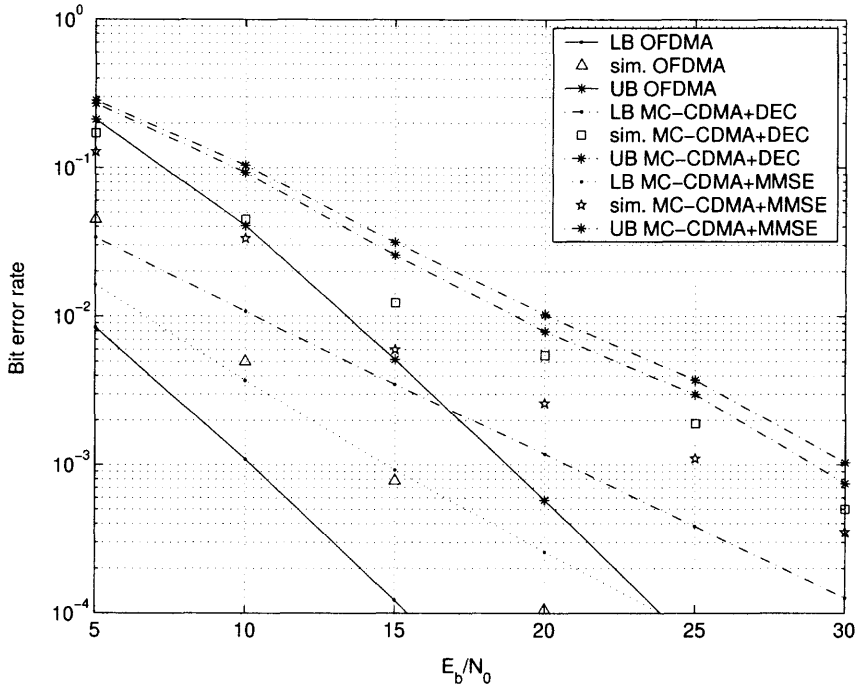

Figure 4.16 Comparison of OFDMA and MC-CDMA at 100% load.

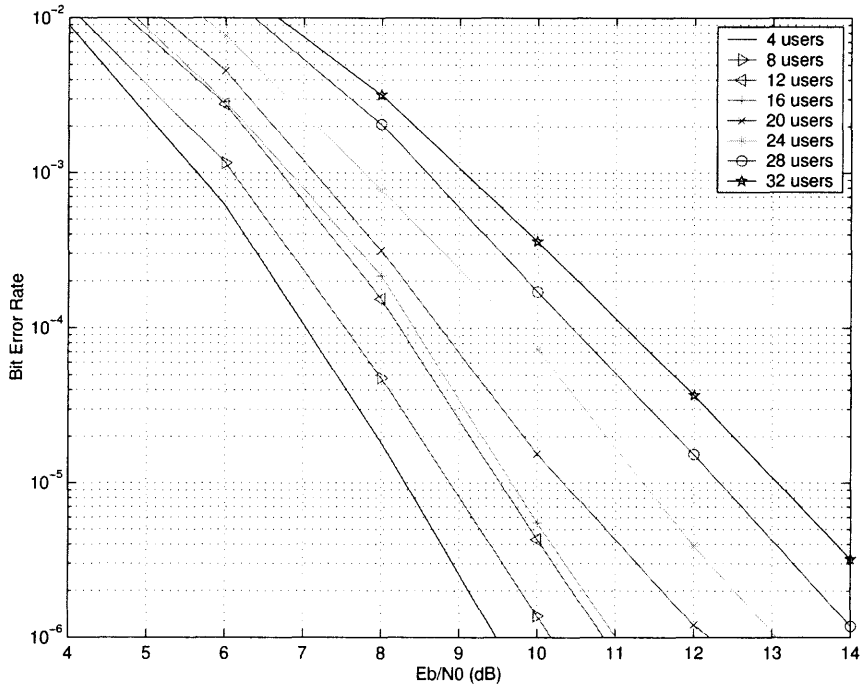

Figure 4.17 Simulated performance of OFDMA for different code rates.

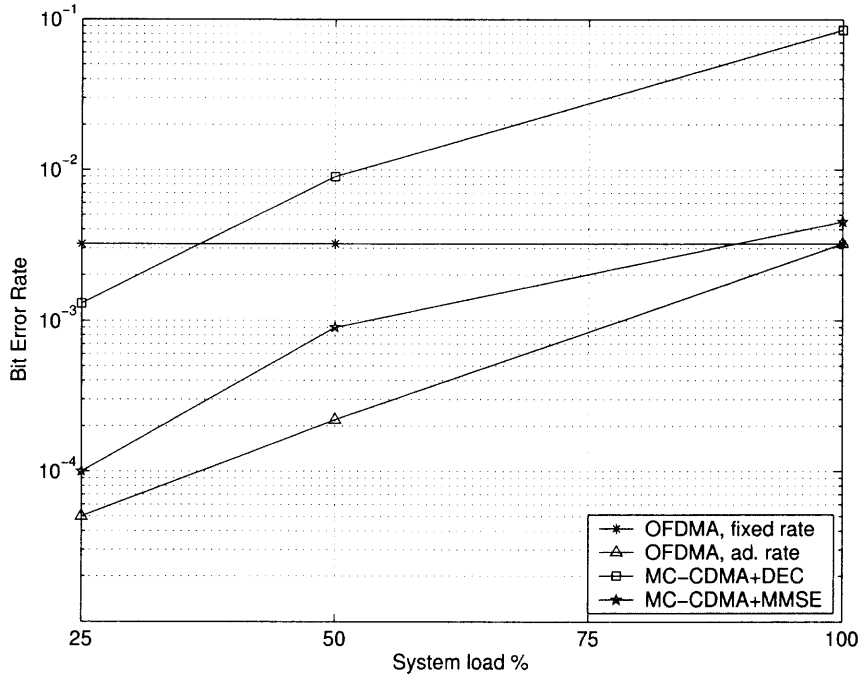

Figure 4.18 Bit error rate of OFDMA and MC-CDMA for $E_b/N_0 = 8dB$.

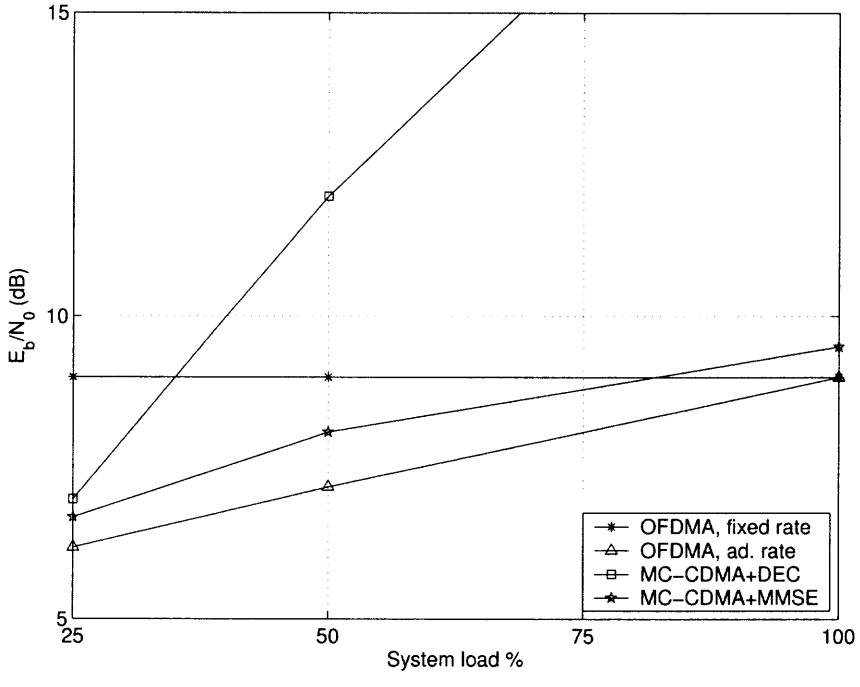

Figure 4.19 E_b/N_0 needed to obtain a BER of 10^{-3} for OFDMA and MC-CDMA.

be greatly improved if rate-adaptive codes are used. In addition, the BER of OFDMA was compared with the BER of MC-CDMA using linear multiuser detectors, through analytical bounds and through simulation, for the MCBFC. The results obtained show superior performance of OFDMA over MC-CDMA for any system load.

CHAPTER 5

MULTI-CARRIER SYSTEMS WITH MULTIPLE FREQUENCY OFFSETS

This chapter focuses on the effects of poor transmitter frequency synchronization on OFDM with macrodiversity for SFN, introduced in Section 2.2.4. The sensitivity of OFDM to frequency synchronization increases when more, narrower sub-carriers are used to compensate for the large delay spread caused by macrodiversity. It is well known that an offset between transmitter carrier and receiver local oscillator frequencies results in ICI, which severely degrades performance. Other causes of ICI are Doppler spread and oscillator phase jitter [58–65]. However, ICI resulting from a transmitter-receiver frequency offset can be easily eliminated by estimating it and correcting it [66]. In addition, various methods have been proposed to make the OFDM signal more robust to ICI [60, 67, 68].

In the context of a macrodiversity system, the effects of multiple transmitter frequency offsets are analyzed. The case where multiple offsets result from poor frequency synchronization of multiple transmitters is considered, which causes ICI that cannot be canceled by simple estimation and correction as in the case of a single offset. A similar problem, although different in nature and scale, arises in frequency dispersive channels when offsets are produced by different Doppler shifts on different signal paths from a single transmitter [62, 63]. Nevertheless, offsets resulting from poor transmitter synchronization can be much larger, and cause serious performance degradation in OFDM due to ICI. In order to counter it, linear and decision feedback interference cancellation schemes for the receiver are proposed. Additionally, noise enhancement due to linear ICI cancellation motivates the use of more complex but more effective decision feedback schemes.

5.1 Macrodiversity Offset Representation

The signal model described in this section is for an OFDM system with macrodiversity, which may represent a SFN (shown in Figure 2.7) or a cellular system performing a soft handoff (depending on the number of transmitters involved). For a system with N_T transmitters, which lack frequency synchronization among them, and between them and receiver, RF frequencies f_c^i, $i = 1, 2, \cdots, N_T$, and f_{lo} are different. For a moving user, f_c^i may also be different due to different Doppler shifts resulting from the signal arriving from different angles with respect to its moving direction, even if the transmitters are synchronized, although lack of frequency synchronization may result in larger frequency offsets than Doppler shifts. For example, a mobile traveling at a speed of 250 km/h receiving a signal at 800 MHz experiences a maximum Doppler shift of 185 Hz, while a local oscillator at the transmitter having a deviation of 7 ppm results in a shift of 5600 Hz. In the following only the effects of synchronization are considered and it is assumed that the channel is time-invariant for the length of an OFDM symbol[1]. It is also assumed that a long enough guard interval is used so that there is no ISI, and, without loss of generality, a single OFDM symbol is considered.

The signal transmitted by station i is given by

$$s_{RF}^i(t) = \Re\left\{\frac{1}{\sqrt{N_s}}\sum_{l=0}^{N_s-1} A_l^i b_l \exp(j2\pi(l\Delta f + f_c^i)t)\right\}. \tag{5.1}$$

In the expression, N_s is the number of sub-carriers, A_l^i is sub-carrier l transmit amplitude, b_l is the information symbol on sub-carrier l, and Δf is the sub-carrier frequency spacing. The complex baseband equivalent is given by

$$x^i(t) = \frac{1}{\sqrt{N_s}}\sum_{l=0}^{N_s-1} A_l^i b_l \exp(j2\pi(l\Delta f + (f_c^i - f_{lo}))t), \tag{5.2}$$

[1]One can assume that, if there are frequency shifts due to Doppler effects, these are superimposed to the offset between local oscillators. That makes the signal model valid even with Doppler shifts.

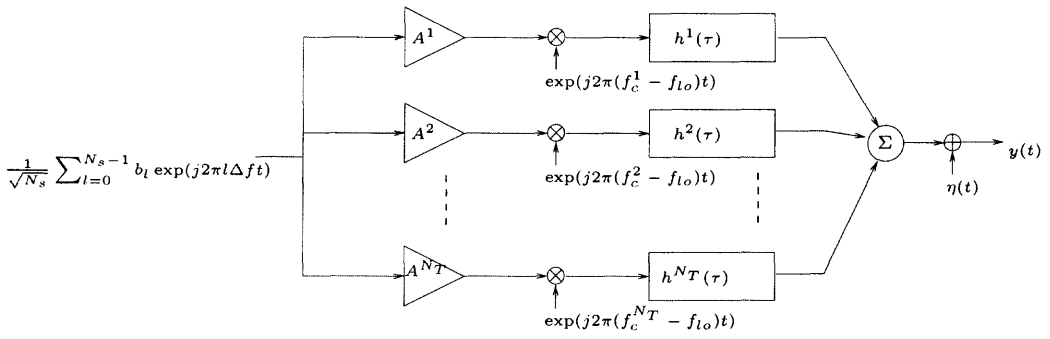

Figure 5.1 Baseband system model, with transmitter frequency offsets.

where the baseband signal is defined as the RF signal translated by f_{lo}, rather than f_c^i, in order to represent the frequency offset $f_c^i - f_{lo}$.

The received complex baseband signal is given by

$$y(t) = \sum_{i=1}^{N_T} \left(\int h^i(\tau) x^i(t-\tau)\, d\tau \right) + \eta(t), \tag{5.3}$$

where $h^i(\tau)$ denotes the complex baseband channel response from station i to the receiver, under the assumption that the channel is time-invariant for the duration of the OFDM symbol (the relative delay of signals from different transmitters is also incorporated in $h^i(\tau)$). In addition, $\eta(t)$ denotes AWGN. The equivalent baseband system model is shown in Figure 5.1. The discrete-time baseband signal in the interval $[0, N_s - 1]$ is obtained by sampling $y(t)$ at a rate $f_s = (N_s + N_{CP})T^{-1}$, where T is the OFDM symbol duration, and N_{CP} the number of samples of the cyclic prefix, which is then discarded:

$$\begin{aligned} y(n) &= \sum_{i=1}^{N_T} h^i(n) \circledast \frac{1}{\sqrt{N_s}} \sum_{l=0}^{N_s-1} A_l^i b_l \exp\left(j2\pi \frac{l+\epsilon^i}{N_s} n \right) \\ &+ \eta(n). \end{aligned} \tag{5.4}$$

In the expression, $\epsilon^i = \frac{f_c^i - f_{lo}}{\Delta f}$ is the frequency offset, normalized by the sub-carrier spacing $\Delta f = f_s/N_s$, $\circledast$ denotes the circular convolution operator, and $\eta(n)$ is AWGN.

After performing DFT on the received signal

$$\begin{aligned} y_k &= \frac{1}{\sqrt{N_s}} \sum_{n=0}^{N_s-1} y(n) \exp(-j2\pi nk/N_s) \\ &= \sum_{i=1}^{N_T} \sum_{l=0}^{N_s-1} H_l^i A_l^i b_l \Phi^i(l-k) + \zeta_k, \end{aligned} \tag{5.5}$$

where H_l^i is the baseband channel response at frequency $f = 2\pi l \Delta f$. Furthermore,

$$\begin{aligned} \Phi^i(l-k) &= \frac{1}{N_s} \sum_{n=0}^{N_s-1} \exp(j2\pi n(l-k+\epsilon^i)/N_s) \\ &= \frac{1}{N_s} \frac{\sin(\pi(l-k+\epsilon^i))}{\sin(\pi(l-k+\epsilon^i)/N_s)} \exp\left(j\pi \frac{(N_s-1)(l-k+\epsilon^i)}{N_s}\right). \end{aligned} \tag{5.6}$$

The term $\zeta_k(n)$ represents AWGN at sub-carrier k and has variance σ_ζ^2 (the same in all sub-carriers). In matrix notation,

$$\mathbf{y} = \sum_{i=1}^{N_T} \mathbf{\Phi}^i \mathbf{H}^i \mathbf{A}^i \mathbf{b} + \boldsymbol{\zeta}, \tag{5.7}$$

where the elements of $\mathbf{\Phi}^i$ are defined as $[\mathbf{\Phi}^i]_{k,j} = \Phi_{kj}^i = \Phi^i(j-k)$.

5.2 Performance Analysis

The performance of the described OFDM macrodiversity system in terms of the SINR is derived in this section. Compared to the SNR of a system with perfect frequency synchronization (and thus without ICI), the SINR will yield the degradation due to frequency offsets. First, closed form expressions for the average SINR of a receiver with no ICI cancellation (which is referred to as *conventional receiver*), and for the optimum local oscillator frequency f_{lo}, are derived.

For calculation of the SINR, consider the received signal on sub-carrier k, which using the signal model in Equation (5.7), is

$$y_k = \sum_{i=1}^{N_T} \Phi_{kk}^i H_{kk}^i A_{kk}^i b_k + \sum_{i=1}^{N_T} \sum_{l \neq k} \Phi_{kl}^i H_{ll}^i A_{ll}^i b_l + \zeta_k. \tag{5.8}$$

The first term in this expression corresponds to the desired signal, the second corresponds to ICI, and the last term is AWGN. The SINR, denoted by γ, is

$$\gamma_k = \frac{E\left[\left|\sum_{i=1}^{N_T} \Phi_{kk}^i H_{kk}^i A_{kk}^i b_k\right|^2\right]}{E\left[\left|\sum_{i=1}^{N_T}\sum_{l\neq k} \Phi_{kl}^i H_{ll}^i A_{ll}^i b_l\right|^2\right] + \sigma_\zeta^2}, \tag{5.9}$$

where the expectation operator $E[\cdot]$ is taken over all channel states and data statistics. In order to obtain simplified, closed-form expressions for γ_k, the following is assumed: first, channel responses from different transmitters are uncorrelated (this is justified by the fact that different transmitters are geographically separated); second, transmitted symbols b_l are uncorrelated and normalized ($E[|b_l|^2] = 1$). Under these circumstances the SINR simplifies to

$$\gamma_k = \frac{\sum_{i=1}^{N_T} \mathcal{L}^i |\Phi_{kk}^i|^2 |A_{kk}^i|^2}{\sum_{i=1}^{N_T}\sum_{l\neq k} \mathcal{L}^i |\Phi_{kl}^i|^2 |A_{kl}^i|^2 + \sigma_\zeta^2}, \tag{5.10}$$

where $\mathcal{L}^i$ denotes the average path loss from transmitter i to the receiver. Furthermore, if all sub-carriers are transmitted with equal power, $|\mathbf{A}^i|^2 = \mathcal{P}^i \mathbf{I}_{N_s}$ (where $\mathbf{I}$ denotes the identity matrix), then all sub-carriers have the same SINR. Its expression further simplifies to

$$\gamma_k = \gamma = \frac{\sum_{i=1}^{N_T} \mathcal{L}^i \mathcal{P}^i |\Phi^i(0)|^2}{\sum_{i=1}^{N_T} \mathcal{L}^i \mathcal{P}^i (1 - |\Phi^i(0)|^2) + \sigma_\zeta^2}, \tag{5.11}$$

where the orthonormality property of $\mathbf{\Phi}$ [66] was used.

A conventional receiver can maximize the SINR with a proper choice of the local oscillator frequency f_{lo}. Doing so is equivalent to maximizing

$$\sum_{i=1}^{N_T} \mathcal{L}^i \mathcal{P}^i |\Phi^i(0)|^2 = \sum_{i=1}^{N_T} \mathcal{L}^i \mathcal{P}^i \left|\frac{1}{N_s}\frac{\sin \pi\epsilon^i}{\sin(\pi\epsilon^i/N_s)}\right|^2, \tag{5.12}$$

where Equation (5.6) was used. Note, however, that the signal suffers from ICI unless $\epsilon^i = 0$ for all i, which is only possible if all transmitters are synchronized. It is shown in Appendix C that, using a second order approximation of the expression in Equation

(5.6), the local oscillator frequency maximizing the left hand side of Equation (5.12) is given by

$$f_{lo} = \frac{\sum_{i=1}^{N_T} \mathcal{L}^i \mathcal{P}^i f_c^i}{\sum_{i=1}^{N_T} \mathcal{L}^i \mathcal{P}^i}, \tag{5.13}$$

which is the average frequency of the received signals, weighted with their respective amplitudes. This agrees with the result by Robertson and Kaiser [62] for the effects of two-path Doppler spread in a single-transmitter OFDM system.

Two examples of local oscillator alignment are shown on Figure 5.2 for a macro-diversity system with 4 transmitters. Dashed lines display relative transmitter amplitudes, and their normalized frequency offset from the nominal carrier frequency f_{nom}. Solid lines display the optimum receiver frequency (obtained maximizing the left hand side of Equation (5.12)), and the frequency obtained by the approximation in Equation (5.13). As one can see from the figure, the synchronization error incurred by the expression in Equation (5.13) is small, even for considerable transmitter offsets. For the remainder of the chapter it is assumed that the conventional receiver is synchronized to the average frequency in order to provide a fair comparison with the proposed improved receivers.

5.3 Multiple Offset Linear ICI Cancellation

It was shown that resilient ICI (after optimal alignment of the local oscillator) limits the performance of a conventional receiver; therefore, further processing at the receiver is considered in order to improve it. The use of a linear transformation $\mathbf{T}$ on the received signal, in the frequency domain (after the DFT at the receiver), is introduced in this section. From Equation (5.7), an equivalent channel response can be defined as $\mathcal{H}$ so that

$$\mathbf{y} = \sum_{i=1}^{N_T} \mathbf{\Phi}^i \mathbf{H}^i \mathbf{A}^i \mathbf{b} + \boldsymbol{\zeta} = \mathcal{H}\mathbf{b} + \boldsymbol{\zeta}. \tag{5.14}$$

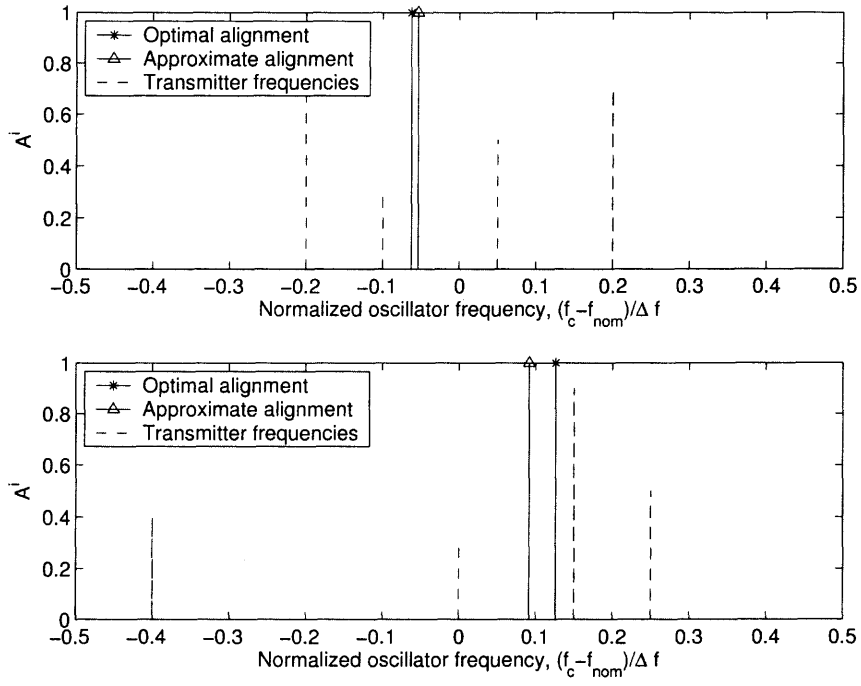

Figure 5.2 Optimal and approximate receiver local oscillator alignment.

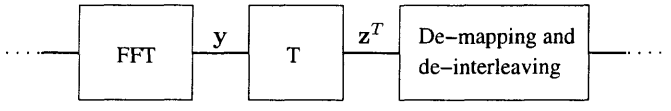

Figure 5.3 Block diagram of a receiver employing linear ICI cancellation.

Figure 5.3 depicts the structure of a receiver implementing linear ICI cancellation, with a matrix filter $\mathbf{T}$[2]. Denote the received signal, after processing, by

$$\mathbf{z}^T = \mathbf{T}(\mathcal{H}\mathbf{b} + \boldsymbol{\zeta}). \tag{5.15}$$

Expressions for $\mathbf{T}$, which lead to the sub-carrier decorrelating (or zero forcing), and to the MMSE solutions, are derived in the following sections.

[2]A linear matrix filter is also used in [69] for block equalization of signals with ISI, and is used to cancel multi-access interference in linear multiuser detectors for CDMA [19], where signals are also processed in blocks.

5.3.1 Decorrelating Transformation

The decorrelating solution, which imposes the elimination of all ICI, can be implemented, provided that matrix $\mathcal{H}$ is invertible, by

$$\mathbf{T} := \mathbf{D} := \mathcal{H}^{-1}. \tag{5.16}$$

The processed received signal vector can then be expressed by

$$\mathbf{z}^D = \mathcal{H}^{-1}\mathbf{y} = \mathbf{b} + \boldsymbol{\zeta}^D, \tag{5.17}$$

where $\boldsymbol{\zeta}^D$ is Gaussian noise with covariance matrix $\mathbf{R}_{\zeta^D} = \sigma_\zeta^2 \mathcal{H}^{-1}(\mathcal{H}^{-1})^H$. Clearly, this operation decorrelates the signal at different sub-carriers if transmitted symbols are independent, which was already assumed.

The SINR of this receiver is simply the SNR, since all ICI has been eliminated,

$$\gamma_k^D = \frac{E[|b_k|^2]}{E[|\zeta_k^D|^2]} = \frac{1}{\rho_k^D \sigma_\zeta^2}. \tag{5.18}$$

Parameter ρ_k^D in Equation (5.18) is defined as the decorrelating noise enhancement factor, $\rho_k^D = \sigma_{\zeta_k^D}^2/\sigma_{\zeta_k}^2 = [\mathcal{H}^{-1}(\mathcal{H}^{-1})^H]_{k,k}$, where $\sigma_{\zeta_k^D}^2 = [\mathbf{R}_{\zeta^D}]_{k,k}$ is the variance of ζ_k^D, the noise in sub-carrier k. The mean SINR is obtained averaging for different sub-carriers and over the channel coefficients $H_{kk}^i, i = 1, 2, \cdots, N_T$. Although the decorrelating transformation succeeds in eliminating all ICI, it also produces noise enhancement, degrading the SNR. Furthermore, it is not the linear transformation that maximizes the SINR.

5.3.2 MMSE Transformation

The linear transformation that minimizes the mean square error (MSE) of the received signal, and its resulting SINR, are derived in this section. The MSE is defined as

$$\xi = E\left[|\mathbf{b} - \mathbf{z}^T|^2\right]. \tag{5.19}$$

The MMSE, which minimizes ξ, also satisfies the orthogonality principle ([70], p.197), that is given by

$$E\left[(\mathbf{b}-\mathbf{z}^T)(\mathbf{z}^T)^H\right]=0. \tag{5.20}$$

The corresponding expression for the MMSE linear transformation, which is easily derived setting $\partial\xi/\partial\mathbf{T}=0$, or from Equation (5.20), is given by

$$\mathbf{T}:=\mathbf{M}\mathcal{H}^H, \tag{5.21}$$

where $\mathbf{M}=(\mathbf{R}_H+\sigma_\zeta^2\mathbf{I})^{-1}$, with $\mathbf{R}_H=\mathcal{H}^H\mathcal{H}$, is the MMSE estimation matrix. The processed received signal vector is described by

$$\mathbf{z}^M=\mathbf{M}\mathbf{R}_H\mathbf{b}+\boldsymbol{\zeta}^M, \tag{5.22}$$

where $\boldsymbol{\zeta}^M=[\zeta_0^M,\zeta_1^M,\cdots,\zeta_{N_s-1}^M]$ is a vector representing Gaussian noise, with covariance $\mathbf{R}_{\zeta^M}=\sigma_\zeta^2\mathbf{M}\mathbf{R}_H\mathbf{M}^H$.

To find the SINR, the received signal, at sub-carrier k, after the transformation, is expressed as

$$z_k^M=[\mathbf{M}\mathbf{R}_H]_{k,k}b_k+\sum_{l\neq k}[\mathbf{M}\mathbf{R}_H]_{k,l}b_l+\zeta_k^M, \tag{5.23}$$

where the first term corresponds to desired signal, the second term represents ICI, and the last Gaussian noise. Having identified these terms, the SINR for sub-carrier k can be expressed, conditioned on the channel state, as

$$\begin{aligned}\gamma_k^M &= \frac{E\left[|[\mathbf{M}\mathbf{R}_H]_{k,k}b_k|^2\right]}{E\left[|\sum_{l\neq k}[\mathbf{M}\mathbf{R}_H]_{k,l}b_l|^2\right]+E[|\zeta_k^M|^2]}\\ &= \frac{|[\mathbf{M}\mathbf{R}_H]_{k,k}|^2}{\sum_{l\neq k}|[\mathbf{M}\mathbf{R}_H]_{k,l}|^2+\rho_k^M\sigma_\zeta^2}.\end{aligned} \tag{5.24}$$

ρ_k^M in Equation (5.24) is defined as the MMSE noise enhancement factor, and is given by $\rho_k^M=\sigma_{\zeta_k^M}^2/\sigma_{\zeta_k}^2=[\mathbf{M}\mathbf{R}_H\mathbf{M}^H]_{k,k}$, with $\sigma_{\zeta_k^M}^2=[\mathbf{R}_{\zeta^M}]_{k,k}$.

The SINR can also be obtained in terms of the minimum mean square error $\mathbf{e}$; first note that the transmitted symbols can be expressed as

$$\mathbf{b} = \mathbf{M}\mathcal{H}^H\mathbf{y} + \mathbf{e}. \tag{5.25}$$

Such representation, referred to in [71] as the backward channel model, is instrumental in deriving the expression for the MMSE-decision feedback interference canceller. Note that Equation (5.21) can be interpreted as the concatenation of a matched filter bank matrix $\mathcal{H}^H$, and the MMSE estimator matrix $\mathbf{M}$. Defining $\bar{\mathbf{y}} = \mathcal{H}^H\mathbf{y}$, $\mathbf{M}$ can be expressed by means of the Wiener-Hopf equation as ([72], p. 327)

$$\mathbf{M} = \mathbf{R}_{b\bar{y}}\mathbf{R}_{\bar{y}\bar{y}}^{-1}, \tag{5.26}$$

where $\mathbf{R}_{b\bar{y}}$ represents the cross-correlation matrix of $\bar{\mathbf{y}}$ and the transmitted signal vector, and $\mathbf{R}_{\bar{y}\bar{y}}$ the auto-correlation matrix of $\bar{\mathbf{y}}$. Using this notation the error covariance is given by [72]

$$\mathbf{R}_e = \mathbf{R}_{bb} - \mathbf{R}_{b\bar{y}}\mathbf{R}_{\bar{y}\bar{y}}^{-1}\mathbf{R}_{\bar{y}b}, \tag{5.27}$$

which, noting that $\mathbf{R}_H^H = \mathbf{R}_H$, yields

$$\begin{aligned} \mathbf{R}_e &= \mathbf{I} - \mathbf{R}_H^H(\mathbf{R}_H\mathbf{R}_H^H + \sigma_\zeta\mathbf{R}_H)^{-1}\mathbf{R}_H \\ &= (\mathbf{M}^{-1} - \mathbf{R}_H)\mathbf{M} \\ &= \sigma_\zeta^2\mathbf{M}. \end{aligned} \tag{5.28}$$

From Equation (5.25), and using the principle of orthogonality, it is possible to obtain the SINR, conditioned on the channel state, as

$$\gamma_k^M = \frac{E[|[\mathbf{M}\mathcal{H}^H\mathbf{y}]_k|^2]}{E[|e_k|^2]} = \frac{E[|b_k|^2] - E[|e_k|^2]}{E[|e_k|^2]} = \frac{1}{[\mathbf{R}_e]_{k,k}} - 1. \tag{5.29}$$

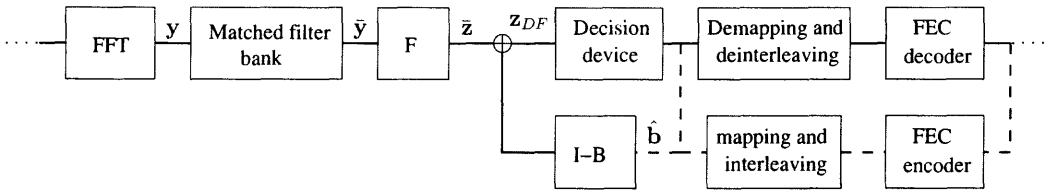

Figure 5.4 Block diagram of a receiver employing decision-feedback ICI cancellation.

5.4 Multiple Offset Decision-feedback ICI Cancellation

As it was shown in the previous section, ICI cancellation by linear methods (decorrelation or MMSE) results in noise enhancement, which degrades the receiver performance. A way to improve performance is decision-feedback ICI cancellation, which uses detected symbols to eliminate interference on succeeding symbols of an OFDM block. Receivers implementing decision-feedback ICI cancellation are described in this section, and their SINR is derived. The proposed scheme is shown in Figure 5.4, and consists of two linear matrix filters: the *feed-forward* filter and the *feedback* filter. After the matched filter bank, the feed-forward matrix $\mathbf{F}$ is used to transform the received signal. The signal is then fed to a decision device whose output is used as the input of the feedback filter. Clearly, the latter (denoted by matrix $\mathbf{I} - \mathbf{B}$) must be strictly causal, i.e. it must be triangular. With the decision-feedback principle, after a symbol carried on a sub-carrier is detected, it is subtracted from the signal on the other sub-carriers. The figure shows two possible feedback methods (dashed lines): either with hard decisions directly taken from the decision device, or with the final decisions after decoding and re-encoding. The latter method adds considerable complexity to the receiver but results in more reliable decisions being fed back. Decision feedback detection is implemented successively across all sub-carriers.

To perform decision feedback ICI cancellation the criteria in Section 5.3 are used, i.e. to completely rid the received signal of ICI, or to minimize the MMSE. The first approach is termed *decorrelating*, or *zero-forcing*, *decision feedback receiver* (D-DF),

while the second approach is termed *MMSE decision feedback receiver* (MMSE-DF). The expressions for feed-forward and feedback matrices, as well as the resulting SINR, are derived in the next subsections.

5.4.1 Decorrelating Decision Feedback

To analyze the decorrelating-decision feedback receiver, denote the received signal, after the matched filter bank in Figure 5.4, by

$$\bar{\mathbf{y}} = \mathbf{R}_H \mathbf{b} + \mathcal{H}^H \bar{\boldsymbol{\zeta}}. \tag{5.30}$$

The feed-forward and feedback matrices can be obtained from the Cholesky factorization of $\mathbf{R}_H$,

$$\mathbf{R}_H = \mathbf{X}^H \mathbf{D}_D^2 \mathbf{X}, \tag{5.31}$$

where $\mathbf{X}$ is upper triangular and all the elements of its diagonal are ones, and $\mathbf{D}_D^2$ is diagonal with real, positive elements (see Appendix B for a derivation of this result). Using, for the feed-forward filter of the detector,

$$\mathbf{F} := \mathbf{D}_D^{-2} (\mathbf{X}^H)^{-1}, \tag{5.32}$$

which is lower-triangular, the received signal, after processing, becomes

$$\bar{\mathbf{z}} = \mathbf{D}_D^{-2} (\mathbf{X}^H)^{-1} \bar{\mathbf{y}} = \mathbf{X}\mathbf{b} + \boldsymbol{\zeta}^{D-DF}, \tag{5.33}$$

where $\boldsymbol{\zeta}^{D-DF}$ is a Gaussian noise vector with covariance matrix $\mathbf{R}_{\zeta^{D-DF}} = \sigma_\zeta^2 \mathbf{D}_D^{-2}$. Based on the structure of $\mathbf{X}$, notice from Equation (5.33) that the N_s^{th} term is not perturbed by ICI, and therefore it can be detected without further processing. After detection, it can be subtracted (properly modified by the corresponding term in $\mathbf{X}$) from the other sub-carrier signals, eliminating its contribution to ICI. The detection

strategy is thus

$$\begin{aligned} \hat{b}_{N_s-1} &= \text{decision}(\bar{z}_{N_s-1}) \\ \hat{b}_{N_s-l} &= \text{decision}\left(\bar{z}_{N_s-l} - \sum_{i=1}^{l-1} X_{N_s-l,N_s-l+i}\ \hat{b}_{N_s-l+i}\right) \\ l &= 2, \cdots, N_s, \end{aligned}$$

meaning that the corresponding feedback matrix is given by

$$\mathbf{B} := \mathbf{X}. \tag{5.34}$$

Finally, the decision process can be expressed in matrix notation as

$$\hat{\mathbf{b}} = \text{decision}(\mathbf{D}_D^{-2}(\mathbf{X}^H)^{-1}\bar{\mathbf{y}} + (\mathbf{I} - \mathbf{X})\hat{\mathbf{b}}). \tag{5.35}$$

The SINR of the received signal was calculated assuming that all decisions are correct. In such case, the decision variables have no ICI, and the SINR for sub-carrier k is

$$\gamma_k^{D-DF} = \frac{E[|b_k|^2}{E[|\zeta_k^{D-DF}|^2]} = \frac{1}{\sigma_\zeta^2 \rho_k^{D-DF}} \tag{5.36}$$

where, as in the previous sections, $\rho_k^{D-DF} = [D^{-2}]_{k,k}$ is defined as the noise enhancement factor.

5.4.2 MMSE Decision Feedback

The MMSE-DF receiver has the same structure as the D-DF receiver, but it differs in the criterion used to derive its feed-forward and feedback matrices, which are chosen to minimize the mean square error, rather than to completely eliminate interference (as in Section 5.4.1). The error for the decision-feedback receiver is

$$\xi^{DF} = E[|\mathbf{b} - \mathbf{z}^{DF}|^2], \tag{5.37}$$

where $\mathbf{z}^{DF}$ is the received signal, after filtering by the feed-forward and feedback matrices, given by (ignoring decision errors)

$$\mathbf{z}^{DF} = \bar{\mathbf{z}} + (\mathbf{I} - \mathbf{B})\mathbf{b}, \tag{5.38}$$

from which it follows that

$$\xi^{DF} = E[|\mathbf{B}\mathbf{b} - \bar{\mathbf{z}}|^2]. \tag{5.39}$$

As in Section 5.3, the MMSE solution must minimize ξ_{DF}, or, equivalently, satisfy the principle of orthogonality,

$$E[(\mathbf{B}\mathbf{b} - \bar{\mathbf{z}})\bar{\mathbf{z}}^H] = 0. \tag{5.40}$$

From Equation (5.25) and noting that $\mathcal{H}^H\mathbf{y} = \bar{\mathbf{y}}$, $\bar{\mathbf{y}} = \mathbf{M}^{-1}(\mathbf{b} - \mathbf{e})$ results. Denote by $\mathbf{K}^H\mathbf{D}_M^2\mathbf{K}$ the Cholesky decomposition of $\mathbf{M}^{-1}$; $\mathbf{K}$ is upper-triangular, with all ones in the diagonal, and $\mathbf{D}_M^2$ is diagonal, with real, positive elements. The feed-forward filter is implemented by (see Appendix B for a derivation of this result)

$$\mathbf{F} := \mathbf{D}_M^{-2}(\mathbf{K}^H)^{-1}, \tag{5.41}$$

which is upper-triangular, to yield

$$\bar{\mathbf{z}} = \mathbf{D}_M^{-2}(\mathbf{K}^H)^{-1}\bar{\mathbf{y}} = \mathbf{K}\mathbf{b} + \tilde{\mathbf{e}}, \tag{5.42}$$

where the error was redefined as $\tilde{\mathbf{e}} = -\mathbf{K}\mathbf{e}$, which, using the result in Equation (5.28), has variance

$$R_{\tilde{\mathbf{e}}} = \sigma_\zeta^2\mathbf{K}\mathbf{M}\mathbf{K}^H = \sigma_\zeta^2\mathbf{D}_M^{-2}. \tag{5.43}$$

Since $\mathbf{K}$ in Equation (5.42) is upper triangular, data on the N_s^{th} sub-carrier can first be detected, and the interference it is causing on other terms can be canceled by

decision feedback. The detection strategy is similar to that for the D-DF receiver, and it can be described as

$$\begin{aligned} \hat{b}_{N_s-1} &= \text{decision}(\bar{z}_{N_s-1}) \\ \hat{b}_{N_s-l} &= \text{decision}\left(\bar{z}_{N_s-l} - \sum_{i=1}^{l-1} K_{N_s-l,N_s-l+i}\ \hat{b}_{N_s-l+i}\right) \\ l &= 2, \cdots, N_s, \end{aligned}$$

and the feedback matrix is given by

$$\mathbf{B} := \mathbf{K}. \tag{5.44}$$

Finally, as in the decorrelating-decision feedback receiver, the decision process is expressed in matrix notation as

$$\hat{\mathbf{b}} = \text{decision}(\mathbf{D}_M^{-2}(\mathbf{K}^H)^{-1}\bar{\mathbf{y}} + (\mathbf{I} - \mathbf{K})\hat{\mathbf{b}}). \tag{5.45}$$

To calculate the SINR, decision errors are ignored; under such assumption, the SINR for sub-carrier k is, as in Equation (5.29),

$$\gamma_k^{M-DF} = \frac{1}{[\mathbf{R}_{\tilde{\mathbf{e}}}]_{k,k}} - 1. \tag{5.46}$$

5.5 Numerical Results

In this section numerical results for the performance of the receivers previously derived are presented. First, for two transmitters with a fixed frequency offset, the mean SINR (averaged over the fading channel) as a function of mean SNR, and as a function of the offset, was calculated. The SINR distribution is also shown. Second, the performance of a SFN, with several transmitters contributing to the received signal was evaluated, with each transmitter having a random offset from the

nominal frequency, and undergoing a channel with independent fading and lognormal shadowing[3].

OFDM and channel parameters used in this section are summarized in Table 5.1. It is always assumed that the channel delay spread is shorter than the cyclic prefix to prevent ISI. While the parameters used are representative of a macro-cellular system, more simulations were carried out with different parameter sets (e.g. parameters from an indoor channel), yielding similar results. Performance of the conventional receiver and of a system with no offset is shown on all figures for comparison.

Table 5.1 Simulation Parameters

sub-carriers (N_s)	freq. spacing (Δ_f)	offset (ϵ^i)
128	50 kHz	$\pm$ 0.1, random in [-0.3,0.3]
transmitters (N_T)	**delay spread (τ_{rms})**	**shadowing std. dev. (σ)**
2,8	250 ns	8 dB

Figures 5.5 and 5.6 show numerical results of the average SINR of all proposed receivers for two-transmitter macrodiversity with frequency offsets. Both transmitters have same power and path loss (no shadowing), and channel fading is Rayleigh-distributed. Fading correlation among sub-carriers is generated according to an exponential delay spread (see Table 5.1 for the r.m.s. delay spread, τ_{rms}). Figure 5.5 shows the SINR as a function of an increasing offset ($\epsilon^1 = -\epsilon^2$), and Figure 5.6 shows the SINR as a function of SNR for an offset $\epsilon^1 = -\epsilon^2 = 0.1$. Figure 5.7 shows the cumulative distribution function (cdf) of the received SINR, for $\epsilon^1 = -\epsilon^2 = 0.1$,

[3]Results are limited to average SINR and its distribution, which provide an idea of how a system performs in terms BER without limiting the validity of the results to a particular modulation and coding scheme. Actual BER calculation is left as a topic for future research.

and SNR=20 dB. The cdf was calculated for the average SINR of all sub-carriers, rather than for the SINR of an individual sub-carrier.

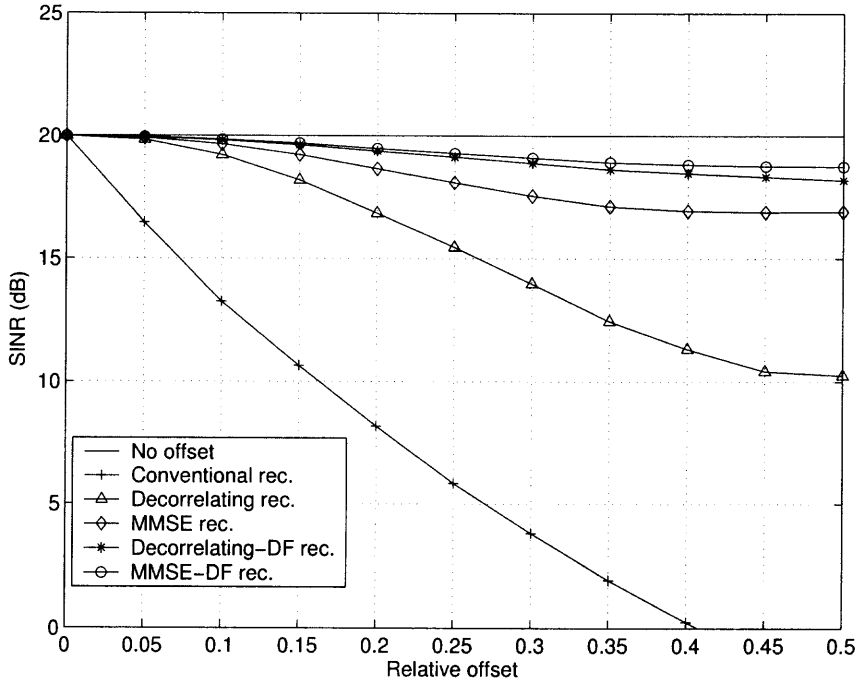

Figure 5.5 Average receiver SINR vs transmitter frequency offset on a Rayleigh fading channel, SNR=20 dB, $\epsilon^1 = -\epsilon^2$.

In order to simulate a SFN, a macrodiversity system with several nearby transmit stations contributing to the received signal was modeled (farther stations were assumed to arrive with larger delay than the cyclic prefix and thus to contribute to noise). In this case, to model poor frequency synchronization, different transmitters used a carrier frequency chosen randomly from the interval $[f_c - \epsilon_{max}\Delta f, f_c + \epsilon_{max}\Delta f]$, where f_c is the nominal carrier frequency, ϵ_{max} is the maximum relative offset, and Δf is the sub-carrier frequency spacing. Furthermore, signals undergo independent lognormal shadowing channels, with standard deviation of 8dB, for different transmitters[4].

Figures 5.8 and 5.9 show (respectively) received average SINR and outage probability of the SFN described, when the maximum offset is $\epsilon_{max} = 0.3$ and an outage

[4]The same parameters can be used for simulation of soft handoff. The main difference is that the latter usually involves only two transmitters, while a SFN involves more than two.

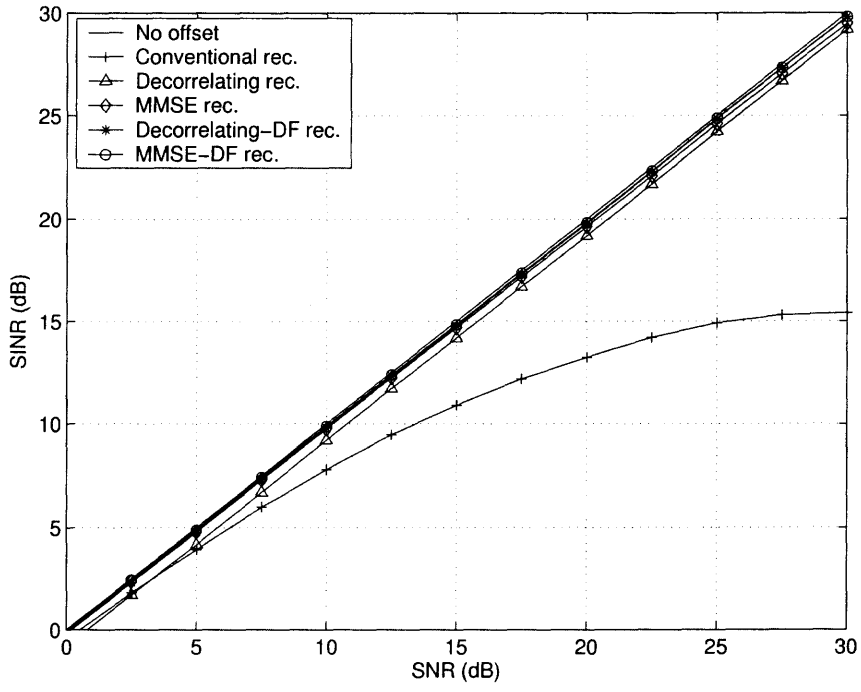

Figure 5.6 Average receiver SINR vs SNR on a Rayleigh fading channel, $\epsilon = \pm 0.1$.

is declared if the receiver SINR falls below 10 dB. In addition, Figure 5.10 shows the cdf of the received SINR for SNR=20dB. Dash-dotted lines correspond to a system with 2 contributing transmitters, while solid lines correspond to a system with 8. As before, the cdf is calculated on the average SINR of all sub-carriers. Notice that, with more contributing transmitters, the SINR of the conventional receiver decreased, due to its inability to synchronize to all transmitters. On the other hand, the SINR of the proposed receivers, which are robust to ICI, improved as a result of an increase in diversity (except for the decorrelating detector, whose performance deteriorated due to increased noise enhancement). Furthermore, in Figure 5.10 the cdf has a heavier tail than in Figure 5.7, which shows the effects of shadowing.

From figures 5.5-5.10 one can conclude that, with any of the proposed ICI cancellation receivers, robustness to transmitter frequency offsets was achieved, which performed almost as well as a system with no offset at all. It can also be seen from figures 5.6 and 5.8 that the SINR for a conventional receiver saturated at high SNR

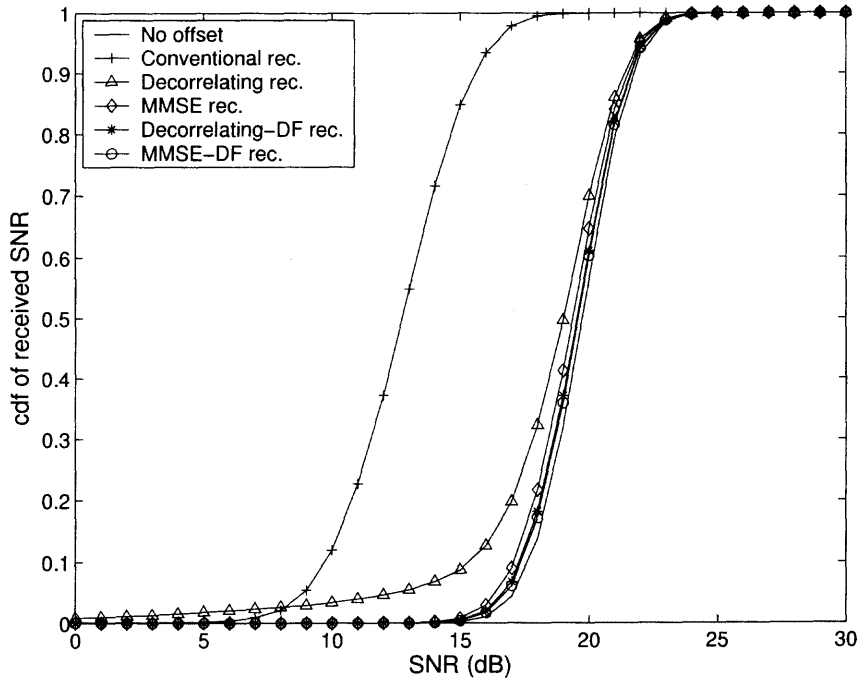

Figure 5.7 SINR cdf for SNR=20 dB, $\epsilon = 0.1$, Rayleigh fading channel.

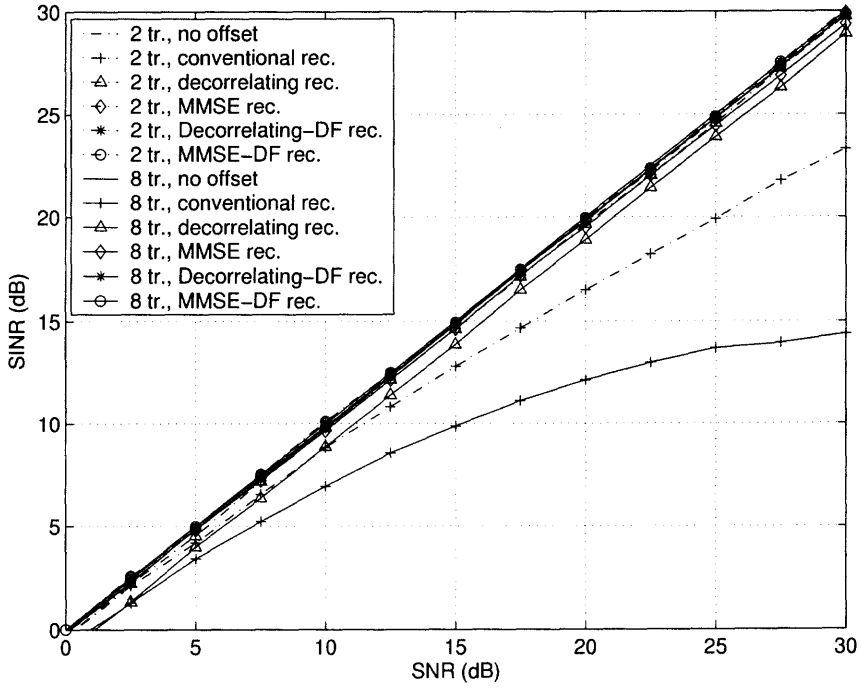

Figure 5.8 Average receiver SINR vs SNR for SFN simulation, with $\epsilon_{max} = 0.3$.

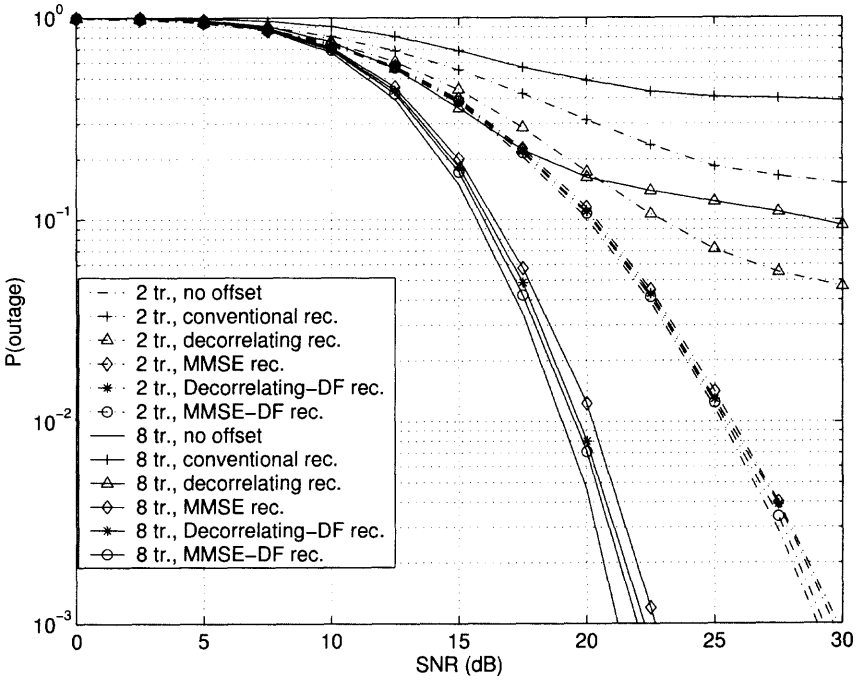

Figure 5.9 Outage probability for SFN simulation, with $\epsilon_{max} = 0.3$.

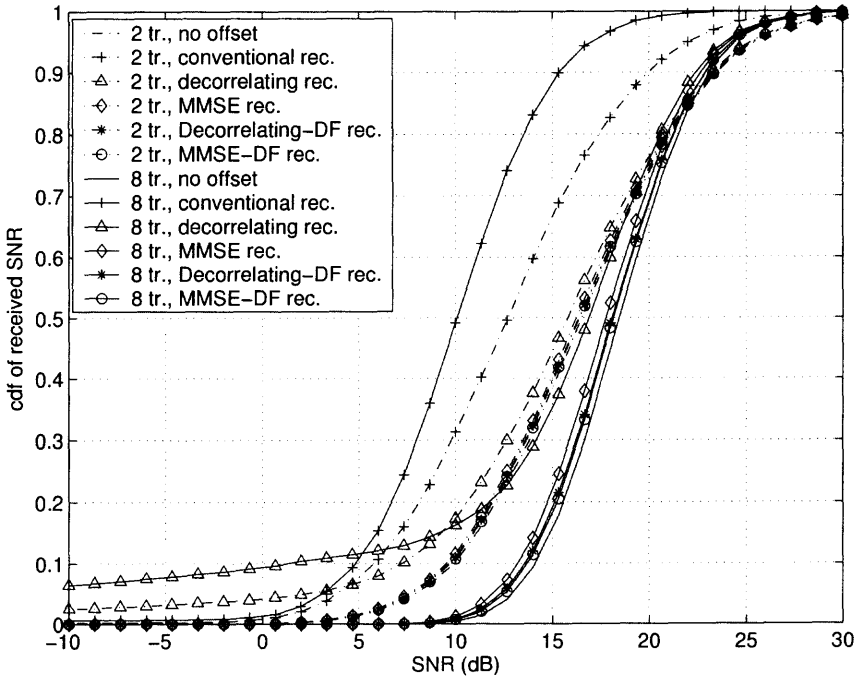

Figure 5.10 SINR cdf for SFN simulation, with SNR=20 dB, and $\epsilon_{max} = 0.3$.

levels, since ICI becomes dominant, while the SINR of ICI cancellation receivers did not. Furthermore, as expected, decision-feedback ICI cancellation outperformed linear, and MMSE-based detectors outperformed decorrelating-based, in terms of average received SINR and outage probability. However, improved performance comes at the expense of increased complexity: in the first case, because decision-feedback requires extra processing; and in the second, because MMSE requires knowledge of the received SNR, and of the transmitted signal amplitudes, while the decorrelating receiver does not.

5.6 Chapter Summary

This chapter analyzed the effects of multiple transmit frequency offsets on an OFDM system with macrodiversity. Multiple offsets may arise in macrodiversity systems, such as a single frequency networks, or cellular systems in soft handoff, as a result of poor frequency synchronization. It was shown that ICI resulting from frequency offsets severely degraded system performance, and expressions for the SINR degradation were obtained. It was also found that, in order to maximize the SINR, receivers must synchronize to the *average* received frequency, although that approach is not sufficient to mitigate strong ICI. In order to counter the effects of ICI, robust receivers, based on linear and decision-feedback ICI cancellation, were proposed. In either case, both decorrelating and MMSE solutions were given, as well as expressions for their SINR. Finally, simulation results showed significant performance improvement with these ICI cancellation receivers, which performed almost as well as a system with no offset at all.

CHAPTER 6

TIME-FREQUENCY DUALITY OF MC AND DS CDMA FOR MULTI-ANTENNA SYSTEMS

The combination of multiple antenna systems and CDMA offers high data rate multiuser wireless communications systems. The capacity of multiple transmit and receive antenna systems, or what is also known as multiple input-multiple output (MIMO) systems increases linearly with the number of antennas on rich scattering channels [34]. The existing literature suggests exploiting this increased capacity for multiuser systems by means of direct sequence (DS) CDMA. Research in this area has focused on receiver design. In [73] the Bell Labs layered space-time (BLAST) structure is used as the detection algorithm of a MIMO CDMA system. Among other proposals, in [74] a linear decorrelating detector is used, [75] includes transmit and receive filters, or beamformers, and [76] uses turbo-codes and iterative MMSE detection. MIMO MC-CDMA systems have also been proposed (see, e.g. [77–79]) offering significant capacity increases. DS and MC CDMA has been compared for single antenna systems by many authors [12, 13, 80–84], but such comparisons focus on performance results. It was observed that performance depends on factors not intrinsic to DS or MC CDMA, which causes the disparity in the results obtained by different authors.

A duality relationship between MIMO DS and MC CDMA systems, which provides the tools to effectively compare equivalent MC and DS CDMA systems on fading channels, and provides insight into what may determine any performance differences, is established in this chapter. With such duality and a system function representation of the channel a framework is formulated from which dual matched filter structures for MC and DS CDMA, a unified multiuser detection approach, and

a criterion for the selection of good spreading sequences are derived. Time-frequency duality between DS and MC CDMA in shown in Section 6.2. The significance of this relationship in TDFD channels is shown in Section 6.3. In Section 6.4, from the receiver matched filter structures of time dispersive (TD) channels, new structures for frequency dispersive (FD) and TDFD channels are presented. Further applications of duality can be found in the design of spreading sequences described in Section 6.5.

6.1 Multiple Antenna CDMA Systems

For both DS and MC CDMA, a system with N_t transmit and N_r receive antennas is considered. To achieve a higher rate per user it is assumed that a user data stream is divided into M substreams, which are then multiplied by a signature waveform (or spreading code) and transmitted simultaneously over L antennas, each with a different spreading code. Code allocation and transmit diversity should be performed so as to optimize the distribution of resources at the base station, namely power, spreading codes, and bandwidth (see [73] for more details). A general block diagram of a multiple antenna CDMA transmitter is shown in Figure 6.1. The IDFT blocks apply to MC-CDMA only. Prior to transmission, the MC-CDMA signal is converted from frequency domain to time domain by means of an IDFT, performed by the FFT algorithm. The fundamental difference between DS and MC CDMA is that, in DS-CDMA, spreading is performed in the time domain, whereas in MC-CDMA it is performed in the frequency domain. It is assumed that the channel is perfectly known at the receiver, and thus receiver beamforming filters are used, as part of the space-time (in DS-CDMA) or space-frequency (in MC-CDMA) matched filter, as it is explained in detail in Section 6.4.

The performance of a multiple antenna system is greatly influenced by the channel characteristics. The amount of scattering and the DOA distribution determine the spatial channel fading correlation. Channel correlation is of great relevance since it

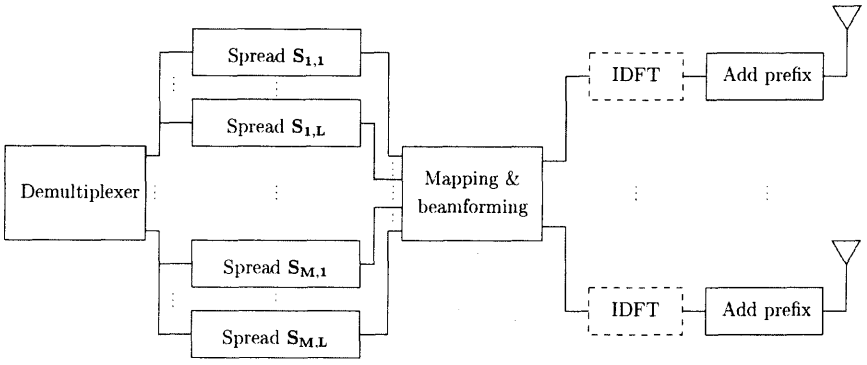

Figure 6.1 Multiple antenna CDMA transmitter with code diversity.

has been shown that the Shannon capacity of the system is directly proportional to the rank of the channel matrix [34]. A general model for a Gaussian WSS channel in delay, Doppler and DOA domains, like the one in [30, 31], is considered. The stationarity assumption allows us to fully characterize the channel by means of the space-time-frequency correlation function, $R(\Delta x, \Delta f, \Delta t)$, or the direction-delay-Doppler power spectrum $P(\Omega, \tau, \nu)$ [30], which are extensions of the functions defined in Section 2.3.3 to include the space domain. Such model is general enough to consider the effects of time selectivity (or time variance), frequency selectivity, and space selectivity.

6.2 Time-Frequency Duality of MC and DS CDMA

It is possible to show that MC and DS CDMA are duals by their expressions in time and frequency domains. The most general case involves the use of continuous signature waveforms, while an approach of practical interest, which allows for a finite sub-carrier implementation of MC-CDMA, restricts user signatures to be (usually binary) discrete sequences. Throughout this chapter it is assumed that the channel delay spread is much smaller than the symbol interval, so that ISI can be eliminated by inserting a guard interval between symbols without significantly penalizing spectral efficiency. Under this assumption the CDMA signals can be represented for one symbol period only without loss of generality, both for MC and DS.

Denote the spreading operation of a DS-CDMA symbol, in the discrete time domain, as

$$\mathbf{x}_{DS,i} = \mathbf{S}_i b_i, \tag{6.1}$$

where $\mathbf{S}_i = [\mathbf{s}_{i,1}^T, \mathbf{s}_{i,2}^T, \cdots, \mathbf{s}_{i,L}^T]^T$ is a column vector formed by the concatenation of L signature sequences each with processing gain N, used to transmit symbol b_i with diversity L[1]. Assuming that M symbols are transmitted in parallel, the transmitted signal is given by

$$\mathbf{x}_{DS} = \sum_{i=1}^{M} \mathbf{B}_{T,i}\mathbf{S}_i b_i = \mathbf{B}_T \mathbf{S}\mathbf{b}, \tag{6.2}$$

where $\mathbf{B}_{T,i}$, $NN_t \times NL$, maps $\mathbf{x}_{DS,i}$ onto the transmit antennas[2], $\mathbf{B}_T = [\mathbf{B}_{T,1}, \mathbf{B}_{T,2}, \cdots, \mathbf{B}_{T,M}]$, $\mathbf{S} = \text{diag}\{\mathbf{S}_1, \mathbf{S}_2, \cdots, \mathbf{S}_M\}$ is block-diagonal, and $\mathbf{b} = [b_1, b_2, \cdots, b_M]^T$.

In MC-CDMA the spreading operation is done in the frequency domain. A symbol is copied on N sub-carriers, multiplied by a signature sequence, and then transformed to the time domain using the IDFT, as in OFDM[3]. In order to avoid ISI, it is customary in MC-CDMA to add a guard interval with a cyclic prefix extension. In this section the transmitted signal is considered prior to the cyclic extension, and the discussion on the latter is deferred to Section 6.4. Denote the spreading of MC-CDMA symbols by

$$\mathbf{X}_{MC,i} = \tilde{\mathbf{S}}_i b_i, \tag{6.3}$$

---

[1]Parameter L represents the number of antennas used to transmit each symbol, satisfying $1 \leq L \leq N_t$

[2]If the channel is known at the transmitter, besides providing a mapping from spread symbols to transmit antennas, $\mathbf{B}_{T,i}$ can be designed as time-variant linear filter used for beamforming.

[3]We consider an implementation of MC-CDMA similar to the one in [85], [82].

where $\tilde{\mathbf{S}}_i = [\tilde{\mathbf{s}}_{i,1}^T, \tilde{\mathbf{s}}_{i,2}^T, \cdots, \tilde{\mathbf{s}}_{i,L}^T]^T$ denotes the MC-CDMA spreading sequences. The time domain signal is obtained after the IDFT, for $m = 0, \cdots, L-1$, as

$$[\mathbf{x}_{MC,i}]_n = \sum_{l=0}^{N-1} [\mathbf{x}_{MC,i}]_{l+mN} \exp(j2\pi \frac{l n_{mod\ N}}{N}) \ , \ n = mN, \cdots, (m+1)N-1, \quad (6.4)$$

where $n_{mod\ N}$ denotes the modulo-N operation on n. The modulo-N IDFT is represented in matrix notation as $\mathcal{F}_N^{-1}$, which, for L blocks is denoted by $\mathcal{F}_{L,N}^{-1} = \text{diag}\{\mathcal{F}_N^{-1}, \cdots, \mathcal{F}_N^{-1}\}$. Therefore, $\mathbf{x}_{MC,i} = \mathcal{F}_{L,N}^{-1} \tilde{\mathbf{S}}_i b_i$ and, for M symbols transmitted in parallel,

$$\mathbf{x}_{MC} = \sum_{i=1}^{M} \mathbf{B}_{T,i} \mathcal{F}_{L,N}^{-1} \tilde{\mathbf{S}}_i b_i = \mathcal{F}_{N_t,N}^{-1} \sum_{i=1}^{M} \mathbf{B}_{T,k} \tilde{\mathbf{S}}_i b_i = \mathcal{F}_{N_t,N}^{-1} \mathbf{B}_T \tilde{\mathbf{S}} \mathbf{b}. \quad (6.5)$$

Note that because $\mathbf{B}_{T,i}$ is a mapping of the spread symbols to the transmit antennas, it is composed of diagonal blocks $\mathbf{I}_N$, and therefore the order of $\mathcal{F}^{-1}$ and $\mathbf{B}_{T,i}$ can be reversed by changing the number of IDFT blocks in $\mathcal{F}^{-1}$.

Looking at the expressions for DS-CDMA and MC-CDMA in time and frequency domains notice the following:

- If $\tilde{\mathbf{S}} = \mathbf{S}$, i.e. the same signature sequences are used, then the MC-CDMA signal, before the IDFT, is $\mathbf{X}_{MC} = \mathbf{B}_T \mathbf{S} \mathbf{b}$, and $\mathbf{X}_{MC} = \mathbf{x}_{DS}$, which means that MC and DS CDMA modulators are dual elements. This relationship is displayed in the diagram of Figure 6.2, which contains the expressions for time and frequency domains.

- If $\tilde{\mathbf{S}} = \mathcal{F}_{ML,N} \mathbf{S}$, i.e. if the DFT of the spreading sequences of DS-CDMA is used for MC-CDMA, then $\mathbf{X}_{MC} = \mathbf{B}_T \mathcal{F}_{ML,N} \mathbf{S} \mathbf{b} = \mathcal{F}_{N_t,N} \mathbf{B}_T \mathbf{S} \mathbf{b} = \mathcal{F}_{N_t,N} \mathbf{x}_{DS}$, which means that MC and DS spreading are dual operators which represent CDMA spreading in time and frequency domains respectively, and $\mathbf{x}_{MC} = \mathcal{F}_{N_t,N}^{-1} \mathbf{B}_T (\mathcal{F}_{ML,N} \mathbf{S}) \mathbf{b} = \mathbf{B}_T \mathcal{F}_{ML,N}^{-1} \mathcal{F}_{ML,N} \mathbf{S} \mathbf{b} = \mathbf{B}_T \mathbf{S} \mathbf{b} = \mathbf{x}_{DS}$, so the output

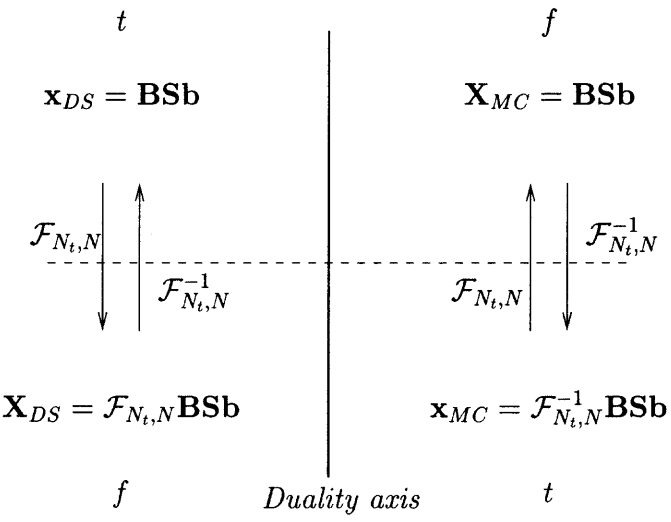

Figure 6.2 Duality diagram for DS and MC CDMA for equal spreading sequences $\tilde{\mathbf{S}} = \mathbf{S}$.

of the modulator is the same. Therefore $\mathbf{x}_{DS}$ and $\mathbf{X}_{MC}$ can also be viewed as implementations of the same CDMA system in dual domains.

It is possible to extend the duality relationship to continuous time and frequency domains, after pulse-shaping or windowing. Denote the DS-CDMA signal transmitted from antenna m, $m \in \{0, \cdots, N_t\}$, as

$$x^c_{DS,m}(t) = \sum_{n=0}^{N-1} [\mathbf{x}_{DS}]_{Nm+n}\, p(t - nN^{-1}T), \tag{6.6}$$

where T is the symbol period, and $p(t)$ denotes the pulse shape, which is assumed to be a Nyquist pulse with respect to the sampling frequency $F_s = NT^{-1}$. $p(t)$ determines the duration and bandwidth of a DS-CDMA chip, which is assumed to be approximately $N^{-1}T$ seconds and NT^{-1} Hz respectively. As mentioned earlier, MC-CDMA uses the multicarrier structure of OFDM. Therefore, spectral shaping is carried out by means of a time window $w(t)$ on the time-domain signal. Denote the windowed MC-CDMA signal transmitted from antenna m as

$$x^c_{MC,m}(t) = w(t) \sum_{l=0}^{N-1} [\mathbf{X}_{MC}]_{Nm+l} e^{j2\pi l T^{-1} t}, \tag{6.7}$$

and in the frequency domain

$$\begin{aligned} X^c_{MC,m}(f) &= \int w(t) \sum_{l=0}^{N-1} [\mathbf{X}_{MC}]_{Nm+l} e^{j2\pi l T^{-1} t} e^{-j2\pi f t}\, dt \\ &= \sum_{l=0}^{N-1} [\mathbf{X}_{MC}]_{Nm+l} \int w(t) e^{j2\pi l T^{-1} t} e^{-j2\pi f t}\, dt \\ &= \sum_{l=0}^{N-1} [\mathbf{X}_{MC}]_{Nm+l} W(f - lT^{-1}), \end{aligned} \tag{6.8}$$

where $W(f)$ denotes the Fourier transform of $w(t)$. The window function defines the duration and bandwidth of a MC-CDMA chip, that is assumed to be approximately T seconds and T^{-1} Hz, which is different from that of a DS-CDMA chip. From Equations (6.6) and (6.8) it is concluded that pulse shaping and windowing are dual operations. The DS-CDMA signal of antenna m in the frequency domain, obtained from Equation (6.6) completes the duality and is given by

$$\begin{aligned} \mathbf{X}^c_{DS,m}(f) &= \int \sum_{n=0}^{N-1} [\mathbf{x}]_{DS,Nm+n}\, p(t - nN^{-1}T) e^{-j2\pi f t}\, dt \\ &= \sum_{n=0}^{N-1} [\mathbf{x}]_{DS,Nm+n} \int \left[p(t) * \delta(t - nN^{-1}T)\right] e^{-j2\pi f t}\, dt \\ &= P(f) \sum_{n=0}^{N-1} [\mathbf{x}]_{DS,Nm+n} e^{j2\pi n N^{-1} T f}, \end{aligned} \tag{6.9}$$

where $P(f)$ is denotes the Fourier transform of $p(t)$.

The results on duality can be further generalized to systems using random sequences or continuous waveforms. For random sequences the following definition on the duality of random processes is needed [26]:

Definition 1 *Two random processes are statistically dual if their individual statistics are dual functions.*

If $s_{i,j}$ and $\tilde{s}_{i,j}$ are identically distributed random processes (e.g. random binary sequences), they are statistically dual, since they are defined in dual domains. As a result, DS and MC CDMA signals are statistically dual.

For continuous waveforms the DS-CDMA signal vector is denoted by

$$\mathbf{x}_{DS}^{c}(t) = \mathbf{B}_{T}^{c}\mathbf{S}^{c}(t)\mathbf{b}, \tag{6.10}$$

where the superscript ^{c} stands for continuous waveforms, $\mathbf{S}^{c}(t) = \text{diag}\{\mathbf{s}_1^c(t), \mathbf{s}_2^c(t), \cdots, \mathbf{s}_M^c(t)\}$, with $\mathbf{s}_i^c(t) = [s_{i,1}^c(t); s_{i,2}^c(t); \cdots; s_{i,L}^c(t)]^T$ containing the waveforms used to spread the i^{th} symbol b_i. The waveforms are constrained to have their energy concentrated within $t \in [0, T]$ and within the frequency band $f \in [-NT^{-1}/2, NT^{-1}/2]$. In MC-CDMA, the signature waveform is used in the frequency domain and the time-domain signal is obtained with an inverse Fourier Transform (IFT). Note that by using a continuous signature waveform it is implicitly assumed that MC-CDMA is using an infinite number of sub-carriers, hence the use of the continuous IFT rather than the corresponding IDFT used in discrete domains. Denote the MC-CDMA signal vector by

$$\mathbf{x}_{MC}^{c}(t) = \int \mathbf{B}_{T}^{c}\tilde{\mathbf{S}}^{c}(f)\mathbf{b}e^{j2\pi ft}\, df, \tag{6.11}$$

where $\tilde{\mathbf{S}}^{c}(f)$ and $\mathbf{B}_{T}^{c}$ are the corresponding spreading sequence matrix and the mapping to the N_t antennas for MC-CDMA. The corresponding expressions for DS and MC CDMA in the frequency domain are as follows:

$$\mathbf{X}_{DS}^{c}(f) = \int \mathbf{B}_{T}^{c}\mathbf{S}^{c}(t)\mathbf{b}e^{-j2\pi ft}\, dt \tag{6.12}$$

$$\mathbf{X}_{MC}^{c}(f) = \mathbf{B}_{T}^{c}\tilde{\mathbf{S}}^{c}(f)\mathbf{b}. \tag{6.13}$$

From Equations (6.10)-(6.13) and (6.11)-(6.12):

- If the same (conveniently translated and scaled) spreading waveform is used in DS and MC-CDMA in time and frequency domains respectively, then the DS and MC-CDMA modulators, together with their respective beamformers, are dual devices.

- If $\tilde{\mathbf{S}}^c(f) = \int \mathbf{S}^c(t)e^{-j2\pi ft}\, dt$, i.e. the frequency-domain spreading waveform in MC-CDMA is set to the FT of the time-domain spreading sequence of the DS-CDMA system, then, as for discrete sequences, $\mathbf{X}^c_{MC}(f) = \mathbf{B}^c_T \int \mathbf{S}^c(t)e^{-j2\pi ft}\, dt\, \mathbf{b}$ $= \int \mathbf{x}^c_{DS}(t)e^{-j2\pi ft}\, dt$, which means that Equations (6.10)-(6.13) define dual operators, and DS-CDMA and MC-CDMA are dual descriptions of the same CDMA system.

As it was already mentioned, the beamformer can be optimized for a particular channel if it is known at the transmitter. In that case symbol mapping is replaced by a transmit beamformer, which is matched to the channel, and

$$\mathbf{x}^c_{DS}(t) = \mathbf{B}^c_T(t,\tau) * \mathbf{S}^c(t)\mathbf{b} \tag{6.14}$$

$$\mathbf{X}^c_{MC}(f) = \tilde{\mathbf{B}}^c_T(f,\nu) * \tilde{\mathbf{S}}^c(f)\mathbf{b}, \tag{6.15}$$

where $\mathbf{B}^c_T(t,\tau)$ and $\tilde{\mathbf{B}}^c_T(f,\nu)$ denote beamforming time-variant filter and frequency-variant frequency domain filter matrices, respectively. The corresponding expressions for DS and MC CDMA with transmit beamforming in frequency and time domains can be similarly obtained.

A final remark on duality regards self-dual sequences. A sequence is self-dual if it is the same in time and frequency domains, which means it is invariant to a DFT. Similarly, a random sequence is self-dual if it has the same distribution as its DFT (an example of a random self-dual sequence is an i.i.d. complex Gaussian sequence). If signature sequences, deterministic or random, are self-dual, then the DS and MC CDMA signals in time and frequency domains are equal, or equally distributed.

6.3 Time and Frequency Dispersive MIMO Channels

Wireless channels are often both time and frequency dispersive. Multipath propagation causes time dispersion when paths have different delays, and transmitter or receiver movement causes Doppler frequencies which cause frequency dispersion. The

effects of a TDFD channel on MC and DS CDMA signals are analyzed using a description based on system functions, including spatial correlation [31]. Time and frequency dispersion can lead to frequency selectivity and time variation. A channel is considered to be frequency-selective (FS) if its response is not constant over the signal bandwidth. Similarly, it is considered to be time-variant (TV) if its response is not constant over a symbol period.

Assume the channel response is doubly spread in time and frequency, with dispersion in time limited to τ and in frequency limited to ν. Assume also that the channel is underspread, i.e. its time-bandwidth product satisfies $\tau\nu \ll 1$, and therefore it can be estimated at the receiver. For a CDMA signal, define the chip signal bandwidth and duration as B_c and T_c respectively. For DS-CDMA, a symbol bandwidth satisfies $B = B_c$, and its period $T = NT_c$. For MC-CDMA, $B = NB_c$, and $T = T_c$. If the chip pulse satisfies $B_cT_c \approx 1$, it results in a CDMA symbol time-bandwidth product of $BT = NB_cT_c \approx N$ for both DS and MC. Define the coherence time of the channel as the minimum time separation t_{coh} so that the correlation $R(0, 0, t_{coh}) = 0$, and the coherence bandwidth as the minimum frequency separation B_{coh} satisfying $R(0, f_{coh}, 0) = 0$[4]. The channel is selective in frequency only, or *time-flat, frequency-selective* if $b_{coh} < B$ and $t_{coh} \gg T$. This is typical of a CDMA system with short chip pulses and a small processing gain N, which corresponds to a system with a few users and high data rate. On the other hand, the channel is selective in time only, or *time-selective, frequency-flat* if $t_{coh} < T$ and $b_{coh} \gg B$, which corresponds to a CDMA system with longer chip pulses and large spreading gain (e.g. with a large number of low-rate users). Finally, the channel is doubly dispersive in time and frequency if both $t_{coh} < T$ and $b_{coh} < B$. These situations are shown in the diagram of Figure 6.3.

[4]Coherence bandwidth and time in wireless channels are often approximated from the r.m.s. delay spread, τ_{rms}, as $B_{coh} \approx \frac{1}{2\pi\tau_{rms}}$, and from the maximum Doppler spread as $t_{coh} \approx \nu^{-1}$.

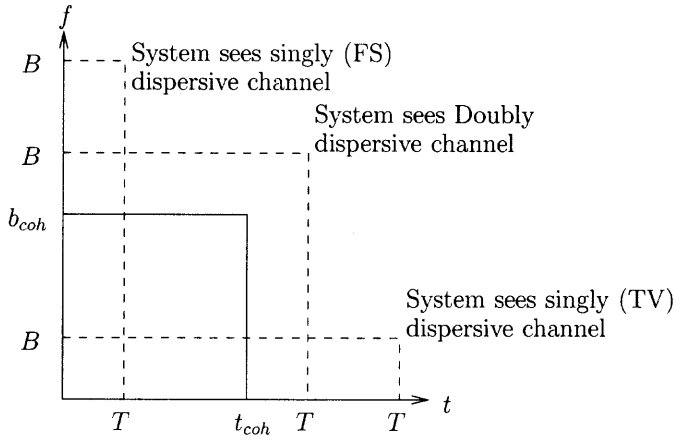

Figure 6.3 Different CDMA systems on a dispersive channel.

Let us characterize an $N_r \times N_t$ MIMO TDFD channel in the time domain by its matrix *input delay-spread function*, $\mathbf{G}^c(t,\tau)$, which represents the continuous time channel as a function of time and delay spread [5]. $\mathbf{G}^c(t,\tau)$ can be obtained from any of the system functions for space-time-frequency WSS channels. A straightforward method to obtain the columns of $\mathbf{G}^c(t,\tau)$ is sampling what Kattenbach [31] defines as the *Time-and-Aperture-Variant Impulse Response*, $g(t,\tau,x)$, where x denotes position in space (within the appropriate set of coordinates), at the position of each receive antenna elements. Repeating the procedure for all transmit antennas all the columns in $\mathbf{G}^c(t,\tau)$ can be obtained. The received signal for DS-CDMA can then be expressed as

$$\mathbf{y}^c_{DS}(t) = \int \mathbf{G}^c(t,\tau)\mathbf{x}^c_{DS}(t-\tau)\,d\tau + \boldsymbol{\eta}^c(t). \tag{6.16}$$

$\boldsymbol{\eta}^c(t)$ represents a vector of AWGN with covariance matrix $\mathbf{R}_{\boldsymbol{\eta}} = \sigma^2\mathbf{I}_{N_r}$.

For MC-CDMA it is more convenient to express the signal in the frequency domain, therefore the received signal is denoted by

$$\mathbf{Y}^c_{MC}(f) = \int \mathbf{H}^c(f,\nu)\mathbf{X}^c_{MC}(f-\nu)\,d\nu + \boldsymbol{\zeta}^c(t), \tag{6.17}$$

[5] the notation in [27] is retained, but using capital letters to denote matrix, rather than scalar, channels.

where $\mathbf{H}^c(f,\nu)$, $N_r \times N_t$, is defined as the matrix *input Doppler-spread function*, which represents the channel as a function of frequency and Doppler spread and is a dual operator of $\mathbf{G}^c(t,\tau)$. As another system function, $\mathbf{H}^c(f,\nu)$ can be obtained from $\mathbf{G}^c(t,\tau)$ by a direct and inverse Fourier transformation in time and delay domains respectively. Otherwise, it can be obtained by sampling the *Doppler-Resolved Aperture-Variant Transfer function* [31], $H(\nu,f,x)$, at the position of every receive antenna and repeating the procedure for every transmit antenna.

At the receiver, a beamformer performs match-filtering of the space-time channel, and subsequently the user's signal is despread by correlating it with the spreading waveform, yielding

$$\begin{aligned}\mathbf{z}^c_{DS} &= \int_{T_B}^{T_B+T} (\mathbf{S}^c(t-T_B))^T \mathbf{B}^c_R(t,\tau) * \mathbf{y}^c_{DS}(t)\, dt \\ &= \int_{T_B}^{T_B+T} (\mathbf{S}^c(t-T_B))^T \mathbf{B}^c_R(t,\tau) * \mathbf{G}^c(t,\tau) * \mathbf{B}^c_T \mathbf{S}^c(t)\mathbf{b}\, dt + \boldsymbol{\xi}^c_{DS}, \quad (6.18)\end{aligned}$$

where a delay T_B is introduced to retain causality of the receive beamformer, which is matched to the channel. Similarly, for MC-CDMA,

$$\begin{aligned}\mathbf{Z}^c_{MC} &= \int_{\frac{-N}{2T}}^{\frac{N}{2T}} (\tilde{\mathbf{S}}^c(f))^T \tilde{\mathbf{B}}^c_R(f,\nu) * \mathbf{Y}^c_{MC}(f)\, df \\ &= \int_{\frac{-N}{2T}}^{\frac{N}{2T}} (\tilde{\mathbf{S}}^c(f))^T \tilde{\mathbf{B}}^c_R(f,\nu) * \mathbf{H}^c(f,\nu) * \tilde{\mathbf{B}}^c_T \tilde{\mathbf{S}}^c(f)\mathbf{b}\, df + \boldsymbol{\xi}^c_{MC}. \quad (6.19)\end{aligned}$$

A look at Equations (6.16)-(6.19) reveals an interesting relationship between DS and MC CDMA. When they are used upon dual channels (i.e. channels a and b having input delay-spread and input Doppler-spread functions that satisfy $\mathbf{G}^c_a(t,\tau) = \mathbf{H}^c_b(f,\nu)$), then:

- If the same spreading sequences are used, i.e. $\tilde{\mathbf{S}}^c(f) = \mathbf{S}^c(t)$, the whole transmitter-channel-receiver chains are dual systems, resulting in the received signal being identical. Furthermore the receiver noise has the same covariance matrix;

therefore both CDMA systems will exhibit the same performance. More generally, one can say that Frequency dispersion and Time dispersion have equivalent effects on MC and DS CDMA.

- If $\mathbf{G}_a^c(t,\tau) = \mathbf{G}_a^c(\tau)$, i.e. channel a is frequency dispersive only, and DS-CDMA is used, then the performance of MC-CDMA on channel b, which is time-dispersive only and therefore $\mathbf{H}_b^c(f,\nu) = \mathbf{H}_b^c(\nu)$, is the same. Furthermore, one can expect the transceiver design to be also dual, with the same structures being implemented on dual domains. The same conclusion can be reached for the dual case when $\mathbf{G}_a^c(t,\tau) = \mathbf{G}_a^c(t)$, i.e. channel a is time dispersive only.

This relationship is shown on Figure 6.4 for all possible cases. This conclusion is possible because channels of the form $\mathbf{G}_1^c(t,\tau) = \mathbf{H}_2^c(f,\nu)$ have eigenvalue decompositions yielding equal eigenvector distributions. Such channels are said to be equivalent [28]. The same conclusion can be drawn deriving the received signal of DS and MC CDMA in terms of the matrix *channel delay-Doppler spread function* $\mathbf{U}^c(\nu,\tau)$ and *Doppler-delay spread function* $\mathbf{V}^c(\tau,\nu)$ [27]:

$$\mathbf{y}_{DS}^c(t) = \int\int \mathbf{U}^c(\tau,\nu)\mathbf{x}_{DS}^c(t-\tau)e^{j2\pi\nu t}\,d\tau d\nu \tag{6.20}$$

$$\mathbf{Y}_{MC}^c(f) = \int\int \mathbf{V}^c(\nu,\tau)\mathbf{X}_{MC}^c(f-\nu)e^{-j2\pi\tau f}\,d\nu d\tau. \tag{6.21}$$

Noting that Equations (6.20) and (6.21) are identical in terms of dual variables f-t and τ-ν and dual channel functions **U**-**V**, it can also be concluded that dual delay and Doppler dispersion has equivalent effects on dual signals (DS and MC CDMA).

6.4 Dual Matched Filter Structures

A discrete-time, discrete-frequency domain representation of the received signal, which takes into account the effects of the dispersive channel, is used in this section to see the implications of the results in the previous section to CDMA design. TDFD channels

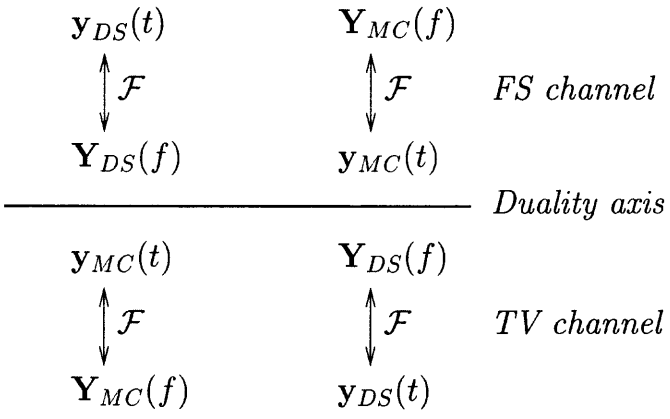

Figure 6.4 Double duality diagram for DS and MC CDMA on TD and FD channels.

distort CDMA signals by increasing its duration and bandwidth. If the channel has time dispersion (delay spread) of τ_D its duration is increased to $T_y = T + \tau_D$. DS and MC CDMA cope with time dispersion by inserting a guard interval or a cyclic prefix between symbols. If the channel has frequency dispersion (Doppler spread) of $\pm B_D$, the symbol bandwidth is increased to $B_y = B + B_D$. In the following sections it is shown that the dual counterparts of guard interval and cyclic prefix play a role in frequency dispersive channels, leading to simplified matched filter structures. A receiver structure for TDFD channels will also be derived based on an approximate discrete-time model of the channel.

6.4.1 Frequency-selective MIMO Channels

Here the channel input delay-spread function is a time-invariant, frequency-selective filter $\mathbf{G}(t,\tau) = \mathbf{G}(\tau)$. It is assumed that the channel response spans L_T chip intervals, and that $L_T \ll N$. The discrete-time channel input delay-spread function, from transmit antenna n_t to receive antenna n_r, is given by $g_{n_t,n_r}(n) := [r(t) * [\mathbf{G}]_{n_t,n_r}(t) * p(t)]_{t=nT}$, where $p(t)$ and $r(t)$ are the transmitter chip pulse waveform and receiver matched filter, respectively. The symbol period should be extended to $N_{GI} \geq N + L_T$ chips to avoid ISI.

In DS-CDMA the additional samples of the symbol period are set to zero as a guard interval. This operation is represented by $\mathbf{\Theta}_{DS,t}$, a block-diagonal matrix containing blocks $\mathbf{\Theta}^m_{DS,t} = [\mathbf{I}_N; \mathbf{0}_{N \times L_T}]^T$. From Equation (6.2), the discrete-time received signal is given by

$$\mathbf{y}_{DS} = \mathbf{G}\mathbf{\Theta}_{DS,t}\mathbf{B}_T\mathbf{S}\mathbf{b} + \boldsymbol{\eta}. \tag{6.22}$$

$\mathbf{G}$ consists of $N_r N_t$ blocks of size $N_{GI} \times N_{GI}$ given by $[\mathbf{G}_{n_t,n_r}]_{i,j} = g_{n_t,n_r}(i-j)$, which have Toeplitz structure. The receiver matched filter consists of the receive beamforming matrix $\mathbf{B}_R$, composed of MLN_r blocks $\mathbf{B}_R^{n_r,m}$ each of size $N \times N_{GI}$ representing matrix filters for the n^{th} antenna onto the l^{th} spread i^{th} symbol, and despreading matrix, $\mathbf{S}^T$. Matching the receive beamformer to the channel, $\mathbf{B}_R = (\mathbf{G}\mathbf{\Theta}_{DS,t}\mathbf{B}_T)^H$. Since the channel is time-invariant, so is $\mathbf{B}_R$, and its implementation has the structure of a Rake receiver in space and time, or 2D Rake, shown in Figure 6.5. The received signal, after despreading, can be expressed as

$$\mathbf{z}_{DS} = \mathbf{S}^T\mathbf{B}_T^H\mathbf{\Theta}_{DS,t}^H\mathbf{G}^H\mathbf{y}_{DS} = \mathbf{S}^T\mathbf{B}_T^H\mathbf{\Theta}_{DS,t}^H\mathbf{G}^H\mathbf{G}\mathbf{\Theta}_{DS,t}\mathbf{B}_T\mathbf{S}\mathbf{b} + \boldsymbol{\xi}_{DS}. \tag{6.23}$$

In MC-CDMA the additional samples are used to cyclically extend the symbol. This is done by adding the last L_T chips of a MC-CDMA symbol in the time domain (after the IDFT), and removing them at the receiver. This is represented by processing at the transmitter with block-diagonal matrix $\mathbf{\Theta}_{MC,t}$, consisting of n_t blocks $\mathbf{\Theta}^m_{MC,t} = [\mathbf{I}_{N,L_T}; \mathbf{I}_N]^T$, where $\mathbf{I}_{N,L_T}$ denotes a matrix consisting of the last L_T columns of the identity matrix $\mathbf{I}_N$, and by processing at the receiver with block-diagonal matrix $\mathbf{\Xi}_{MC,t}$, whose blocks are $\mathbf{\Xi}^m_{MC,t} = [\mathbf{0}_{N \times L_T}; \mathbf{I}_N]$. From Equation (6.5), the discrete-time received signal is

$$\mathbf{y}_{MC} = \mathbf{G}\mathbf{\Theta}_{MC,t}\mathcal{F}^{-1}_{N_t,N}\mathbf{B}_T\tilde{\mathbf{S}}\mathbf{b} + \boldsymbol{\eta}. \tag{6.24}$$

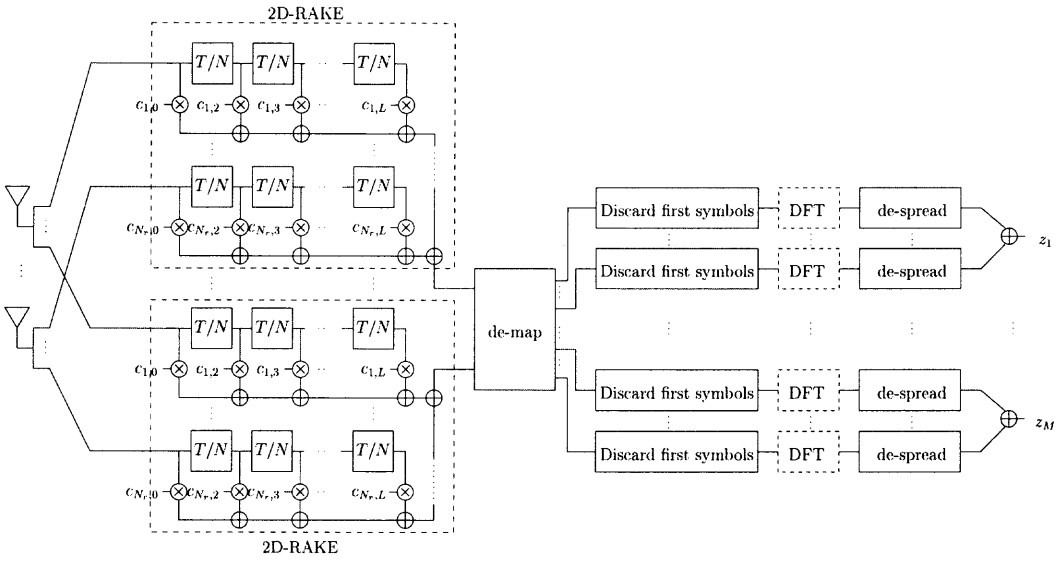

Figure 6.5 2D Rake receiver for DS-CDMA on TD channels and MC-CDMA on FD channels.

As a result of cyclic prefix addition and removal $\Xi^m_{MC,t}\mathbf{G}_{n_r,n_t}\Theta^m_{MC,t}$ become circulant. Since the DFT matrix diagonalizes circulant matrices, $\mathcal{F}_N\Xi^m_{MC,t}\mathbf{G}_{n_r,n_t}\Theta^m_{MC,t}\mathcal{F}_N^{-1}$ are diagonal. Defining $\bar{\mathbf{H}} = \mathcal{F}_{N_r,N}\Xi_{MC,t}\mathbf{G}\Theta_{MC,t}\mathcal{F}^{-1}_{N_t,N}$ the received signal after despreading is

$$\mathbf{z}_{MC} = \tilde{\mathbf{S}}^T\mathbf{B}_R^H\bar{\mathbf{H}}\mathbf{B}_T\tilde{\mathbf{S}}\mathbf{b} + \boldsymbol{\xi}_{MC}, \tag{6.25}$$

which indicates that to match the receiver beamformer to the channel it must be $\mathbf{B}_R := (\bar{\mathbf{H}}\mathbf{B}_T)^H$. An implementation of $\mathbf{B}_R$ is shown in Figure 6.7, where it can be seen that the structure corresponds to a maximal ratio combiner (MRC).

6.4.2 Time-variant MIMO Channels

It was shown in Section 6.3 that time-variant channels are the time-frequency duals of frequency selective channels. Consequently the channel input Doppler-spread function is a frequency-invariant frequency domain filter $H(f,\nu) = H(\nu)$, which means that it can be characterized in the time domain by a time-varying multiplicative coefficient. It is assumed that Doppler spread spans L_F MC-CDMA chip intervals, and that

$L_F \ll N$. The discrete-time channel input Doppler-spread function, from transmit antenna n_t to receive antenna n_r, is $H_{n_t,n_r}(k) := [R(f) * [\mathbf{H}]_{n_t,n_r}(t) * P(f)]_{f=kT^{-1}}$, where $P(f)$ and $R(f)$ are the transmitter chip pulse spectrum and receiver matched filter spectrum, respectively. Channel duality can be used to determine the receiver structures of dual MC and DS CDMA. A first consequence is that the symbol bandwidth shall be extended to $N_{GI} \geq N + L_F$ chips.

For MC-CDMA the additional L_F samples shall be set to zero, as a guard band to prevent Doppler spread from causing out-of-band interference, and then discarded at the receiver[6]. This operation is denoted by matrix $\mathbf{\Theta}_{MC,f} := \mathbf{\Theta}_{DS,t}$ defined earlier[7], and the discrete-frequency received signal is

$$\mathbf{Y}_{MC} = \mathbf{H}\mathbf{\Theta}_{MC,f}^{T}\mathbf{B}_T\tilde{\mathbf{S}}\mathbf{b} + \boldsymbol{\zeta}. \tag{6.26}$$

With these provisions, DS-CDMA and MC-CDMA are system duals, as shown in Figure 6.6(a). Consequently, the matched filter for MC-CDMA on frequency-dispersive channels is $\mathbf{B}_R = \mathbf{B}_T^H\mathbf{\Theta}_{MC,f}^{T}\mathbf{H}^H$, which has an identical structure as the matched filter for DS-CDMA in TD channels (shown in Figure 6.5), and corresponds to a space-frequency rake receiver. The received signal after despreading is therefore

$$\mathbf{z}_{MC} = \tilde{\mathbf{S}}^T\mathbf{B}_T^H\mathbf{\Theta}_{MC,f}^{T}\mathbf{H}^H\mathbf{y}_{MC} = \tilde{\mathbf{S}}^T\mathbf{B}_T^H\mathbf{\Theta}_{MC,f}^{T}\mathbf{H}^H\mathbf{H}\mathbf{\Theta}_{MC,f}^{T}\mathbf{B}_T\tilde{\mathbf{S}}\mathbf{b} + \boldsymbol{\xi}_{MC}. \tag{6.27}$$

For DS-CDMA, denote the insertion of a cyclic guard band (dual of cyclic prefix) at the transmitter, in the frequency domain, and its removal at the receiver by $\mathbf{\Theta}_{DS,f} := \mathbf{\Theta}_{MC,t}$, and $\mathbf{\Xi}_{DS,f} := \mathbf{\Xi}_{MC,t}$, respectively. The received signal is given by

$$\mathbf{Y}_{DS} = \mathbf{H}\mathbf{\Theta}_{MC,t}\mathcal{F}_{N_t,N}\mathbf{B}_T\mathbf{S}\mathbf{b} + \boldsymbol{\zeta}. \tag{6.28}$$

[6]This operation is described for strict duality of the notation. The transmitter simply does not transmit on those sub-carriers.

[7]The guard interval in time is left at the end of the symbol assuming that the receiver is synchronized to the path with least delay. Similarly, the guard band is concentrated on one side assuming that the receiver is synchronized to the path with lowest frequency shift.

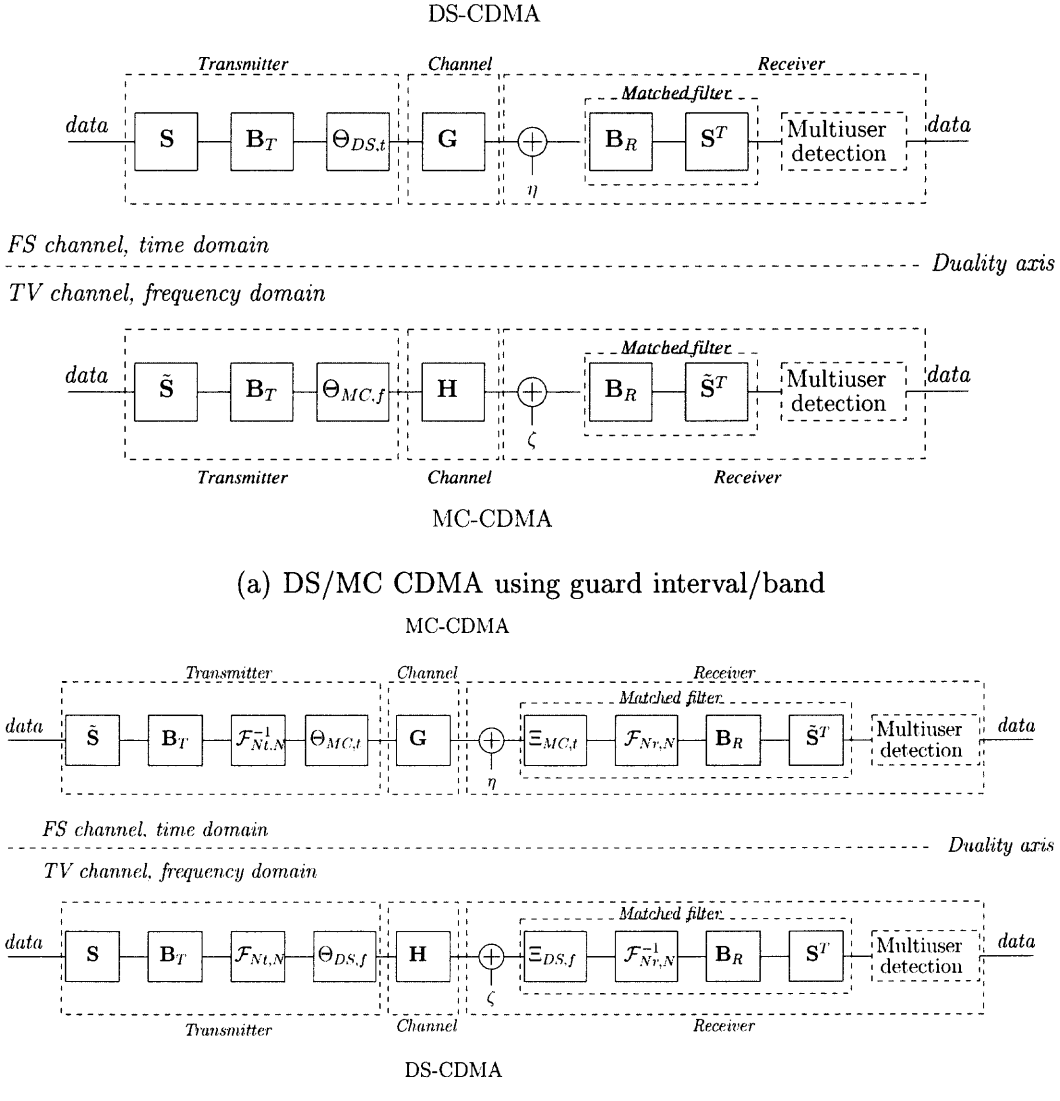

(a) DS/MC CDMA using guard interval/band

(b) MC/DS CDMA using cyclic prefix/band

Figure 6.6 Duality of DS and MC CDMA on FSTV channels.

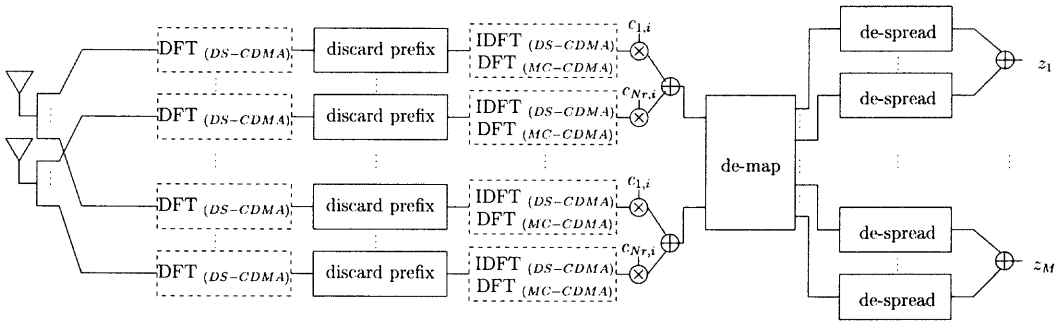

Figure 6.7 2D MRC receiver for MC-CDMA on TD channels and DS-CDMA on FD channels.

It follows from the duality of the channel that, $\mathcal{F}_N^{-1}\Xi_{MC,t}^m \mathbf{H}_{n_r,n_t}\Theta_{MC,t}^m \mathcal{F}_N$ are diagonal, and that defining $\bar{\mathbf{G}} = \mathcal{F}_{N_r,N}^{-1}\Xi_{MC,t}\mathbf{H}\Theta_{MC,t}\mathcal{F}_{N_t,N}$ then the received signal after despreading is

$$\mathbf{z}_{DS} = \mathbf{S}^T\mathbf{B}_R^H\bar{\mathbf{G}}\mathbf{B}_T\mathbf{S}\mathbf{b} + \boldsymbol{\xi}_{DS}, \tag{6.29}$$

which indicates that to match the receiver beamformer to the channel it must be $\mathbf{B}_R := (\bar{\mathbf{G}}\mathbf{B}_T)^H$ corresponding to a space-time MRC combiner (shown in Figure 6.7). The described system is therefore dual to MC-CDMA on a time-dispersive channel, as seen from Equations (6.25) and (6.29), and the block diagrams of Figure 6.6(b).

Simulations were carried out to confirm the duality of MC and DS CDMA for FS and TV channels. Figure 6.8 shows the performance of a 2×2 MIMO system with a single user and $M = L = 2$. The processing gain is $N = 8$, and the spreading codes are Walsh-Hadamard sequences. 2-path dual channels with either time or frequency dispersion of 1 chip was simulated. The performance of MC and DS CDMA on dual channels is identical, confirming the results in this section. In Figure 6.9 a system using a self-dual spreading sequence set (random Gaussian-distributed) is simulated on the same channels, with a spreading gain of $N = 16$. The results show that both systems exhibit the same performance on both channels, showing that MC and DS CDMA are equal when self-dual sequences are used.

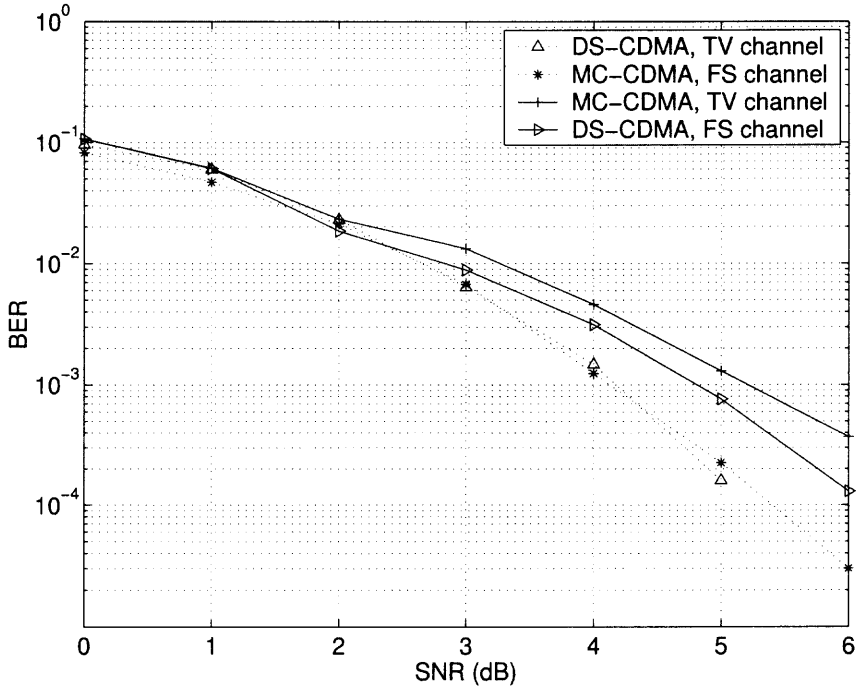

Figure 6.8 MC and DS CDMA using Walsh-Hadamard sequences on FS and TV dual channels.

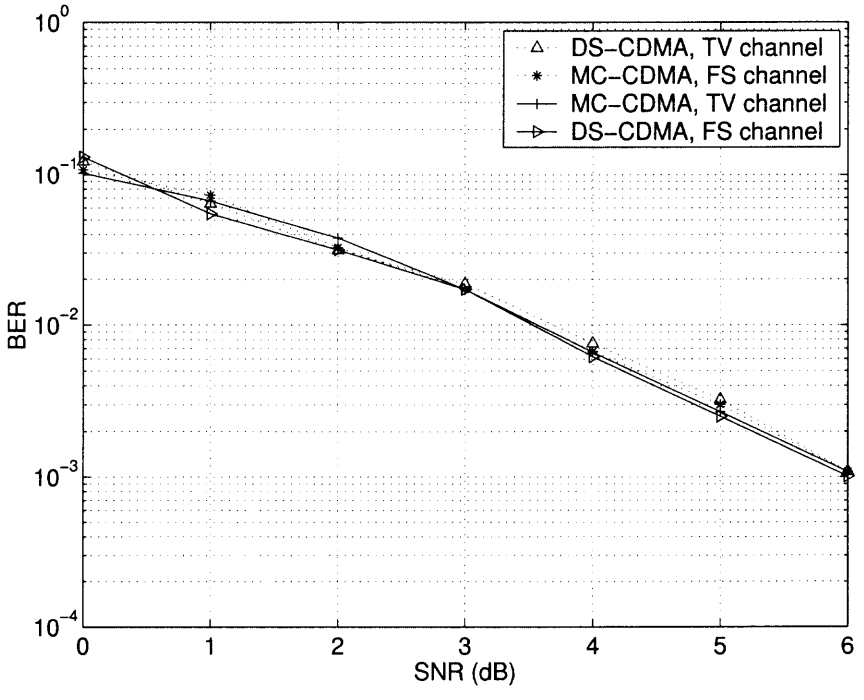

Figure 6.9 MC and DS CDMA using self-dual sequences on FS and TV dual channels.

6.4.3 Doubly-dispersive MIMO Channels

Assume a transmission channel with both time and frequency dispersion spanning for L_T DS-CDMA chips and L_F MC-CDMA chips so that $L_T \ll N$ and $L_F \ll N$. The discrete-time channel input delay-spread function from transmit antenna n_t to receive antenna n_r can be found as

$$g_{n_t,n_r}(n,m) := [r(t) * [\mathbf{G}_{n_t,n_r}](t,\tau) * p(t)]_{t=nT,\tau=mT}, \tag{6.30}$$

or, alternatively, the discrete-frequency input Doppler-spread function is given by

$$h_{n_t,n_r}(l,e) := [R(f) * [\mathbf{H}_{n_t,n_r}](f,\nu) * P(f)]_{f=lT^{-1},\nu=eT^{-1}}, \tag{6.31}$$

and

$$[\mathbf{G}_{n_t,n_r}]_{i,j} = g_{n_t,n_r}(i,i-j) \tag{6.32}$$

$$[\mathbf{H}_{n_t,n_r}]_{i,j} = h_{n_t,n_r}(i,i-j). \tag{6.33}$$

Notice that $g_{n_t,n_r}(n,m)$ in Equation (6.30) and $h_{n_t,n_r}(l,e)$ in Equation (6.31) are time and frequency variant respectively; therefore $\mathbf{G}_{n_t,n_r}$ in Equation (6.32) and $\mathbf{H}_{n_t,n_r}$ in Equation (6.33) are not Toeplitz matrices and cannot be diagonalized by adding and removing a cyclic prefix neither in time nor frequency domains. Hence it is logical to add a guard interval to prevent ISI in both DS and MC CDMA, rather than a cyclic prefix which would not be useful. Nevertheless, the channel representation in Equations (6.32) or (6.33) leads to a matched filter implementation involving time-varying filters, whose coefficients can be difficult to estimate.

For MC-CDMA it is more useful to represent the received signal using the expression in Equation (6.21) in discrete form. If the windowing function is well contained in time in $[0,T]$ and in frequency in $[-T^{-1}/2, T^{-1}/2]$ then it is possible to

represent the received signal by

$$\mathbf{Y}_{MC} \approx \sum_{m} \mathbf{V}(m)\mathbf{X}_{MC}e^{j2\pi m/N}, \tag{6.34}$$

where

$$[\mathbf{V}_{n_t,n_r}(m)]_{i,j} = V_{n_t,n_r}(i-j,m) \tag{6.35}$$

is the matrix representation of the discrete Doppler-delay spread function, which in turn can be approximated under the stated conditions by

$$V_{n_t,n_r}(e,m) = V_{n_t,n_r}(\nu,\tau)_{|\nu=eT^{-1},\ \tau=mT}. \tag{6.36}$$

The derivation of Equation (6.34) is deferred to Appendix D.

Similarly, for DS-CDMA, from Equation (6.20), if the pulse shape is well contained in time in $[0, N^{-1}T]$ and in frequency in $[-NT^{-1}/2, NT^{-1}/2]$ then the received signal also admits the representation

$$\mathbf{y}_{DS} \approx \sum_{e} \mathbf{U}(e)\mathbf{x}_{DS}e^{j2\pi e/N}, \tag{6.37}$$

where

$$[\mathbf{U}_{n_t,n_r}(e)]_{i,j} = U_{n_t,n_r}(i-j,e) \tag{6.38}$$

is the matrix representation of the delay-Doppler spread function (dual of the Doppler-delay spread function), approximated by

$$U_{n_t,n_r}(m,e) = V_{n_t,n_r}(\tau,\nu)_{|\tau=mN^{-1}T,\ \nu=eNT^{-1}}. \tag{6.39}$$

With the representation of Equations (6.34) and (6.37) the channel matched filter is given by $(\sum_m \mathbf{V}(m)e^{j2\pi m/N})^H$ and $(\sum_e \mathbf{U}(e)e^{j2\pi e/N})^H$. This notation is useful to realize that for both DS and MC CDMA, although the matched filter is a time-variant filter bank, only the coefficients of the discrete channel spreading function

need to be estimated for its implementation. An interpretation of this matched filter is shown in Figure 6.10, which is a space-time-frequency, or 3D, Rake receiver.

6.5 Interference Minimization and Multiuser Detection

So far the structure of the transmitted signal and implementation of the receiver matched filter have been addressed, but other parameters that greatly determine the performance of a CDMA system such as co-channel interference, and the ability of the receiver to mitigate it, have not been examined. Channel dispersion can corrupt the cross-correlation properties of spreading sequences, hence the need for multiuser detection. In MIMO CDMA systems, even single user system suffers from interference between sub-streams (*self-interference*), but a multiuser system also suffers from interference from other users, or MAI.

For the single user case, the received signal, can be expressed as

$$\mathbf{z}_{DS} = \mathbf{R}_{DS}\mathbf{b} + \boldsymbol{\xi}_{DS}, \tag{6.40}$$

and

$$\mathbf{z}_{MC} = \mathbf{R}_{MC}\mathbf{b} + \boldsymbol{\xi}_{MC}, \tag{6.41}$$

where $\mathbf{R}_{DS}$ and $\mathbf{R}_{MC}$ represent the channel-modified code cross-correlation matrices, given by the normalized concatenation of all matrix operations in Equations (6.23), (6.25), (6.27), and (6.29), are generally different from the code cross-correlation matrix, $\mathbf{R} = \mathbf{S}^T\mathbf{S}$ so that even when orthogonal codes are used, time or frequency dispersion result in loss of orthogonality for both DS and MC CDMA, resulting in $\{\mathbf{R}_{DS}, \mathbf{R}_{MC}\} \neq \mathbf{I}_M$.

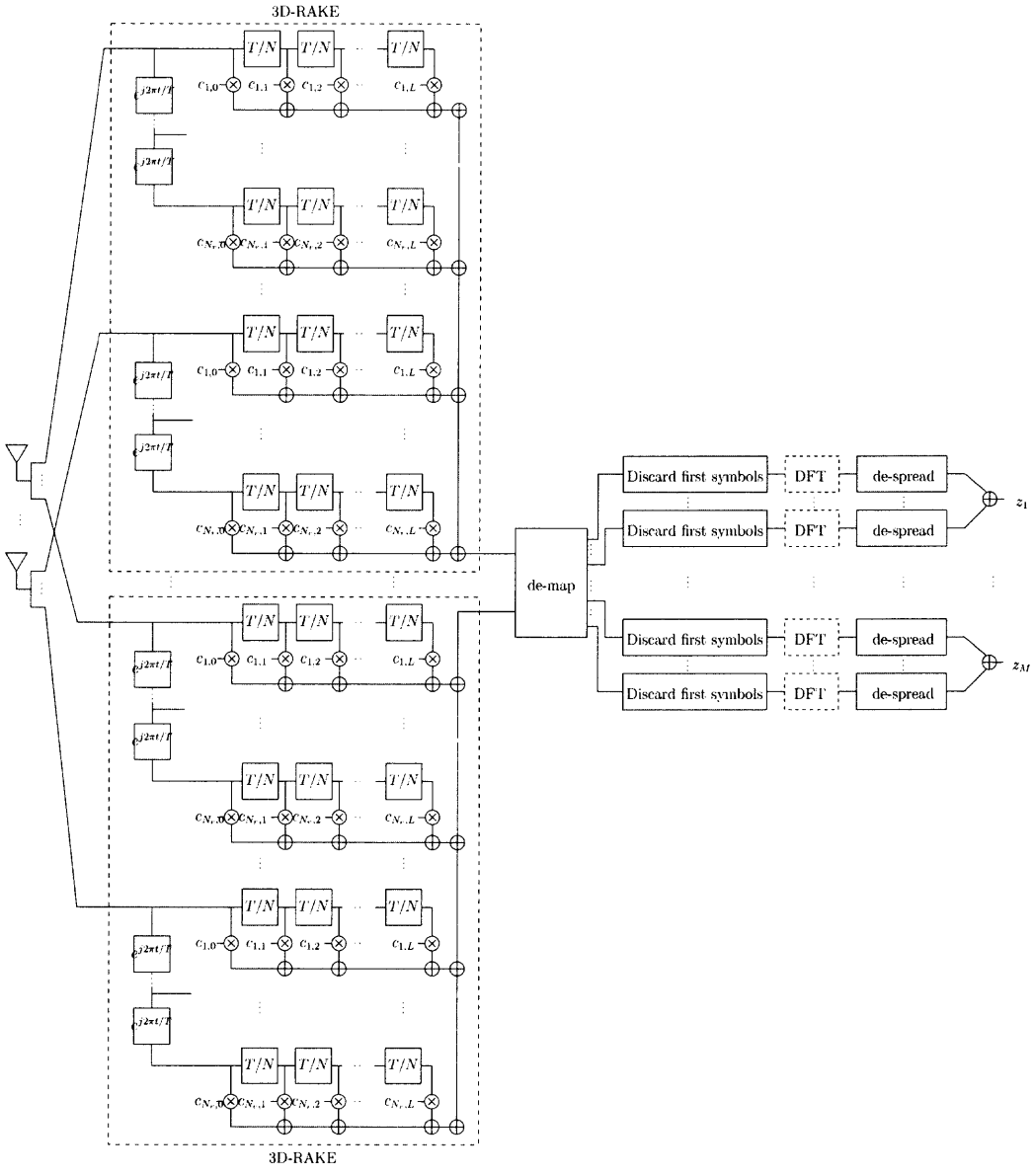

Figure 6.10 3D Rake receiver for DS-CDMA and MC-CDMA on TDFD channels.

The multiuser case can be treated in a similar way. The received signal of a multiuser system can be expressed, for the downlink, after despreading, as

$$\mathbf{y}_{DS,k} = \mathbf{B}_{R,k}\mathbf{G}_k \sum_{k=1}^{K} \mathbf{\Theta}_{DS,t}\mathbf{B}_{T,k}\mathbf{S}_k\mathbf{b}_k + \eta_k \tag{6.42}$$

$$\mathbf{y}_{MC,k} = \tilde{\mathbf{B}}_{R,k}\mathbf{H}_k \sum_{k=1}^{K} \mathbf{\Theta}_{MC,f}\mathbf{B}_{T,k}\tilde{\mathbf{S}}_k\mathbf{b}_k + \zeta_k, \tag{6.43}$$

where K is the number of active users, and, for the uplink, as

$$\mathbf{y}_{DS,k} = \mathbf{B}_{R,k} \sum_{k=1}^{K} \mathbf{G}_k\mathbf{\Theta}_{DS,t}\mathbf{B}_{T,k}\mathbf{S}_k\mathbf{b}_k + \eta_k \tag{6.44}$$

$$\mathbf{y}_{MC,k} = \tilde{\mathbf{B}}_{R,k} \sum_{k=1}^{K} \mathbf{H}_k\mathbf{\Theta}_{MC,f}\mathbf{B}_{T,k}\tilde{\mathbf{S}}_k\mathbf{b}_k + \zeta_k, \tag{6.45}$$

where perfect time and frequency synchronization among users was assumed. The despread signal can be represented by

$$[\mathbf{z}_{DS,1}^T; \cdots ; \mathbf{z}_{DS,K}^T]^T = \mathbf{R}_{DS}[\mathbf{b}_1^T; \cdots ; \mathbf{b}_K^T]^T + \xi_{DS}, \tag{6.46}$$

and

$$[\mathbf{z}_{MC,1}^T; \cdots ; \mathbf{z}_{MC,K}^T]^T = \mathbf{R}_{MC}[\mathbf{b}_1^T; \cdots ; \mathbf{b}_K^T]^T + \xi_{MC}, \tag{6.47}$$

where self-interference and MAI result from the non-diagonal terms in $\mathbf{R}_{DS}$, $\mathbf{R}_{MC}$ (of size $KM \times KM$). Multiuser systems can experience what is defined as *multiuser dispersion.* Signals from different users have time offsets at the receiver due to different propagation delays, to channel time dispersion, and, in quasi-synchronous systems, due to small synchronization errors (of the order of a few DS-CDMA chips). If the receiver is synchronized to the user with smallest delay, then all other users experience a positive delay, and the received signal experiences *multiuser time dispersion* due to different user delays, even if the channel is not time-dispersive. Similarly, signals from different users have different frequency offsets at the receiver due to different

moving speed and direction causing different Doppler shifts, and due to small carrier frequency synchronization errors of their local oscillator (of the order of a few sub-carriers, or MC-CDMA chips). The received signal experiences *multiuser frequency dispersion* even if the channel is not frequency-dispersive. In the following sections the implications of duality on spreading sequence design and MUD are discussed.

6.5.1 Spreading Sequence Design

The case of DS-CDMA on TD channels has been treated extensively. Multiple path delays cause interference proportional to the correlation of the time-shifted, zero-padded sequences (due to the use of a guard interval),

$$\rho_{i,j}(m) = \sum_{n} [\mathbf{s}_i]_n [\mathbf{s}_j]_{n+m}. \tag{6.48}$$

Therefore, well-chosen spreading sequences should minimize $\rho_{i,j}(m)$ for any i,j, and m, except for $\rho_{i,i}(0)$. But, from Equation (6.21) one can see that the effects of time delays on MC-CDMA result in a modulation of the spreading sequence, so that interference is proportional to

$$\mu_{i,j}(m) = \sum_{l} [\tilde{\mathbf{s}}_i]_l [\tilde{\mathbf{s}}_j]_l e^{j2\pi m/N}. \tag{6.49}$$

The expressions for cross-correlation can be derived for FD channels from its duality with TD channels, and for TDFD channels from Equations (6.34) and (6.37), which are summarized in Table 6.1

The auto-correlation and cross-correlation of time and frequency shifted sequences is shown in Figures 6.11 and 6.12 respectively, for Walsh-Hadamard, Gold, and binary random sequences. Auto-correlation and cross-correlation of these sequences with both time and frequency shifts is shown in Figures 6.13(a)-6.13(b), 6.14(a)-6.14(b), and 6.15(a)-6.15(b).

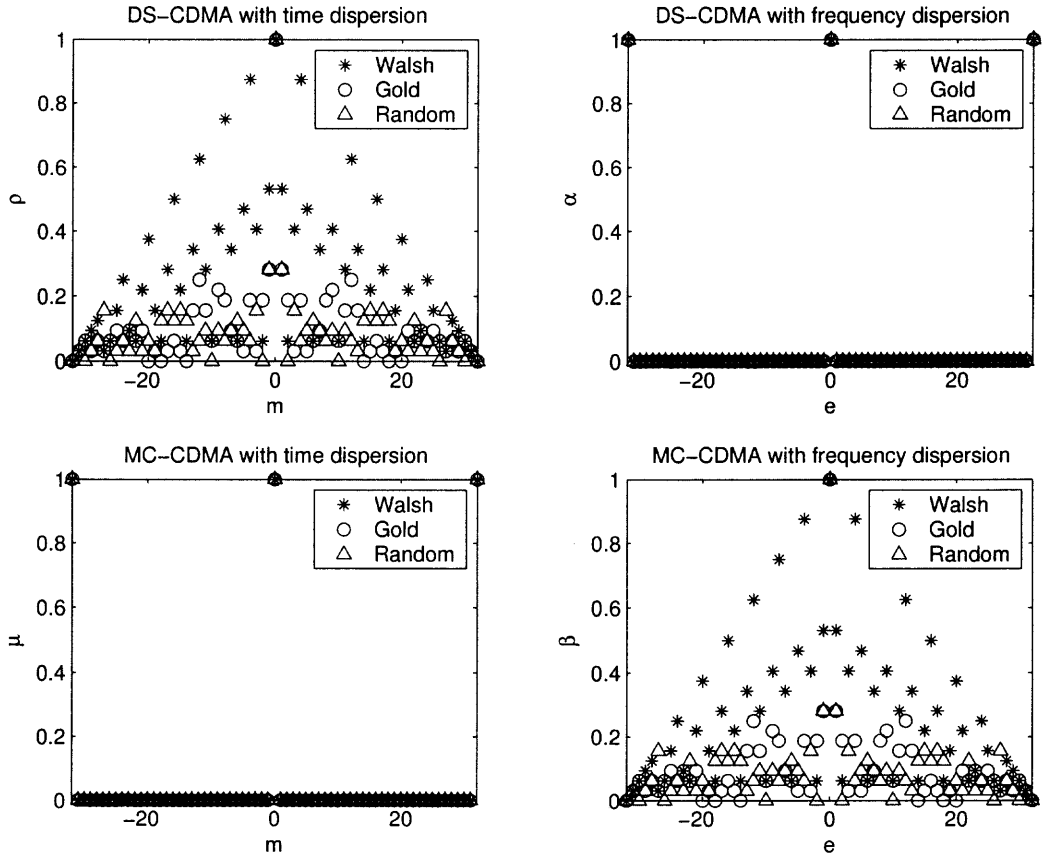

Figure 6.11 Auto-correlation of spreading sequences for MC and DS CDMA.

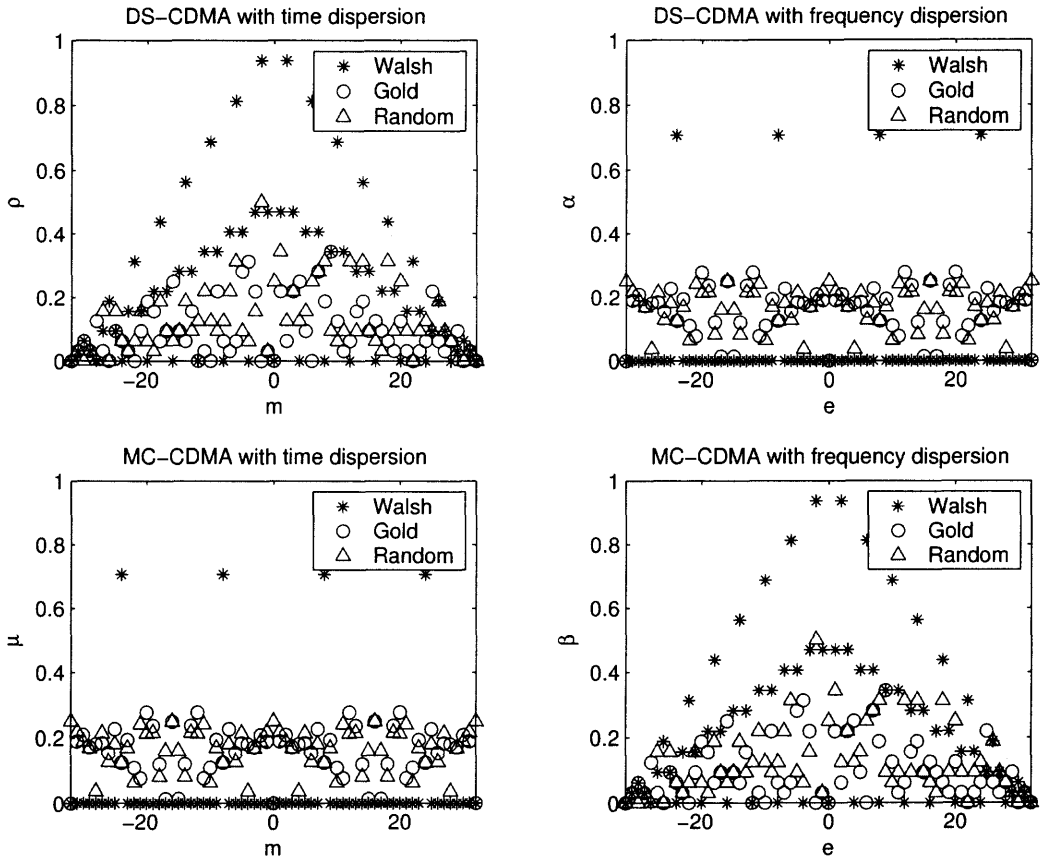

Figure 6.12 Cross-correlation of spreading sequences for MC and DS CDMA.

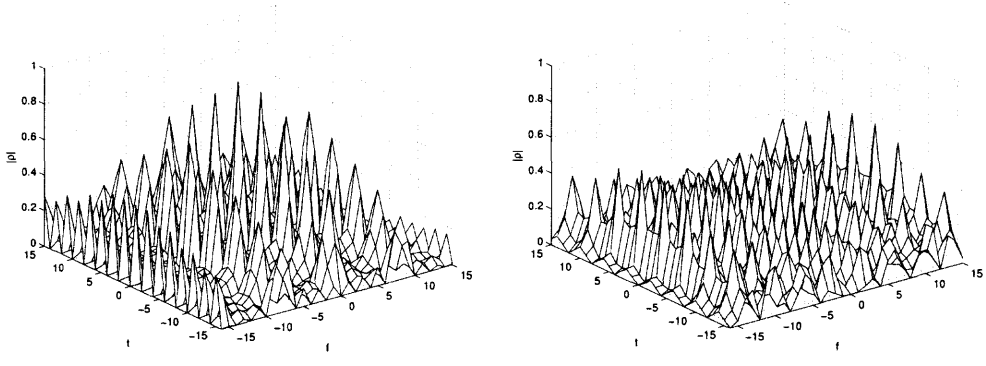

(a) Autocorrelation of a time and frequency shifted Walsh-32 sequence.

(b) Cross-correlation of two time and frequency shifted Walsh-32 sequences.

Figure 6.13 Time-frequency correlation of Walsh sequences.

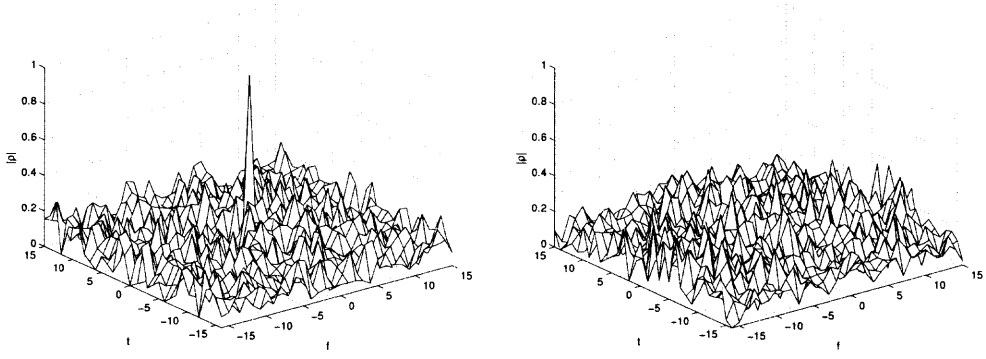

(a) Autocorrelation of a time and frequency shifted Gold-31 sequence.

(b) Cross-correlation of two time and frequency shifted Gold-31 sequences.

Figure 6.14 Time-frequency correlation of Gold sequences.

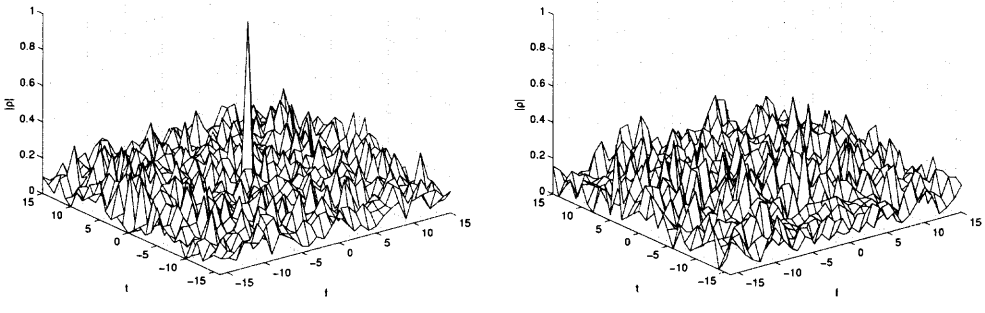

(a) Autocorrelation of a time and frequency shifted PN-32 sequence.

(b) Cross-correlation of two time and frequency shifted PN-32 sequences.

Figure 6.15 Time-frequency correlation of PN sequences.

Table 6.1 Design Criteria for Spreading Sequences for Dispersive Channels

channel	DS-CDMA	MC-CDMA
TD	$\rho_{i,j}(m) = \sum_n [\mathbf{s}_i]_n [\mathbf{s}_j]_{n+m}$	$\mu_{i,j}(m) = \sum_l [\tilde{\mathbf{s}}_i]_l [\tilde{\mathbf{s}}_j]_l e^{j2\pi m/N}$
FD	$\alpha_{i,j}(e) = \sum_n [\mathbf{s}_i]_n [\mathbf{s}_j]_n e^{j2\pi e/N}$	$\beta_{i,j}(e) = \sum_l [\tilde{\mathbf{s}}_i]_l [\tilde{\mathbf{s}}_j]_{l+e}$
TDFD	$\gamma_{i,j}(m,e) = \sum_n [\mathbf{s}_i]_n [\mathbf{s}_j]_{n+m} e^{j2\pi e/N}$	$\delta_{i,j}(e,m) = \sum_l [\tilde{\mathbf{s}}_i]_l [\tilde{\mathbf{s}}_j]_{l+e} e^{j2\pi n/N}$

6.5.2 Unified Multiuser Detection Approach

A second approach against interference from other codes is to use multiuser detection. A lot of research has been done on the area, and the consideration of particular MUD schemes is beyond the scope of this chapter (see, e.g., [19,86,87] for DS-CDMA, [82, 85,88,89] for MC-CDMA, and [73,90,91], for MIMO DS-CDMA). The performance of DS and MC-CDMA depends on the code cross-correlation matrices, $\mathbf{R}_{DS}$ and $\mathbf{R}_{MC}$. Nevertheless, all multiuser processing operates on the despread vectors $\mathbf{z}_{DS}, \mathbf{z}_{MC}$, and from the derivations it should be clear that the implications for MUD of the use of MC or DS CDMA are equivalent to the choice of a particular set of spreading sequences, thus a unified design approach can be followed in TD, FD, and TDFD channels.

6.6 Comparing MC-CDMA and DS-CDMA Using Time-frequency Duality

It was shown that MC and DS CDMA exhibit the same performance on dual channels. The performance of MC-CDMA and DS-CDMA on the same channel can also be addressed from this analysis (e.g. the performance on a typical wireless channel). First, note that if the spreading sequences of MC and DS CDMA are related by a Fourier transform, the transmitted CDMA signals are identical. Secondly, note that, thanks to the unified multiuser detection approach, the MUD does not have any impact on the comparison, since for a fair comparison both should use exactly the

same MUD. From these facts it follows that, with the same MUD, and for spreading sequences related by a Fourier transform, the same performance can be expected from MC and DS CDMA. Therefore, any difference in the performance comparison of these two CDMA schemes can be attributed to the choice of spreading sequences. Furthermore, the performance of any of the two systems can be matched by its counterpart by a proper spreading sequence choice. As a conclusion, it can be said that MC or DS CDMA should perform equally on any channel if care is taken in choosing a good set of spreading sequences.

6.7 Conclusion

A time-frequency duality relationship between MC and DS CDMA multiple antenna systems was formulated on time and frequency dispersive channels. It is shown that MC and DS CDMA are system duals when operating on dual channels. Optimum matched filter structures were determined for TD, FD, and TDFD channels and also related by duality. Furthermore, it is shown that multiuser detection and spreading sequence design can be addressed from a unified approach for MC and DS CDMA in dispersive channels, or in systems suffering from multiuser dispersion.

CHAPTER 7

SUMMARY

Great interest on multicarrier systems has resulted in the adoption of OFDM in several standards for wireless communication. A substantial amount of research has been carried out in different aspects of multicarrier transmission, such as detection, estimation, synchronization, and coding. The use of multicarrier modulation for multiuser systems has opened many new problems. This dissertation has addressed the topics of outage capacity, coding, and ICI cancellation for multiuser multicarrier systems. The original contributions are:

- Calculation of outage capacities of a multicarrier downlink system for time, frequency, and code division implemented with MC-CDMA.
- Performance comparison of coded OFDMA with rate-adaptive encoding and MC-CDMA.
- Derivation of the SINR of macrodiversity OFDM systems with multiple frequency offsets, and of linear and decision-feedback ICI cancellation receivers for such systems.
- Study of time-frequency duality between single carrier and multicarrier multiple antenna CDMA systems, and of its implications to receiver and spreading sequence design.

The results presented have opened new areas of research, which can be summarized as:

- Study of the capacity and performance of a cellular OFDMA system with single frequency reuse in terms of capacity and bit error rate.

- Assessment of the effects of windowing on the SINR of macrodiversity OFDM systems with multiple frequency offsets, and its implications on the design of low-complexity ICI cancellation receivers. Also, study of the impact of channel and offset estimation on their performance

- Study of space-time-frequency duality between direct sequence CDMA, multi-carrier CDMA and space division multiple access on space, time, and frequency dispersive channels.

APPENDIX A

DERIVATION OF LINEAR BLOCK DECORRELATING AND MMSE RECEIVERS

In this appendix the expressions for linear block decorrelating and MMSE receivers are derived. Results apply to multiuser detectors for MC-CDMA used in Chapters 3 and 4, and to linear ICI cancellation schemes proposed in Chapter 5. The general problem of detecting a vector of N symbols using a linear transformation followed by a symbol by symbol detector can be expressed as

$$\mathbf{z} = \mathbf{T}\mathbf{y}, \tag{A.1}$$

where $\mathbf{y} = (\mathbf{RAb} + \boldsymbol{\zeta})$, $\mathbf{R} = \mathbf{V}^H\mathbf{V}$ is a Hermitian symmetric matrix that represents the concatenation of the channel response and the matched filter, which introduces inter-block interference[1], and $\mathbf{T}$ is designed to improve detection. In addition, $\mathbf{b} = [b_0, b_1, \cdots, b_{N-1}]$ is a vector of symbols with covariance $E[\mathbf{b}\mathbf{b}^H] = \mathbf{I}_N$, $\mathbf{A} = \text{diag}\{A_0, A_1, \cdots, A_{N-1}\}$ represents symbol amplitudes, and $\boldsymbol{\zeta}$ is a vector of colored Gaussian noise with covariance $\sigma_\zeta^2\mathbf{R}$.

A.1 Decorrelating Detector

The *decorrelating detector*, also known as *zero-forcing detector*, is easily obtained by forcing that $E[\mathbf{TRAb}(\mathbf{TRAb})^H] = \mathbf{A}^2$, which immediately gives the solution

$$\mathbf{T} = \mathbf{R}^{-1}. \tag{A.2}$$

[1]The causes of inter-block interference (IBI) depend on what the signal vector is representing. In CDMA, inter-block interference is MAI. In OFDM, it is ICI.

The SNR of the decorrelating detector for symbol b_k is

$$\gamma_k = \frac{A_k^2 E[b_k b_k^*]}{E[[(\mathbf{R}^{-1}\boldsymbol{\zeta})(\mathbf{R}^{-1}\boldsymbol{\zeta})^H]_{k,k}]} = \frac{A_k^2}{\sigma_\zeta^2 [\mathbf{R}^{-1}]_{k,k}}. \tag{A.3}$$

The decorrelating detector incurs a performance loss, as a result of noise enhancement, which, as it can be seen from Equation (A.3), is independent of the signal power. The noise enhancement factor is defined as $\rho_k^D = [\mathbf{R}^{-1}]_{k,k}$ and represents the SNR penalty incurred.

A.2 MMSE Detector

The *MMSE detector* minimizes the mean square error of the received signal,

$$\xi = E[|\mathbf{e}|^2], \tag{A.4}$$

where $\mathbf{e} = \mathbf{Ab} - \mathbf{z}$. The solution of this quadratic, unconstrained optimization problem is obtained setting $\partial\xi/\partial\mathbf{T} = 0$. There is an important geometric interpretation of the MMSE detector: the solution is given by the element in the Hilbert subspace $V(\mathbf{z})$ that is closest to $\mathbf{Ab}$. Such element is the projection of $\mathbf{Ab}$ in $V(\mathbf{z})$, and the error, $\mathbf{e}$ is orthogonal to $V(\mathbf{z})$,

$$E[\mathbf{z}\mathbf{e}^H] = 0 \tag{A.5}$$

This result is known as the *principle of orthogonality*, and yields

$$E[\mathbf{z}(\mathbf{Ab})^H] - E[\mathbf{z}\mathbf{z}^H] =$$
$$\mathbf{A}^2\mathbf{R}^H\mathbf{T}^H - \mathbf{A}^2\mathbf{T}\mathbf{R}\mathbf{R}^H\mathbf{T}^H - \sigma_\zeta^2\mathbf{T}\mathbf{R}\mathbf{T}^H = 0. \tag{A.6}$$

Solving for $\mathbf{T}$,

$$\begin{aligned} \mathbf{T} &= \mathbf{A}^2(\mathbf{R}\mathbf{A}^2 + \sigma_\zeta\mathbf{I})^{-1} \\ &= (\mathbf{R} + \sigma_\zeta^2\mathbf{A}^{-2})^{-1}. \end{aligned} \tag{A.7}$$

The error covariance is given by

$$\begin{aligned} E[\mathbf{e}\mathbf{e}^H] &= E[\mathbf{A}\mathbf{b}(\mathbf{A}\mathbf{b})^H] - E[\mathbf{A}\mathbf{b}\mathbf{z}^H] - E[\mathbf{z}(\mathbf{A}\mathbf{b})^H] + E[\mathbf{z}\mathbf{z}^H] \\ &= \mathbf{A}^2 - \mathbf{A}^2\mathbf{R}^H\mathbf{M} \\ &= \mathbf{M}(\mathbf{A}^2\mathbf{M}^{-1} - \mathbf{A}^2\mathbf{R}^H) \\ &= \mathbf{M}(\mathbf{A}^2(\mathbf{R} + \sigma_\zeta^2\mathbf{A}^{-}2) - \mathbf{A}^2\mathbf{R}^H) \\ &= \sigma_\zeta^2\mathbf{M}, \end{aligned} \tag{A.8}$$

where by the principle of orthogonality $E[\mathbf{z}\mathbf{z}^H] - \mathbf{z}(\mathbf{A}\mathbf{b})^H] = 0$. The received signal before the symbol by symbol detector can be described as

$$z_k = [\mathbf{MR}]_{k,k}A_k b_k + \sum_{j \neq k}[\mathbf{MR}]_{k,j}A_j b_j + [\mathbf{MR}]_{k,k}\zeta_k, \tag{A.9}$$

where the first term is the desired signal, the second term represents IBI, and the third term is Gaussian noise. Equation (A.9) yields a first expression for the SINR for symbol k:

$$\begin{aligned} \gamma_k &= \frac{E[|[\mathbf{MR}]_{k,k}A_k b_k|^2]}{E[|\sum_{j\neq k}[\mathbf{MR}]_{k,j}A_j b_j|^2] + E[|[\mathbf{MR}]_{k,k}\zeta_k|^2]} \\ &= \frac{|[\mathbf{MR}]_{k,k}|^2 A_k^2}{\sum_{j\neq k}|[\mathbf{MR}]_{k,j}|^2 A_j^2 + [\mathbf{MRM}^H]_{k,k}}. \end{aligned} \tag{A.10}$$

A second expression for the SINR can be given as a function of the MMSE. Note that, by the Pythagorean Theorem for Hilbert spaces, the desired signal power is given by

$$E[|[\mathbf{MR}]_{k,k}|^2 A_k b_k] = E[|A_k b_k|^2] - E[|e_k]|^2], \tag{A.11}$$

hence the SINR is

$$\gamma_k = \frac{E[|[\mathbf{Ab}]_k|^2] - E[|[\mathbf{e}]_k|^2]}{E[|[\mathbf{e}]_k|^2]} = \frac{[\mathbf{A}^2]_{k,k}}{\sigma_\zeta^2[\mathbf{M}]_{k,k}} - 1. \tag{A.12}$$

APPENDIX B

DERIVATION OF DECISION FEEDBACK BLOCK DECORRELATING AND MMSE RECEIVERS

In this appendix the expressions for decision feedback block decorrelating and MMSE receivers are derived for the ICI cancellation schemes proposed in Chapter 5. Unlike in the derivation of linear receivers in Appendix A, where symbol by symbol detection is assumed, recursive detection is assumed in decision feedback receivers. Mathematically, the input of a recursive detector is represented by $\mathbf{XAb}$, where $\mathbf{X}$ is upper triangular and monic (with ones in the diagonal), and $\mathbf{A}$, introduced to make this result more general, represents the symbol amplitudes. The structure of $\mathbf{X}$ provides the causality required by the recursive detection process.

B.1 Decorrelating Decision Feedback Detector

The decorrelating detector completely eliminates interference. This is ensured by forcing

$$E[\mathbf{FRAb}(\mathbf{FRAb})^H] = \mathbf{XA}^2\mathbf{X}^H, \tag{B.1}$$

where $\mathbf{F}$ is the feed-forward matrix (see Figure 5.4). This criterion gives

$$\mathbf{FRA}^2\mathbf{R}^H\mathbf{F}^H = \mathbf{XA}^2\mathbf{X}^H. \tag{B.2}$$

Denote the Cholesky decomposition of $\mathbf{R}$ by

$$\mathbf{R} = (\mathbf{LD})^H\mathbf{LD} = \mathbf{L}^H\mathbf{D}^2\mathbf{L}, \tag{B.3}$$

where $\mathbf{L}$ is upper-triangular and monic, and $\mathbf{D}$ is diagonal with real elements. Since the Cholesky factorization is unique, it follows that $\mathbf{FR}$ and $\mathbf{X}$ must be Cholesky

factors of $\mathbf{R}$,

$$\mathbf{FR} = \mathbf{X} = \mathbf{L}, \tag{B.4}$$

and therefore $\mathbf{F}$ is given by

$$\mathbf{F} = \mathbf{LR}^{-1} = \mathbf{D}^{-2}(\mathbf{L}^H)^{-1}. \tag{B.5}$$

The SINR for symbol k, ignoring decision errors, is given by

$$\gamma_k = \frac{E[|A_k b_k|^2]}{E[|\zeta_k|^2]} = \frac{A_k^2}{\sigma_\zeta^2[\mathbf{D}^{-2}]_{k,k}}. \tag{B.6}$$

B.2 MMSE Decision Feedback Detector

For the decision-feedback version of the MMSE detector the desired signal is constrained to $\mathbf{XAb}$ rather than $\mathbf{Ab}$, with $\mathbf{X}$ being a fixed upper-triangular matrix to be determined. Therefore the error is defined as $\mathbf{e} = \mathbf{z}_F - \mathbf{XAb}$. The principle of orthogonality also applies in this case, and the optimal solution satisfies

$$\begin{aligned} E[\mathbf{z}_F \mathbf{e}^H] &= 0; \\ E[\mathbf{z}_F \mathbf{z}_F^H] &= E[\mathbf{z}_F (\mathbf{XAb})^H]. \end{aligned} \tag{B.7}$$

Developing Equation (B.7),

$$(\mathbf{A}^2\mathbf{R}^H + \sigma_\zeta^2)\mathbf{F}^H = \mathbf{A}^2\mathbf{X}^H$$

$$\mathbf{F} = ((\mathbf{R} + \sigma_\zeta^2\mathbf{A}^{-2})\mathbf{X}^{-1})^{-1} = (\mathbf{M}^{-1}\mathbf{X}^{-1})^{-1} = \mathbf{XM}. \tag{B.8}$$

where the $\mathbf{X}$ that minimizes the MSE has to be determined. The error covariance is given by

$$\begin{aligned}
\mathbf{R_{ee}} = E[\mathbf{ee}^H] &= \mathbf{X}E[\mathbf{Abb}^H\mathbf{A}^H]\mathbf{X}^H - \mathbf{XA}E[\mathbf{bz}^H] - E[\mathbf{zb}^H]\mathbf{A}^H\mathbf{X}^H + E[\mathbf{zz}^H] \\
&= \mathbf{XA}^2\mathbf{X}^H - \mathbf{XA}^2\mathbf{R}^H\mathbf{M}^H\mathbf{X}^H \\
&= \mathbf{X}(\mathbf{A}^2 - \mathbf{A}^2\mathbf{R}^H\mathbf{M}^H)\mathbf{X}^H \\
&= \mathbf{XM}(\mathbf{A}^2\mathbf{M}^{-1} - \mathbf{A}^2\mathbf{R}^H)\mathbf{X}^H \\
&= \mathbf{XM}(\mathbf{A}^2(\mathbf{R} + \sigma_\zeta^2\mathbf{A}^{-2}) - \mathbf{A}^2\mathbf{R}^H)\mathbf{X}^H \\
&= \sigma_\zeta^2\mathbf{XMX}^H, \qquad \text{(B.9)}
\end{aligned}$$

where by the principle of orthogonality $E[\mathbf{zz}^H] - E[\mathbf{zb}^H]\mathbf{A}^H\mathbf{X}^H = 0$. Since the estimation is of an innovations representation of the error, the prediction error e_k is orthogonal to the subspace $V(b_1, \cdots, b_{k-1})$ in the Hilbert space $V(\mathbf{b})$ defined by $\mathbf{b}$. Define the Cholesky factorization of $\mathbf{M}$ as

$$\mathbf{M} = (\mathbf{DK})^H(\mathbf{DK}) = \mathbf{K}^H\mathbf{D}^2\mathbf{K}, \qquad \text{(B.10)}$$

where $\mathbf{K}$ is lower-triangular and monic, and $\mathbf{D}$ is diagonal with real elements. The error covariance in terms of the Cholesky factors of $\mathbf{M}$ is

$$\mathbf{R_{ee}} = \sigma_\zeta^2\mathbf{XK}^H\mathbf{D}^2\mathbf{KX}^H. \qquad \text{(B.11)}$$

Since $\mathbf{D}$ is diagonal and both $\mathbf{K}$ and $\mathbf{X}$ are monic by definition, it follows that the solution which decorrelates the error is

$$\mathbf{X} = \mathbf{K}. \qquad \text{(B.12)}$$

Furthermore, since the Cholesky factors are unique, $\mathbf{K}$ is the unique MMSE solution, with the error given by

$$\mathbf{R_{ee}} = \sigma_\zeta^2\mathbf{D}^2. \qquad \text{(B.13)}$$

APPENDIX C

DERIVATION OF THE OPTIMAL RECEIVER SYNCHRONIZATION FREQUENCY IN THE PRESENCE OF MULTIPLE OFFSETS

In Chapter 5 it was found that the frequency that maximizes the SINR of the received signal maximizes the function

$$\mathcal{J}(f_{lo}) = \sum_{i=1}^{N_T} \mathcal{L}^i \mathcal{P}^i |\Phi_{kk}^i|^2 = \sum_{i=1}^{N_T} \mathcal{L}^i \mathcal{P}^i \left| \frac{1}{N_s} \frac{\sin\left(\pi \frac{f_c^i - f_{lo}}{\Delta f}\right)}{\sin\left(\pi \frac{1}{N_s} \frac{f_c^i - f_{lo}}{\Delta f}\right)} \right|^2 . \tag{C.1}$$

To make the problem mathematically tractable the exact discrete Fourier transform expression of Φ_{kk}^i in Equation (5.6) is approximated by its continuous counterpart

$$\begin{aligned} \Phi_{kk}^i &= \frac{1}{N_s T} \int_0^{N_s T} \exp\left(j2\pi \frac{1}{N_s} \frac{f_c^i - f_{lo}}{\Delta f} t\right) dt \\ &= \exp\left(j\pi T \frac{f_c^i - f_{lo}}{\Delta f}\right) sinc\left(T \frac{f_c^i - f_{lo}}{\Delta f}\right). \end{aligned} \tag{C.2}$$

Thus,

$$|\Phi_{kk}^i|^2 = sinc^2\left(T \frac{f_c^i - f_{lo}}{\Delta f}\right). \tag{C.3}$$

Using the second order Taylor series expansion, for small offsets,

$$sinc^2(x) = \frac{\sin^2(\pi x)}{(\pi x)^2} \simeq 1 - \frac{\pi^2 x^2}{3}, \tag{C.4}$$

and the function to maximize becomes

$$\mathcal{J}^*(f_{lo}) = \sum_{i=1}^{N_T} \mathcal{L}^i \mathcal{P}^i \left(1 - \frac{\pi^2}{3} \left(T \frac{f_c^i - f_{lo}}{\Delta f}\right)^2\right). \tag{C.5}$$

Setting the derivative to zero

$$\frac{\partial \mathcal{J}^*(f_{lo})}{\partial f_{lo}} = \sum_{i=1}^{N_T} \mathcal{L}^i \mathcal{P}^i \frac{\pi^2}{3} \frac{2T}{\Delta f} \left(\frac{f_c^i - f_{lo}}{\Delta f}\right) = 0 \tag{C.6}$$

yields, after simple manipulations,

$$f_{lo} = \frac{\sum_{i=1}^{N_T} \mathcal{L}^i \mathcal{P}^i f_c^i}{\sum_{i=1}^{N_T} \mathcal{L}^i \mathcal{P}^i}. \tag{C.7}$$

APPENDIX D

DISCRETE-TIME MODEL FOR TIME AND FREQUENCY DISPERSIVE CHANNELS

In this appendix it is shown that continuous time and frequency expressions for the received signal of DS and MC CDMA

$$\mathbf{Y}^c_{MC}(f) = \int\int \mathbf{V}^c(\nu,\tau)\mathbf{X}^c_{MC}(f-\nu)e^{-j2\pi\tau f}\,d\nu d\tau \tag{D.1}$$

$$\mathbf{y}^c_{DS}(t) = \int\int \mathbf{U}^c(\tau,\nu)\mathbf{x}^c_{DS}(t-\tau)e^{j2\pi\nu t}\,d\tau d\nu \tag{D.2}$$

admit a discrete representation given by

$$\mathbf{Y}_{MC} \approx \sum_m \mathbf{V}(m)\mathbf{X}_{MC}e^{j2\pi m/N} \tag{D.3}$$

$$\mathbf{y}_{DS} \approx \sum_e \mathbf{U}(e)\mathbf{x}_{DS}e^{j2\pi e/N}. \tag{D.4}$$

Consider the representation of $\mathbf{Y}^c_{MC}(f)$ in terms of the frequency-dependent modulation function $\mathbf{M}^c(t,f) = \int\int \mathbf{V}^c(\nu,\tau)e^{-j2\pi f\tau}e^{j2\pi\nu t}\,d\tau d\nu$, so that the contribution of the signal transmitted from antenna n_t to the signal received by antenna n_r is given by

$$Y^c_{n_r,MC}(f) = \int x^c_{n_t,MC}(t)M^c_{n_t,n_r}(t,f)e^{-j2\pi ft}\,dt. \tag{D.5}$$

If the transmitter and receiver windowing functions are assumed to be contained in time in $[0,T]$ and in frequency in $[-T^{-1}/2, T^{-1}/2]$ respectively[1], the following channel

[1]If the same transmit and receive windowing function is used then the derivation is an approximation, since no function can be both time and frequency limited.

functions will produce the same output:

$$\tilde{M}^c_{n_t,n_r}(t,f) = \text{rect}\left(\frac{t-T/2}{T}\right) M(t,f)^c_{n_t,n_r} \text{rect}\left(\frac{f}{T^{-1}}\right) \quad \text{(D.6)}$$

$$\tilde{\tilde{M}}^c_{n_t,n_r}(t,f) = \text{rect}\left(\frac{t-T/2}{T}\right) \sum_n \sum_l \tilde{M}^c_{n_t,n_r}(t-nT,f) \text{rect}\left(\frac{f-lT^{-1}}{T^{-1}}\right) \quad \text{(D.7)}$$

It was shown in [27] that the Doppler-delay spread function corresponding to Equation (D.7) is

$$\tilde{\tilde{V}}^c_{n_t,n_r}(\nu,\tau) = \sum_e \sum_m V^c_{n_t,n_r}\left(\frac{e}{T}, \frac{m}{T^{-1}}\right) \delta\left(\nu - \frac{m}{T}\right) \delta\left(\tau - \frac{e}{T^{-1}}\right), \quad \text{(D.8)}$$

so that the output under such constraints is

$$\begin{aligned} Y^c_{n_r,MC}(f) &= \int\int \tilde{\tilde{V}}^c_{n_t,n_r} X^c_{n_t,MC}(f-\nu) e^{j2\pi\tau f}\, d\tau d\nu \\ &= \sum_e \sum_m V^c_{n_t,n_r}\left(\frac{e}{T}, \frac{m}{T^{-1}}\right) X^c_{n_t,MC}\left(f - \frac{e}{T^{-1}}\right) e^{j2\pi f m/T}. \end{aligned} \quad \text{(D.9)}$$

Since $X^c_{n_t,MC}\left(f - \frac{e}{T}\right) = [\mathbf{X}_{MC}]_e$, after sampling in the frequency domain for $f = lT^{-1}$,

$$[\mathbf{Y}_{MC}]_l = \sum_e \sum_m V(e,m)[\mathbf{X}_{MC}]_{l-e} e^{j2\pi ml}, \quad \text{(D.10)}$$

which with the matrix notation introduced in Equation (6.35) becomes

$$\mathbf{Y}_{MC} = \sum_m \mathbf{V}(m)\mathbf{X}_{MC} e^{j2\pi ml}. \quad \text{(D.11)}$$

For DS-CDMA the dual derivation begins from the representation of $\mathbf{y}^c_{DS}(t)$ in terms of the time-variant transfer function $\mathbf{T}^c(f,t) = \int\int \mathbf{U}^c(\tau,\nu) e^{-j2\pi f\tau} e^{j2\pi\nu t}\, d\tau d\nu$, as

$$y^c_{n_r,DS}(t) = \int X^c_{n_t,DS}(f) T^c_{n_t,n_r}(f,t) e^{j2\pi ft}\, df. \quad \text{(D.12)}$$

If the Fourier transform of the transmitter and receiver time domain pulse shape and matched filter are assumed to be band-limited to $[-NT^{-1}/2, NT^{-1}/2]$ and time-limited to $[0, N^{-1}T]$ then following the same approach as for MC-CDMA it is easily

proven that DS-CDMA admits the representation in Equation (D.4) sampling the delay-Doppler function at

$$U_{n_t,n_r}(m,e) = U_{n_t,n_r}(\tau,\nu)_{\tau=mN^{-1}T,\ \nu=eNT^{-1}}. \tag{D.13}$$

APPENDIX E

ABBREVIATIONS

AWGN:	additive white Gaussian noise
BC:	broadcast channel
BER:	bit error rate
BFC:	block fading channel
BLAST:	Bell-Labs layered space-time
BPSK:	binary phase shift keying
cdf:	cumulative density function
CDM:	code division multiplexing
CDMA:	code division multiple access
CFSL:	coded fixed spreading length
CSIT:	transmitter channel state information
DAB:	digital audio broadcasting
D-DF:	decorrelating decision feedback
DFT:	discrete Fourier transform
DS:	direct sequence
DS-CDMA:	direct sequence code division multiple access
DVB-T:	terrestrial digital video broadcasting
ETSI:	European Telecommunications Standards Institute
FD:	frequency dispersive
FDM:	frequency division multiplexing
FDMA:	frequency division multiple access
FFT:	fast Fourier transform
FS:	frequency selective

FSL:	fixed spreading length
FT:	Fourier transform
IBI:	inter-block interference
ICI:	inter-carrier interference
IDFT:	inverse discrete Fourier transform
IEEE	Institute of Electrical and Electronics Engineers
IFT:	inverse Fourier transform
i.i.d.:	independent, identically distributed
ISI:	inter-symbol interference
LOS	line of sight
MAC:	multiple access channel
MAI:	multi-access interference
MC:	multicarrier
MCBFC:	multicarrier block fading channel
MC-CDMA:	multicarrier code division multiple access
MC-DS-CDMA:	multicarrier direct sequence code division multiple access
MCM:	multicarrier modulation
MC-SS:	multicarrier spread spectrum
MFSL:	multi-code fixed spreading length
MIMO:	multiple-input, multiple-output
MMSE:	minimum mean square error
MMSE-DF	minimum mean square error decision feedback
MRC:	maximal ratio combining
MSE	mean square error
MT-CDMA:	multi-tone code division multiple access
MUD:	multiuser detector
OFDM:	orthogonal frequency division multiplexing

OFDMA:	orthogonal frequency division multiple access
PAPR	peak to average power ratio
pdf:	probability density function
PEP:	pairwise error probability
QPSK:	quadrature phase shift keying
RCPC:	rate-compatible punctured convolutional
r.m.s.:	root mean square
SFN:	single frequency network
SINR:	signal to interference plus noise ratio
SNR:	signal to noise ratio
TD:	time dispersive
TDFD:	time dispersive, frequency dispersive
TDM:	time division multiplexing
TDMA:	time division multiple access
TV:	time variant
US:	uncorrelated scattering
VSL:	variable spreading length
WLAN:	wireless local area network
WSS:	wide sense stationary
WSSUS:	wide sense stationary, uncorrelated scattering

BIBLIOGRAPHY

[1] M. L. Doelz, E. T. Heald, and D. L. Martin, "Binary data transmission techniques for linear systems," *Proc. IRE*, vol. 45, pp. 656–661, May 1957.

[2] J. Bingham, "Multicarrier modulation for data transmission: an idea whose time has come," *IEEE Communications magazine*, pp. 5–14, May 1990.

[3] R. W. Chang, "Synthesis of band-limited orthogonal signals for multichannel data transmission," *Bell System Technical Journal*, vol. 45, pp. 1775–1796, December 1966.

[4] S. Weinstein and P. Ebert, "Data transmission by frequency-division multiplexing using the discrete Fourier transform," *IEEE. Trans. on Comm. Tech.*, vol. COM-19, no. 5, pp. 626–634, October 1971.

[5] ETSI, "Radio broadcasting systems; digital audio broadcasting (DAB) to mobile, portable and fixed receiver," ETS 300-401, May 1997.

[6] ETSI, "Digital video broadcasting: Framing structure, channel coding, and modulation for digital terrestrial television," EN 300-744, Aug. 1997.

[7] IEEE 802.11a 1999, *Wireless LAN medium access control (MAC) and Physical layer (PHY) specifications: High-speed physical layer in the 5 GHz band.*

[8] ETSI TS 101 475 V1.2.2, *Broadband radio access networks (BRAN); HIPERLAN type 2; physical (PHY) layer*, February 2001.

[9] V. M. DaSilva and E. S. Sousa, "Multicarrier orthogonal CDMA signals for quasi-synchronous communication systems," *IEEE J. Select. Aresas Commun.*, pp. 842–852, June 1994.

[10] S. Kondo and L. B. Milstein, "Performance of multicarrier DS CDMA systems," *IEEE Transactions on Communications*, vol. 44, no. 2, pp. 238–246, February 1996.

[11] L. Vandendorpe, "Multitone spread spectrum multiple access communications system in a multipath Rician fading channel," *IEEE Transactions on Vehicular Technology*, vol. 44, no. 2, pp. 327–337, May 1995.

[12] S. Kaiser, "On the performance of different detection techniques for OFDM-CDMA in fading channels," in *Proc. IEEE Globecom*, Nov. 1995, pp. 2059–2063.

[13] S. Hara and R. Prasad, "Overview of multicarrier CDMA," *IEEE communications magazine*, pp. 126–133, December 1997.

[14] T. Cover and J. Thomas, *Elements of information theory*, John Wiley, 1991.

[15] R. van Nee and R. Prasad, *OFDM for wireless multimedia communications*, Artech House, 2000.

[16] N. Yee, J.P. Linnartz, and G. Fettweis, "Multi-Carrier CDMA in indoor wireless radio networks," in *IEEE PIMRC International Conference*, 1993, pp. 109–113.

[17] M. Tan and Y. Bar-Ness, "Performance comparison of multi-code fixed spreading length (MFSL) scheme and variable spreading length (VSL) scheme for multi-rate MC-CDMA," submitted to ISSSTA 2002.

[18] M. Tan and Y. Bar-Ness, "Maximum spectral utilization efficiency multi-code FSL scheme for multi-rate MC-CDMA," in *to appear in Proceedings 3G Wireless*, 2002.

[19] S. Verdu, *Multiuser Detection*, Cambridge University Press, 1998.

[20] G. Malmgren, "On the performance of single frequency networks in correlated shadow fading," *IEEE Transactions on Broadcasting*, vol. 43, no. 2, pp. 155–165, June 1997.

[21] W. C. Jakes, *Microwave mobile communications*, New York, Wiley, 1974.

[22] T. S. Rappaport, *Wireless Communications. Principles and Practice*, Prentice Hall, 1996.

[23] T. Okumura, E. Ohmori, and K. Fukuda, "Field strength and its variability in VHF and UHF land mobile service," *Review Electrical Communication Laboratory*, vol. 16, no. 9-10, pp. 825–873, September-October 1968.

[24] M. Hata, "Empirical formula for propagation loss in land mobile radio services," *IEEE Trans. on Vehicular Technology*, vol. VT-29, no. 3, pp. 317–325, August 1980.

[25] R. H. Clarke, "A statistical theory of mobile-radio reception," *Bell Syst. Tech. Journal*, vol. 47, pp. 957–1000, 1968.

[26] P. Bello, "Time-frequency duality," *IEEE Trans. on Information Theory*, vol. IT-10, pp. 18–33, January 1964.

[27] P. Bello, "Characterization of randomly time-variant linear channels," *IRE Trans. on Comm. Systems*, pp. 360–393, December 1963.

[28] R. S. Kennedy, *Fading Dispersive Communication Channels*, Wiley & Sons, 1969.

[29] T. Kailath, "Time-variant communication channels," *IEEE Trans. on Information Theory*, vol. IT-9, pp. 233–237, October 1963.

[30] B. H. Fleury, "First- and second-order characterization of direction dispersion and space selectivity in the radio channel," *IEEE Trans. on Information Theory*, vol. 46, no. 6, pp. 2027–2044, Sept. 2000.

[31] R. Kattenbach, "Statistical modeling of small-scale fading in directional radio channels," *IEEE Journal on Selected Areas in Commun.*, vol. 20, no. 3, pp. 584–592, April 2002.

[32] D. S. Shiu, G. J. Foschini, M. J. Gans, and J. M. Kahn, "Fading correlation and its effect on the capacity of multielement antenna systems," *IEEE Trans. on Commun.*, vol. 48, no. 3, pp. 502–513, March 2000.

[33] J. Salz and J. H. Winters, "Effect of fading correlation on adaptive arrays in digital mobile radio," *IEEE Trans. on Vehicular Technol.*, vol. 43, no. 4, pp. 1049–1057, Nov. 1994.

[34] I. E. Telatar, "Capacity of multi-antenna gaussian channels," *European Trans. on Telecommun. (ETT)*, vol. 10, pp. 585–595, Nov.-Dec. 1999.

[35] M. A. Visser, *Adaptive Interference Cancelation Techniques for Multicarrier Modulated Systems*, Ph.D. thesis, NJIT, May 1999.

[36] M. J. Gans, "A power spectral theory of propagation in the mobile radio environment," *IEEE Trans. on Vehicular Tehcnol.*, vol. VT-21, pp. 27–38, february 1972.

[37] S. Benedetto and E. Biglieri, *Principles of Digital Transmission With Wireless Applications*, Plenum, 1999.

[38] R. Wesel and J. Cioffi, "Fundamentals of coding for broadcast OFDM," in *Proc. Asilomar Conf. '95*, 1995, pp. 2–6.

[39] E. Biglieri, "Theory and applications of coded modulation," ELE539 class notes, Princeton Univ. Spring 2000.

[40] R. Knopp and P. Humblet, "On coding for block fading channels," *IEEE Trans. on Information Theory*, vol. 46, no. 1, pp. 189–205, January 2000.

[41] T. Cover, "Comments on broadcast channels," *IEEE Trans. on Information Theory*, vol. 44, no. 6, pp. 2524–2530, October 1998.

[42] L. Li and A. Goldsmith, "Capacity and optimal resource allocation for fading broadcast channels: Part I: ergodic capacity," *IEEE. Trans. on Information Theory*, vol. 47, no. 3, pp. 1083–1102, March 2001.

[43] L. Li and A. Goldsmith, "Capacity and optimal resource allocation for fading broadcast channels: Part II: outage capacity," *IEEE. Trans. on Information Theory*, vol. 47, no. 3, pp. 1103–1127, March 2001.

[44] T. Cover, "Broadcast channels," *IEEE Trans. on Information Theory*, vol. IT-18, no. 1, pp. 2–14, January 1972.

[45] P. Bergmans, "A simple converse for broadcast channels with additive white Gaussian noise," *IEEE Trans. on Information Theory*, vol. IT-20, pp. 279–280, March 1974.

[46] G. Caire, G. Taricco, and E. Biglieri, "Optimum power control over fading channels," *IEEE Transactions on Information Theory*, vol. 45, no. 5, pp. 1468–1489, July 1999.

[47] D. Hughes-hartogs, *The capacity of the degraded spectral broadcast channel*, Ph.D. thesis, Stanford U., 1975.

[48] D. Tse, "Optimal power allocation over parallel Gaussian broadcast channels," unpublished.

[49] A. Leon-Garcia, *Probability and Random Processes for Electrical Engineering*, Addison-Wesley, 1994.

[50] R. LeGouable and M. Helard, "Performance of single and multi-user detection techniques for a mc-cdma system over channel model used for HIPERLAN2," in *Proceedings IEEE ISSSTA*, 2000, pp. 718 –722.

[51] S. Hara and R. Prasad, "Design and performance of Multicarrier CDMA system in frequency-selective Rayleigh fading channels," *IEEE Transactions on Vehicular Technology*, vol. 48, no. 5, pp. 1584–1594, September 1999.

[52] Y. S. Leung, S. G. Wilson, and J. W. Ketchum, "Multifrequency trellis coding with low delay for fading channels," *IEEE Trans. on Commmun.*, vol. 41, no. 10, pp. 1450–1458, oct 1993.

[53] E. Malkamaki and H. Leib, "Evaluating the performance of convolutional codes over block fading channels," *IEEE Trans. on Information Theory*, vol. 45, no. 5, pp. 1643–1646, July 1999.

[54] D. N. Rowitch and L. B. Milstein, "Convolutional coding for direct sequence multi-carrier CDMA," in *Proc. IEEE Military Commun. Conference (MILCOM)*, Nov. 1995, vol. 1, pp. 55–59.

[55] R. C. Singleton, "Maximum distance q-nary codes," *IEEE Trans. on Information Theory*, vol. IT-10, pp. 116–118, 1964.

[56] J. Hagenauer, "Rate-compatible punctured convolutional codes (RCPC codes) and their applications," *IEEE Transactions on Communications*, vol. 36, no. 4, pp. 389–400, April 1988.

[57] P. Frenger, P. Orten, T. Ottosson, and A. Svensson, "Multi-rate convolutional codes," Tech. Rep. R021/1998, Chalmers University of Technology, 1998.

[58] M. Russell and G. L. Stuber, "Interchannel interference analysis of OFDM in a mobile environment," in *Proceedings IEEE Vehicular Technology Conference (VTC)*, 1995, pp. 820–824.

[59] T. Pollet, M. VanBladel, and M. Moeneclaey, "BER sensitivity of OFDM systems to carrier frequency offset and wiener phase noise," *IEEE Transactions on Communications*, vol. 43, no. 2/3/4, pp. 191–193, February/March/April 1995.

[60] J. Armstrong, "Analysis of new and existing methods of reducing intercarrier interference due to carrier frequency offset in OFDM," *IEEE Transactions on Communications*, vol. 47, no. 3, pp. 365–369, March 1999.

[61] H. Steendam and M. Moeneclaey, "Analysis and optimization of the performance of OFDM on frequency-selective time-selective fading channels," *IEEE Transactions on Communications*, vol. 47, no. 12, pp. 1811–1819, December 1999.

[62] P. Robertson and S. Kaiser, "The effects of Doppler spread in OFDM(A) mobile radio systems," in *Proceedings IEEE Vehicular Technology Conference (VTC)*, 1999, pp. 329–333.

[63] G. Li and L. J. Cimini, "Bounds on the interchannel interference of OFDM in time-varying impairments," *IEEE Transactions on Communications*, vol. 49, no. 3, pp. 401–404, March 2001.

[64] K. Sathananthan and C. Tellambura, "Performance analysis of an OFDM system with carrier frequency offset and phase noise," in *Proceedings ...*, 2001, pp. 2329–2332.

[65] S. Wu and Y. Bar-Ness, "A phase noise suppression algorithm for OFDM-based WLANs," *IEEE Communications Letters*, vol. 6, no. 12, pp. 535–537, Dec 2002.

[66] M. A. Visser and Y. Bar-Ness, "Frequency offset correction for OFDM using a blind adaptive decorrelator in a time-variant selective Rayleigh fading channel," in *Proceedings IEEE Vehicular Technology Conference (VTC)*, 1999, pp. 1281–1285.

[67] Y. Zhao, J. Leclercq, and S. Haggman, "Intercarrier interference compression in OFDM communication systems by using correlative coding," *IEEE Communications Letters*, vol. 2, no. 8, pp. 214–216, August 1998.

[68] Y. Zhao and S-G Haggman, "Intercarrier interference self-cancellation scheme for OFDM mobile radio communications systems," *IEEE Transactions on Communications*, vol. 49, no. 7, pp. 1185–1191, July 2001.

[69] G. K. Kaleh, "Channel equalization for block transmission systems," *IEEE J-SAC*, vol. 13, no. 1, pp. 110–120, January 1995.

[70] S. Haykin, *Adaptive filter theory*, Prentice Hall, 3rd edition, 1996.

[71] J. M. Cioffi and G. D. Forney, "Generalized decision-feedback equalization for packet transmission with ISI and Gaussian noise," in *Communications, computation, control, and signal processing : a tribute to Thomas Kailath*, A. Paulraj, V. Roychowdhury, and C. Schaper, Eds., pp. 79–127. Kluwer Academic, Boston, MA, 1997.

[72] L. Scharf, *Statistical signal processing*, Addison-Wesley, 1991.

[73] H. Huang, H. Viswanathan, and G. J. Foschini, "Multiple antennas in cellular CDMA systems: Transmission, detection, and spectral efficiency," *IEEE Trans. on Wireless Commun.*, vol. 1, no. 3, pp. 383–392, July 2002.

[74] H. Huang, H. Viswanathan, and G. J. Foschini, "Multiple antennas in random code CDMA systems: Transmission, detection ans spectral efficiency," in *Proc. IEEE Wireless Commun. and Networking Conf.*, 1999, pp. 154–158.

[75] R. L. Choi, K. B. Letaief, and R. D. Murch, "MIMO CDMA antenna systems," in *IEEE International Conf. on Commun.*, 2000, vol. 2, pp. 990–994.

[76] M. Ahmed, J. Pautler, and K. Rohani, "CDMA receiver performance for multiple-input multiple-output antenna systems," in *Proc. IEEE Vehicular Technology Conf. - Fall*, 2001, pp. 1309–1313.

[77] I. Jeong and M. Nakagawa, "Multi-carrier CDMA system using multi-antenna for indoor wireless communication," in *Proc. SBT/IEEE International Telecomm. Symp.*, 1998, vol. 1, pp. 83–88.

[78] C. Li and S. Roy, "Performance of frequency-time MMSE equalizer for MC-CDMA over multipath fading channel," *Wireless Personal Communications*, vol. 18, no. 2, pp. 179–192, Aug 2001.

[79] J. Altuna, B. Mulgrew, and J.M. Zabalegui, "Semi-blind equalisation for multiple-input multiple-output MC-CDMA," in *Proc. 3G Mobile Commun. Technol. conf.*, 2001, pp. 387–391.

[80] S. Kaiser, "OFDM-CDMA versus DS-CDMA: Performance evaluation for fading channels," in *Proc. IEEE ICC*, June 1995, pp. 1722–1726.

[81] S. Hara and R. Prasad, "DS-CDMA, MC-CDMA, and MT-CDMA for mobile multi-media communications," in *Proc. IEEE VTC*, April 1996, pp. 1106–1110.

[82] S. Hara and R. Prasad, "Design and performance of multicarrier CDMA system in frequency-selective Rayleigh fading channels," *IEEE Transactions on Vehicular Technology*, vol. 48, no. 5, pp. 1584–1895, September 1999.

[83] S. B. Slimane, "Bandwidth efficiency of MC-CDMA signals," *IEE Electronics Letters*, vol. 35, no. 21, pp. 1797–1798, Oct 1999.

[84] D. W. Hsuing and J. F. Chang, "Performance of multi-code CDMA in a multipath fading channel," *IEE Proceedings-Communications*, vol. 147, no. 6, pp. 365–370, Dec 2000.

[85] M. A. Visser and Y. Bar-Ness, "Adaptive reduced complexity Multicarrier CDMA (MC-CDMA) structure for downlink PCS," *European Trans. on Telecommunications*, vol. 10, no. 4, pp. 1–10, August 1999.

[86] A. Duel-Hallen, J. Holtzman, and Z. Zvonar, "Multiuser detection for CDMA systems," *IEEE Personal Commun.*, vol. 2, pp. 46–58, Apr. 1995.

[87] X. Wang and H. V. Poor, "Iterative (turbo) soft interference cancellation and decoding for coded CDMA," *IEEE Transactions on Communications*, vol. 47, no. 7, pp. 1046–1061, July 1999.

[88] P. Zong, K. Wang, and Y. Bar-Ness, "Partial sampling MMSE interference supression in asynchronous multi-carrier CDMA system," *IEEE J-SAC*, vol. 19, no. 8, pp. 1605–1613, August 2001.

[89] S. Kaiser and J. Hagenauer, "Multi-carrier CDMA with iterative decoding and soft-interference cancellation," in *Proceedings IEEE Globecom*, 1997, pp. 6 –10.

[90] L. Mailaender, "A multiple antenna successive interference canceller for mixed voice/data systems," in *IEEE Wireless Commun. and Networking Conf. (WCNC)*, 1999, vol. 1, pp. 66–70.

[91] C. B. Papadias and H. Huang, "Linear space-time multiuser detection for multipath CDMA channels," *IEEE J-SAC*, vol. 19, no. 2, pp. 254–265, 2001.